AMERICAN UNIVERSITY OF BEIRUT

EXPLOITING THERMALLY DRIVEN PROCESSES IN THIN-POLYMER FILMS AND ON METAL PARTICLE SURFACES

by
SARAH RAMEZ YASSINE

A thesis
submitted in partial fulfillment of the requirements
for the degree of Master of Science
to the Department of Chemistry
of the Faculty of Arts and Sciences
at the American University of Beirut

Beirut, Lebanon
May 2019

AMERICAN UNIVERSITY OF BEIRUT

EXPLOITING THERMALLY DRIVEN PROCESSES IN THIN-POLYMER FILMS AND ON METAL PARTICLE SURFACES
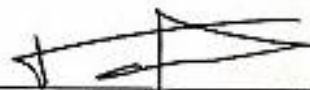
by
SARAH RAMEZ YASSINE

Approved by:

_____

Dr. Pierre Karam, Assistant Professor   Advisor
Chemistry

_____

Dr. Tarek Ghaddar, Full Professor   Member of Committee
Chemistry

_____

Dr. Digambara Patra, Associate Professor   Member of Committee
Chemistry

Date of thesis defense: May 3, 2019

AMERICAN UNIVERSITY OF BEIRUT

THESIS, DISSERTATION, PROJECT RELEASE FORM

Student Name: __Yassine_____ __Sarah_____ __Ramez_____
Last   First   Middle

● Master's Thesis   ○ Master's Project   ○ Doctoral Dissertation

☐   I authorize the American University of Beirut to: (a) reproduce hard or electronic copies of my thesis, dissertation, or project; (b) include such copies in the archives and digital repositories of the University; and (c) make freely available such copies to third parties for research or educational purposes.

■   I authorize the American University of Beirut, to: (a) reproduce hard or electronic copies of it; (b) include such copies in the archives and digital repositories of the University; and (c) make freely available such copies to third parties for research or educational purposes
after : **One ---- year from the date of submission of my thesis, dissertation, or project.**
        Two ---- years from the date of submission of my thesis, dissertation, or project.
        Three ✗-- years from the date of submission of my thesis, dissertation, or project.

_Sarah_____   _07/05/2019_____
Signature   Date

ACKNOWLEDGMENTS

AN ABSTRACT OF THE THESIS OF

Sarah Ramez Yassine   for   Master of Science
                                  Major: Chemistry

Title: Exploiting Thermally Driven Processes in Thin-Polymer Films and On Metal Particle Surfaces

Temperature variations play a pivotal role in deciding the path of many biological and physical processes, yet only few available probes allow measuring these fluctuations at the micro- and nano-scale accurately. In this work, we aim to develop new strategies to map thermal variations in thin polymer films. This acquired knowledge will subsequently allow us to drive chemical reactions using locally generated heat by magnetic nanoparticles with high spatial resolution.

A thermal probe was thus developed through complexing poly (phenylene ethynylene) fluorescent-based conjugated polyelectrolyte (PPE-CO$_2$) with polyvinylpyrrolidone-co-vinyl acetate (PVP-VA). When testing the temperature response in PVP-VA solution, a relative maximum sensitivity of 2.35% was obtained. The polymer complex was then spun cast onto quartz slides and imaged using a DSLR camera at different temperatures between 20.0 °C and 60.0 °C. Finally, these images were analyzed using the ImageJ software to study the change in color upon increasing the temperature.

Building on the previous work, iron-oxide magnetic nanoparticles were complexed with gold nanoparticles via a multi-layer coating method. The heat generated by the magnetic nanoparticles when placed in an alternating magnetic field is transferred to the gold nanoparticle surface where heat-dependent reduction reaction of resazurin, a weakly fluorescent molecule, to a highly fluorescent resorufin is monitored. This level of spatial heat control will allow us to locally catalyze chemical reactions and release reactive oxygen species intracellularly with surgical spatial control.

CONTENT

ILLUSTRATIONS

xiii

TABLES

CHAPTER 1

INTRODUCTION

Temperature is a fundamental physical parameter for a wide range of industrial operation and scientific research.[1] It governs various kinds of chemical reactions, biological processes, and physical laws.[2] These processes occur in either an exothermal or endothermal manner that reflects their thermodynamic behaviors whether occurring inside a biological cellular system or in a solution.[3]

A typical thermally-driven reaction takes place in a restricted location inside the system it belongs to. That by tracking the distribution and fluctuation of the temperature in that specified location, one can infer on the thermodynamics and eventually on its function. For example, scientists can understand the function of a living cell by monitoring the temperature inside its components.[4] In medical applications as well, cellular pathogenesis of diseases is detected and characterized based on the heat produced; cancer as an example.[5] Hence, understanding and studying the role and impact of temperature will undoubtedly help improve our perception of various chemical systems, bio-cellular events, diagnosis, medical therapies, and many others.[3, 6] Therefore, researchers nowadays are exerting a tremendous effort to explore, measure, and control the temperature fluctuations in thermally-driven applications.[7, 8]

1.1 Role of Temperature in Catalysis:

Monitoring temperature in a thermally-dependent system is directly correlated to its efficiency and productivity. One example on this is the 190,000-fold increase observed in the rate of the hydrolysis reaction of polysaccharides when its temperature is raised from 25 to 100 °C. On the other hand, the rate of the hydrolysis of phosphate monoester dianions witnessed a 10,300,000-fold increase for the same temperature rise. [9] In fact, any chemical or biological reaction is enhanced upon increasing the temperature at which it is performed, yet this merit seems to not be assessed the way it should be. Following are some more specific examples on the role of temperature in monitoring extensive scientific reactions and processes.

1.1.1 Cellular Level:

On the intracellular level, triggering a specific function requires the cellular biological reactions to release Gibbs free energy. This will eventually lead to the release of the excess energy in the form of heat elevating the local temperature.[10] For instance, the transfer of a proton within the mitochondrial inner membrane, commonly known as thermogenesis, produces heat inside the cell.[11] Also, the endoplasmic reticulum (ER) produces heat via a calcium-pump activity.[12] These mechanisms, referring to the most probable cases of increase in local temperature intracellularly, cause the shift in the chemical equilibria; thus, accelerating the relative reactions' rates.

Due to this critical role of heat, obtaining a non-homogeneous temperature distribution within the cell will directly correlate to the former's activity affecting its biochemical processes and reactions.

1.1.2   Enzymatic Level:

Temperature, as do other factors, profoundly influence the rate of the reaction of enzymes. In detail, not only do low temperatures lower the enzymatic activity but also at extreme temperatures, the enzymes denature with their activity ceasing. Generally, a 10-degree Celsius rise in the temperature increases the rate of the enzymatic reaction by 2-folds because of a higher enzyme-substrate collision rate. However, this increase in the activity peaks at a specific temperature, unique to each enzyme and commonly known as the optimum temperature, yielding a maximally efficient reaction. Beyond this temperature, the activity starts decaying until ceasing at very high temperatures.[13]

1.1.3   Medicinal & Cancer-treatment Level:

Thermal medicine is the act of manipulating the body or tissue temperature to treat diseases. Reports on using the cold-and-hot thermal therapy first appeared since the earliest practice of medicine. Cancer, for example, is one of the specific medical applications where temperature played a pivotal role in. However, modern thermal medicine intends to further understand the impact of temperature fluctuations on the molecular, cellular, and physiological levels as well as to develop safer and more efficient techniques to manipulate heat in the clinical medicine field.

Hypethermia, for example, refers to the state when the individual's body temperature elevates beyond normal due to a failure in the internal thermoregulation. It occurs when the heat-regulating system in the body is vanquished by the external factors surrounding thus leading to a rise in the body's internal temperature. This thermally-driven condition is being currently implemented in cancer therapy where it is combined with the

radiotherapy and chemotherapy as well as to treat inflation in the body organs through shrinking the respective tissues.[14]

Thermal ablation, the act of destroying abnormal cells through local heating or freezing, is yet another example where the temperature is thoroughly exploited. This therapy is nowadays referred to as the standard health care for a group of cardiac arrhythmia diseases. Endometrial ablation is as well used to treat endometrial bleeding.[15]

Other medical applications relying on temperature as a major contributor include: the storage of viable cells for a long period of time through cryopreservation- applied at a temperature < -80 °C,[16] laser-heating methods for excessive subcutaneous fats that cause obesity and disorders in the body's metabolism,[17] and intravascular heating to eradicate varicose veins by the aid of laser and radiofrequency currents.[17]

1.1.4   Drug Delivery:

One of the very exciting advancements in drug delivery is the development of heat-triggered systems. For instance, scientists are now harnessing thermosensitive liposomal drugs with nanoparticle carriers, that upon heating to a temperature above 40 °C, the chemotherapy agents are released. Such an evolution in the pharmaceutical field allows for specific targeted drug delivery to the tumors while maintaining normal tissues intact. Interestingly, the aforementioned thermal ablation and hyperthermia techniques can be coupled with the heat-activated drug carriers so that the chemotherapy is deposited in the heated-area exclusively.[18]

Chilkoti *et al.* reported the design of the thermally-responsive elastin-like polypeptide (ELP) targeted drug-delivery in an aim to enhance the localization of ELP-drug conjugates inside a solid tumor heated by regional hyperthermia.[19]

1.1.5   Electrochemical:

Local heating has always been challenging for electrochemical systems where most of the conventional heating methods fail. As a result, there has been a pressing need to develop new approaches capable of raising the temperature at a specific location for thermally-driven electrochemical applications. Microwave frequency activation, as an example, is recently being employed to locally heat the tip of the working electrodes based on a focused interaction with the metal. This has led to significant superheating effects growing locally at the surface of the targeted electrode.[20] Another evolving electrochemical heating method applies radiofrequency induction to heat up the surface of the foil electrode. Eventually, the solution's temperature will rise as a function of conduction and convection while flowing around the electrode.[20] These achievements, along with the others, have been considered a breakthrough in the field of localized heating in electrochemical processes.

1.1.6   Chemical Catalysis:

The temperature has a decisive impact also on chemical rates, and hereby on chemical reactions and processes, catalysis in particular. It has, thus, been essential to optimize the activity, selectivity, and stability of the catalytic reactions while monitoring their temperatures.[21] Available heating approaches, despite being sufficient for large-scale catalysis, cannot control catalytic reactions at the nano-scale.

5

Scientists have realized that when it comes to the nano-level, materials and chemical species behave in different manners than they do at large scales, following from their nano-scaled size that increases their surface-to-volume ratios.[22] For this, being able to monitor the temperature changes at that delicate level, enhances the reactions' efficiency and eventually its chemical properties. In order to achieve this goal, many recent advances have evolved to locally heat up thermally-driven catalytic reactions.

For instance, Chen *et al.* used the single-molecule fluorescence approach, that is capable of imaging the individual metal nano-particle, to locally produce fluorescent molecules from locally catalyzed reactions and track its fluorescence emissions at a high resolution.[23] Also, in the field of nanomedicine, scientists recently reported the ability to apply sequential catalysis through locally releasing biocompatible nano-catalysts into specific tumor sites following a very selective manner while keeping normal sites intact.[24]

The concept of localized catalysis will be further discussed in chapter 4 where we report the use of an alternating magnetic field to generate heat from magnetic nanoparticles to drive catalytic chemical reactions.

1.1.7   Thin Films for Micro-Channels and Micro-electronic Devices:

So far, temperature measurements have been extensively explored in a wide range of applications, yet little where those tackling thermal measurements in thin-solid films.

Although highly exploited in micro-channels and microelectronic devices, sensing in thin films still suffers from a lack in the investments and research. One of the major techniques that focused on bridging this gap is the fluorescent-based methodology that will be discussed later in the chapter. These advancements, despite showing some

6

successful results, are still limited in terms of the heat dissipated and the low spatial resolution they exert when mapping thermal changes.

Despite the stated importance of the local temperature profile, scientists still face many difficulties and obstacles in mapping and analyzing properly the local thermal fluctuations. Therefore, we need non-invasive thermometry techniques with a high spatial resolution to read the temperature changes.

Temperature sensing in thin films will be, as well, fully elaborated in a separate chapter, later on in this dissertation.

1.2   Advances in Thermometry:

1.2.1   Contact & Non-Contact Methods:

Among the available temperature-measuring techniques, scientists recognize two major categories: contact methods and non-contact methods. Since contact methods, such as thermistors and thermoelements requiring electrical wiring fail to be implemented in corrosive and delicate environments, non-contact methods evolved.[25]

One of the most common non-contact methods uses infrared (IR) to apply rapid imaging of the temperature. Yet, this technique requires that the material investigated as well as its emissivity should be known prior to the measurements.[26] It also suffers from the wavelength-absorption of its glass material hindering the optical-window measurements. Not to mention, that besides being very expensive, IR-based temperature mode measures thermal fluctuations at the micro-scale, thus, fails to achieve high spatial resolution.[11]

Meanwhile, the field of thermometry has been witnessing huge advances in its various domains.

1.2.2   Brief History on Thermometers:

In 1654, Ferdinand II, the Grand Duke of Tuscany, marked the first milestone in the field of thermometry through his experiment in filling a glass tube with alcohol. However, this early invention lacked any scale or relative, data making it inaccurate. Almost 60 years later, Garbriel Fahrenheit, a German physicist, substituted Ferdinand's alcohol-tube with a mercury one because of the more predictable results of the latter; this yielded more exquisite measurements. Such an advancement was soon backed up by setting the Fahrenheit's temperature-scale.

The temperature has been as well exploited in one of the very early experiments when Lord Kelvin aimed at estimating the age of our planet that was believed to be around 10,000 years old. In 1862, Kelvin took advantage of the cooling speed of a steel ball as a thermal gradient to reach a conclusion that our planet is 100 million-years-old.[27] Later, the Swedish Astronomer Andres Celsius introduced a new thermal scale which he cut down into 100 units ranging between 0 °C -taken as the freezing point- and 100 °C attributed to the boiling point of pure water measured at the sea level.

The effect of thermal knowledge at low scales along with the escalating opportunities displayed in the field of science and technology have triggered the development of several thermometers functioning at the sub-micron scale and exhibiting an acceptable spatial resolution. A spatial resolution is generally defined by the minimum distance needed to obtain a change in the temperature that is greater than the sensitivity of

the thermometer.[28] These micro-scaled thermometries serve the demands in a wide spectra of technological fields including microelectronics, microfluidics, photonics, and micro-optics.[29]

However, with the advancements of science and the increase interest in probing processes at the micro and nanoscale, the available conventional thermometries failed to meet the new standards. Few examples on the challenging demands include the temperature mapping at the intracellular level and in thin chemical films.

1.2.3   Limitations:

Despite the huge demands and expectations in this field, mapping the temperature fluctuations and distributions at a high spatial resolution, up to the nano-scale, hasn't been attained yet. The fact is, conventional thermometers, such as the thermography and thermocouple, suffer from a relatively low spatial resolution (up to 10 μm) making it insufficient for cellular measurements.[30] As a result, available probes fail to detect and track non-homogeneous heat-distributions in heat-dependent systems.

An ideal sufficient thermosensitive technique is expected to satisfy simultaneously, a list of requirements: high temperature resolution, high spatial resolution, function independent of the environmental changes as pH and ionic strength, and function independent of the surrounding biomacromolecules. Alongside, it should be inexpensive, non-invasive, reproducible, and easy to read.

Being unable to satisfy all the aforementioned criteria, blocks and hinders the advancements in thermal sensing in cells as well as in chemical systems and solutions.[3]

This has called for new innovations in the field of thermometry; therefore, nano-thermometry has become essential.

1.2.4   Fluorescent-based Nano-thermometry:

Fluorescent-based nano-thermometry has gained a considerable attention due to the significant advantages it offers from the large scale of imaging to the non-invasive contactless measurements.[31] Various kinds of luminescent nano-thermometers have been implemented into the scientific fields categorized based on the origin of their fluorophore-system. Examples on the diverse systems are the organic dyes,[7, 32] organic-inorganic hybrid nanoparticles,[33] polymer nanoparticles,[33] quantum dots (QDs),[34] polymer dots (PDs),[35, 36] fluorescent proteins,[32] and lanthanide ions (Ln^{3+}).[37, 38] Below, we present some of the work done recently as a result of the remarkable encroachments they have achieved in the field of fluorescent-based nano-thermometry.

1.2.4.1   Ratiometric Probes:

One of the major drawbacks current fluorescence probes suffer from is the effect of the surroundings on the readout of the received signals. Some examples of these factors include photobleaching, dye concentration, and the fluctuations in the excitation sources. These aspects may lead to non-accurate results when mapping the system's temperature. For this, it is of great advantage to rely on fluorescent-based ratiometric nanothermometers to compensate for the above limitations and reduce any error produced by any of the light source, detector, or pathway. Ratiometric probes, therefore, enhance the accuracy of the emission spectra of these thermometers.

1.2.4.2   Lanthanides:

Known for their high stability, biocompatibility, and their ladder-like 4f energy levels, lanthanide ions (Ln^{3+}) have been probed significantly in a wide range of thermal applications in fluorescence nano-thermometry. Although appearing to be extremely transparent when induced in living tissues, these cations are highly emissive in the IR window (700-980 nm).

Suzuki *et al.*, for instance, succeeded in achieving a high thermal sensitivity that allows the detection of different thermal behaviors at distinct spots suggesting a heterogeneous heat production and dissipation. Their work focused on combining Lanthanides β-diketonate chelate europium (III) thenoyltrifluoroacetonate with the organic probe Rhodamine 101 in order to develop a ratiometric sensor.[38]
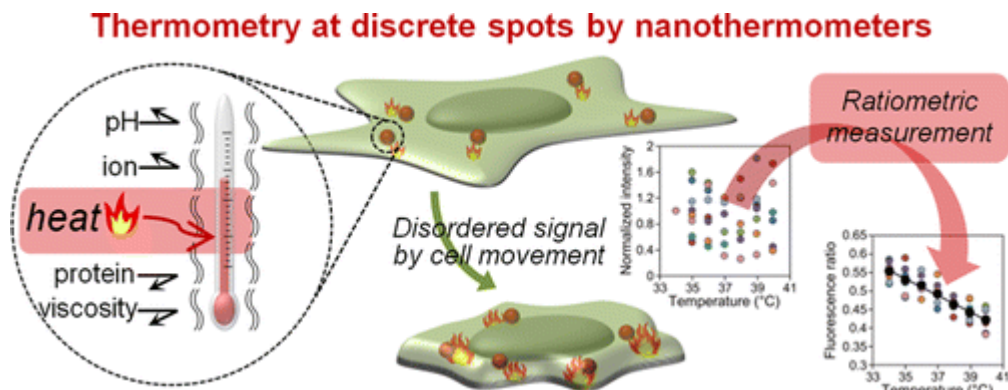
Figure 1.1: Schematic illustration of a ratiometric nanothermometer (RNT) used for intracellular temperature measurements at discrete spots. (Reprinted with permission from Suzuki *et al.*)[38]

Later, lanthanide-based probes were introduced into metal-organic frameworks to enhance their sensitivity and fasten their adaptability with their surroundings more and more.

1.2.4.3   Metal-Organic Frameworks (MOF):

Metal-organic frameworks (MOFs) are hybrid macromolecules used to assemble other specific molecules into a higher hierarchical structure. The fact that the MOF linkers and the locked dyes inside behave and emit light differently and at distinct wavelengths when exerting thermal changes attracts more attention toward this kind of probes.

Example on that is the encapsulation of the rhodamine 101 acting as a fluorescent dye inside the Zirconium-MOF UiO-67. A temperature-dependent fluorescent emission-spectrum acquired over the temperature range 20 to 60 °C displayed a sharp decay in the dye's intensity accompanied by a fixed intensity peak of the organic linker. The reported sensitivity was equal to 1.91 % °C^{-1}.[39] Shen *et al*. reported another interesting MOF-Lanthanide thermal sensor where they introduced Tb^{3+} and Eu^{3+} cations into a thin film. Results revealed an increase in the emission spectra of Eu^{3+} accompanied by a decrease in that of Tb^{3+}. Sensitivity attained was as high as 1.05 % °C^{-1}.[40]
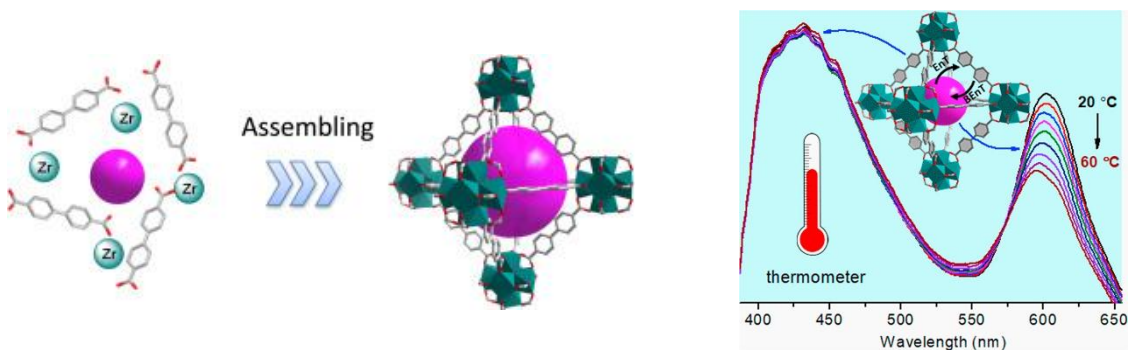
Figure 1.2: Schematic illustration of the formation of Rh101@UiO-67 hybrid by assembling Rh101 dye molecules in the pores of UiO-67 through a one-pot synthesis strategy. (B) Emission spectra of the Rh101@UiO-67 acquired over the temperature range 20 to 60 °C. (Reprinted with permission from Shen *et al*.) [39]

As a rapidly rising field, fluorescent-based nano-thermometry has gained a lot of attention in the applications it can develop even beyond the biomedical discipline. Indeed, it is considered a substantial factor that allows deeper understanding of many applications, including but not limited to, microelectronics, nanofluids, and chemical catalysis. Ideally, a favorable sensing technique should maintain a good stability over time, so it does not require repetitive calibrations leading to non-consistent results.[41] Probes exerting a ratiometric signal can perhaps help to minimize the errors obtained as a result of the fluctuations in the light source, instability, and the fluorophore's concentrations little-effect;[42, 43] this signal ratio accounts for the fluctuations in the excitation source. However, it still fails to account for the fluorophore photobleaching and quenching. Accordingly, scientists aimed for material that (i) consists of a single-component fluorescent system and (ii) emits at two distinct thermally-dependent states.[44]

Notably, conjugated polyelectrolytes, being a class of polymer with exceptional optoelectronic properties and high brightness, appeared as likely prospects at this stage.[41, 45] The reason why we decided to implement into our system presented in chapter 3. In what follows, we'll present a brief background on conjugated polyelectrolytes, addressing their photophysical properties, followed by discussing some of their applications in the field of thermal sensing.

1.2.5 Conjugated Polyelectrolytes:

Conjugated polyelectrolytes (CPEs) are a class of organic semiconductors known for their π-conjugated backbone of alternating single and double bonds functionalized with ionic pendant groups attached to their side chains to increase their solubilities (Figure 1.3).[46] They are categorized based on their charges into two main categories: cationic CPEs, typically connected to quaternary ammonium (NR_3^+) or pyridinium, and anionic CPEs that mostly include carboxylate (CO_2^-), phosphonate (PO_3^{2-}), or sulfonate (SO_3^-) connected to their side chains.[47]

CPEs exhibit high solubility in polar solvents as a function of their charged chain groups and hydrophobic aromatic backbones.[47] Given this advantage in polar media along with their optical and photophysical properties and applications, CPEs hold great promises in the sensing devices and have gained increasing attention by researches nowadays.[46]
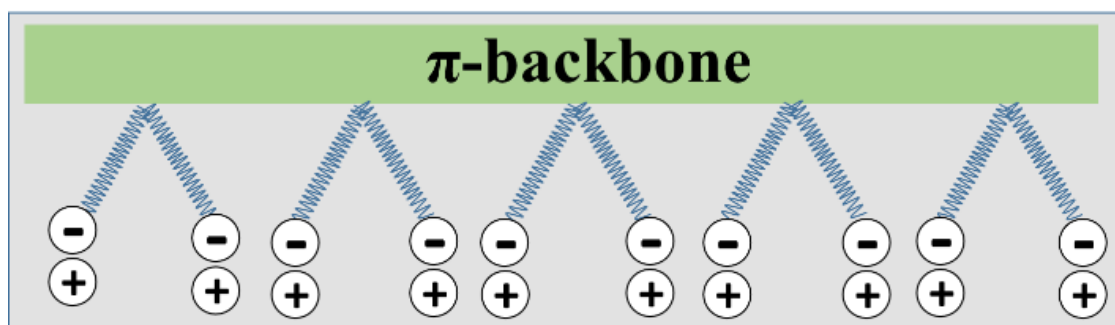
Figure 1.3: Schematic representation of the structural component of an anionic CPE. Modifying the π-backbone colored with green can help to regulate and to control some of the properties of the polymer.

14

1.2.5.1 Photophysical Properties of Conjugated Polyelectrolytes:

Since their discovery in 1987 by Weld Heeger *et al.*, the CPEs properties have been extensively studied and tracked in terms of their π-electron polarization, charge transport, high conductivity, and chemical sensitivity, as well as their band gaps for absorption and emission spectra. The delocalization of their backbone electrons results in attractive optical and electronic properties such as their high efficiency in intra and inter-chain energy transfer and their ability to convert binding events into readable optical and electrochemical responses. Interestingly, factors such as the structure of the polymer and its surrounding environment have a huge impact on monitoring these properties making them excellent objects for sensing. [48] In fact, the energy transfer mechanism and the solvent used affect the degree of aggregation of the CPE that we'll later discuss how it serves our interest in thermal sensing.

1.2.5.1.1 Energy Transfer:

The degree of aggregation affects the delocalization of the π-electrons along the main backbone of the polymer enhancing the thermal response of the system. [49] For this, it is essential to dive deeper into understanding the mechanism of energy transfer and exciton migration in conjugated polyelectrolytes.[50] These polymers possess highly efficient intramolecular and intermolecular energy transfer mechanisms and large extinction coefficient.[51]

There are typically two energy transfer mechanisms: (i) through-space exciton migration that is usually dominant in aggregated polymers, yet not so common in extended chains, and (ii) through-bond energy transfer encountered in the latter case.[52, 53] In the

through-space case, energy is normally transferred through resonance energy transfer in between the CPEs chain segments where the oscillations in a dipole-excited segment are being moved to that in an adjacent one.[49, 54] However, the through-bond mechanism refers to the migration of exciton along the backbone of one single polymer molecule without any chain-to-chain transfer process. This is known as the intrachain energy transfer and is likely to occur in solutions.[49, 50]

1.2.5.1.2   Solvent Effect:

Since CPEs are intrinsically amphiphilic (hydrophobic backbone and hydrophilic side chains), they tend to aggregate in polar organic and aqueous solutions leaving them highly dependent on their solvents.[55] This aggregation influence both the absorption and fluorescence spectra making it an attractive criterion for sensing applications. Since CPEs are amphiphilic, they self-assemble into aggregates through π-stacking in the unfavored aqueous solution.[53, 56]

To illustrate the effect of the solvent, we'll take the study done by C.J Tan and co-workers on PPE-SO$_3^-$ polymer in particular where they compared its fluorescence properties in methanol and in water. They reported that the fluorescence bands of PPE-SO$_3^-$ dissolved in methanol were analogous to that of the neutral PPE, suspended in good solvents like chloroform, CHCl$_3$, in terms of the bands' intensities and chemical shifts. This indicates that PPE-SO$_3^-$ appears as single unaggregated chains and that methanol is serving as a "good" solvent. Also, the similarity between the fluorescence-spectra characteristics exhibited when the CPE was dissolved in water and that of the aggregated

16

conjugated polymer confirms that in an aqueous solution, polymers undergo conformational changes causing their aggregations.[57-59]

The ability of these polymers to alternate their conformation between the aggregated and disaggregated states in response to their structure and environment, made them appealing for a wide range of sensing applications and devices. For instance, the extended conformation is favorable for electroluminescent devices because it maximizes the quantum yield. However, the stacked aggregated status is beneficial for the optimizations and enhancements of the thermal sensing devices; this also relates to the amplified fluorescence quenching discussed in the section below.

1.2.5.2   Conjugated Polyelectrolyte-Based Sensing Applications:

One major factor driving this interest in CPEs for fluorescence sensing is the former's ability to exhibit a signal gain as a response to their interaction with analytes. This signal gain is referred to as amplified fluorescence polymers (AFP) or "super-quenching". One reason behind the increase in the sensitivity (amplification) is the highly efficient transport medium, attained by the conjugated polymer, that transports electronically excited states commonly known as excitons.[60] Generally, excitons are electrically neutral quasiparticles capable of transporting energy via the bounding they form between electrons and electron holes;[61] and in AFP, excitons are so mobile that they undergo diffusion throughout the polymer's chain.

To illustrate further how the energy migration can amplify fluorescence-based sensors, Swager *et al.* did their study on poly(*p*-phenyleneethynylenes) supported by the previous investigations done on this CPE proving its efficiency in energy migration. [62]

They hypothesized that if the energy migration is relatively faster than the fluorescence lifetime, then the excited state will be able to sample every receptor in the polymer. This will eventually allow a single binding site to change the overall emission. In other words, when a quencher occupies a receptor site, it enhances the deactivation.

Swager and co-workers have reported the work they did on several receptor-substituted organic soluble polymers of neutral nature. They accentuated on studying the correlation between the CPE's photophysical properties and its quenching behavior. For instance, they showed that in short CPEs, the quenching constant increases as the molecular weight of the polymer increases. These results paved the way into new detection probes that are based on the principle of energy migration and quietly represented by the amplified fluorescence quenching of conjugated polymers. [63]

In like manner, Karam *et al.* examined the photophysical properties of the negatively charged, hydrophilic conjugated polyelectrolyte: poly[5-methoxy-2-(3-sulfopropoxy)-1,4-phenylenevinylene] (MPS-PPV) at the single-molecule level.[64, 65] In negatively charged vesicles, MPS-PPV was proven to exist as a freely diffusing polymer adopting a collapsed-chain conformation. This collapse will increase the efficiency of the energy migration over several chromophores leading to stepwise photobleaching in fluorescence intensity-time trajectories and emission from low-energy chromophores along the chain, which is consistent with that observed in aqueous solutions. However, in a neutrally charged vesicle, single MPS-PPV adopts an extended conformation.[65]

Based on the properties of the CPEs presented earlier, scientists aimed at studying more how their alternating conformations can be exploited in thermally-driven applications.

Phenylene-based polymers appeared as a pleasing CPE-category , for the fact that they are temperature-sensitive polymers that display a clear shift in their emission spectra while disaggregating to their free-chain status.[66] They, as well, have been utilized as piezochromic probes and membrane reporters.[41] Below is a further discussion on the major characteristics of phenylene-based polymers.

1.2.6   Poly(phenylene ethynylene)s (PPEs):

Poly(phenylene ethynylene) is perhaps the most common type of aromatic conjugated polymers (CP) where all its aromatic groups are benzene rings. Although believed to be rigid rod-like at low molecular weights, PPEs with long chains behave as coil-like worms.[67] Cotts and Swagar verified this discovery through the experiment they carried on a series of PPEs holding different molecular weights. Moreover, it was found that going from the aggregated status to the free chain one, a CPE criterion discussed above, causes a shift in the emission spectra of the short phenylene-based polymers. A property that is expected to enfluence the sensors' thermal response.

Sooner after studying and revealing the properties of the poly (phenylene ethynylene)s (PPEs), a series of studies were done on synthesizing PPEs with ionic side chains and different chain lengths leading to the formation of amphiphilic PPE conjugated polyelectrolytes.[68, 69] Carboxylate, for instance, is one of the most extensively studied ionic groups due to the properties it exhibits including its selectivity in binding to di- or tri-valent

19

metal ions to form coordination complexes. As such, Zhao *et al.* reported the synthesis and characterization of PPE-CO_2-7 conjugated polyelectrolyte.[70]

Herein, this short phenylene-based CPE, PPE-CO_2 was used to build a ratiometric nanothermometer while optimizing its sensitivity and linear range. Following section explains the advantages gained from implementing these thermal-sensitive PPE-CO_2-7 into the field of sensing.

1.2.7 Poly (phenylene ethynylene) Carboxylate (PPE-CO₂):

The synthesis and characterization of poly(phenylene ethynylene)carboxylate polymer is explained in details in ref [70]. Similar to what was obtained when characterizing PPE-SO_3^-, PPE-CO_2 showed changes in absorption and emission spectra when studied in different solvent mixtures. A reason behind this is that in aqueous mixtures such as water, short poly (phenylene ethynylene) carboxylates aggregate. This aggregation is driven by the interaction of the π- π stacking with the polymer's backbone. Consequently, the obtained fluorescence emission witnesses a broadening, structureless, and red-shift in its spectra caused by the excimer species. On the other hand, in polar solvents such as ethanol and methanol, PPE-CO_2 dissolves almost completely in the solvent in the form of an extended- disaggregated individual polymer leading a well-structured emission spectrum.

This sensitivity of the PPE-CO_2 towards the changes in the solvents' polarity along with its distinct behavior when in its aggregated form compared to that when its extended individual chains, made it an exciting and tempting material to build our thermal probe from. In this dissertation, we report the usage of a PPE-CO_2-based fluorescent nanothermometer, to be discussed further in chapter 3.

1.3   Objectives:

Thermal sensing in thin films polymers has been a significant limitation towards optimizing the heat dissipation in micro- and nano-electronic devices as well as many other thin film-based technologies. As a result, it becomes a pressing need to improve the available nano-thermometers while maintaining a high sensitivity. Additionally, controlling temperature with high spatial resolution has been another challenge and the bottleneck for advancing scientific discoveries at the nano-scale level.

In this work, we aim at developing new strategies to map thermal variations in thin polymer films through reporting on a novel fluorescent-based thermal sensor. This acquired knowledge will subsequently allow us to drive chemical reactions using locally generated heat with high spatial resolution. We, herein, exploit the heat generated from magnetic nanoparticles when placed in an alternating magnetic field to drive catalytic chemical reactions.

CHAPTER 2

MATERIALS AND METHODS

In this chapter we present a summary of the materials used and the methodologies followed in the reported experiments of chapters 3 and 4.

2.1 Fluorescent Thermal Sensing using Conjugated Polyelectrolytes in Thin Polymer Films

2.1.1 Materials:

The following materials have been used for our thermal sensing project: Poly (phenylene ethynylene) carboxylate, PPE-CO_2-7, with 7 repeating units were synthesized as previously described by our group and others;[41, 66] Poly (1-vinylpyrrolidone-*co*-vinyl acetate), PVP-VA, M_w= 50K (Aldrich); Poly (1-vinylpyrrolidone-co-styrene), PVP-PS, 38 % emulsion in H_2O, <0.5 µm particle size (Aldrich); Rhodamine B isothiocyanate, $C_{29}H_{30}ClN_3O_3S$, Bio-Reagent, mixed isomers, suitable for protein labeling (Aldrich); Fluorescein 5(6)-isothiocyanate, $C_{21}H_{11}NO_5S$, ≥90% (Aldrich); Ammonium hydroxide, NH_4OH, ACS reagent, 28-30% solution in water (Acros); Hydrogen Peroxide, H_2O_2, puriss., meets analytical specification of Ph. Eur., BP, USP, 30-31% (Aldrich); HEPES solution: N-(2-Hydroxyethyl) piperazine-N′-(2-ethanesulfonic acid), 1 M, pH 7.0-7.6, sterile-filtered, Bio-Reagent, suitable for cell culture (Aldrich); Sodium Chloride, NaCl, extra pure, SLR (Fisher); Quartz slides 25.4 x 25.4 mm^2 (Science Outlet); PELTIER TEC1-12710; Power Supply 30V- 5A D ZHAOXIN, 0.1 volt increment; Fluke 80BK-A Type K Multimeter Thermocouple, and Deionized water (18 µΩ, Nanopure Diamond, CRSL, AUB) for solution preparations and dilutions.

2.1.2   *Methods:*

2.1.2.1   Absorption Measurements:

Absorption spectra were measured using Jasco, V-570 UV/VIS/NIR Spectrophotometer in double beam mode and air as the baseline

 For measurements in solution (Chapter 3):

The mixture solutions were placed in a 1 cm x 1 cm quartz cuvettes, and the total volume was kept constant and equal to 2 mL.

The Reference/Blank Solution consists of 2 mL of 10mM HEPES-150 mM NaCl (pH=7.33) mixture only while that of the control, contains additionally 22 μL of PPE-CO_2-7 (0.45 g/L or 450 μL/mL).

The analyzed solutions consist of 2 mL of 10 mM HEPES-150 mM NaCl (pH=7.33) mixture, 22 μL of PPE-CO_2-7 (0.45 g/L or 450 μL/mL), and different volumes of the respective polymer (PVP-VA or PVP-PS).

 For measurements in thin polymer films (Chapter 3):

The quartz slides coated with 25 μL of different PPE-CO_2-7/polymer mixtures were fixed in the middle of the film holder of the UV-VIS machine. The reference film is plain quartz without any coating, and that of the control is only coated with 25 μL PPE-CO_2-7.

 All runs were taken under the following specifications: Bandwidth: 10.0 nm, scanning speed: 1000 nm/min, data pitch: 2.0 nm, NIR: 40 nm, and a wavelength range: 300-550 nm.

2.1.2.2   Steady State Fluorescent Spectroscopy Thermal Measurements:

Steady-state fluorescent spectroscopy was acquired using a Thermo Fisher Lumina Spectrophotometer equipped with a temperature controller unit (T3 Quantum Northwest). Emission spectra were recorded using Luminous Software- Wave Scan. All solutions were placed in a 1 cm x 1cm quartz cuvettes while keeping the total volume constant and equal to 2 mL.

Before each measurement, the solution was allowed to homogenize through stirring at 400 rpm for five minutes.

The control solution consists of: 2 mL of 10 mM HEPES-150 mM NaCl (pH=7.3) mixture + 22 µL PPE-CO$_2$-7 (450 µg/mL) while the analyzed one contains: 2 mL of 10 mM HEPES-150 mM NaCl mixture, 22 µL PPE-CO$_2$-7 (450 µg/mL), in addition to variable volumes of either PVP-VA or PVP-PS.

All measurements took place at the following specifications: Scan mode: emission (E_M), excitation wavelength = 420 nm, emission wavelength = 435-700 nm.

2.1.2.3   Quartz Cleaning:

Quartz slides were cleaned in boiling ethanol (100%) for 30 min, dipped for 10 min in a warm NH$_3$/H$_2$O$_2$ solution (of ratio 7:3 (v/v) of 28% NH$_3$- 30% H$_2$O$_2$), rinsed in deionized water, and then air dried.

2.1.2.4   PPE-CO$_2$-7/ PVP-VA Film Assembly:

PPE-CO$_2$/Polymer mixtures were coated on the quartz slide using the WS-650MZ-23NPP spin coater machine and via a static-6-steps process. The cleaned quartz slide was first fixed in the middle and vacuumed before adding the desired solution. The first 3 steps were relatively low in speed, starting with 100 rpm and 200 rpm for the first two- 30 sec runs, followed by a one-minute 300 rpm-run. This speed was then increased in the other half of the process to 1000 rpm and 1500 rpm for a 30-sec run each, reaching the maximum speed, 2000 rpm, in the final minute.

2.1.2.5   Thermal Imaging of Thin Polymer Films:

The quartz coated with the PPE-CO$_2$-7/polymer mixtures were placed on a thermoelectric cooler (TECL) - Peltier (TEC1-12710) device- and imaged, under UV light exposure (365 nm), using a regular DSLR Canon 750D camera- 60 mm macro lens- (exposure time 1/5 s, f/5.6, ISO 100). The temperature was regulated using a DC power supply connected to the Peltier by ranging the applied voltage between 0 V and 6 V with 1 V increment. Before each imaging, and after setting the voltage, the quartz was kept for 5 min for the temperature to stabilize.

Temperature changes were measured using a Fluke 80BK-A Type K Multimeter thermocouple (-40 to 260ºC) connected directly to the top of the quartz.
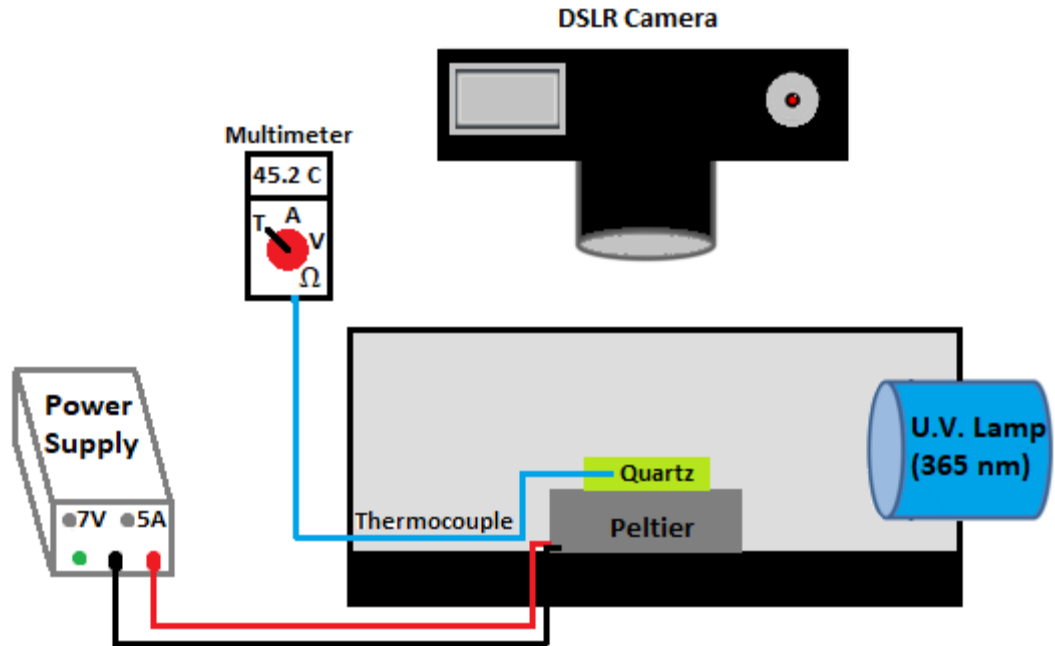
Figure 2.1: Schematic illustration of the thermal imaging setup. The filmed quartz is placed on a thermoelectric cooler (Peltier) and heated via a DC power supply. The thermal fluctuations are measured with a thermocouple connected to a multimeter. Film's excitation was obtained using a UV lamp while images were acquired using a DSLR Canon 750D camera.

2.1.2.6   Analysis of Images:

To analyze the images, saved as RAW files, we first converted them into jpeg using the lightroom software. These jpeg images were then dissected into their three-color components, red-green-blue, and intensity-analyzed using the ImageJ software.

2.1.2.7   Scanning Electron Microscopy (SEM):

The morphology and the thickness of the proposed system were determined using a MIRA3 Tescan scanning electron microscope (SEM). For this purpose, filmed quartz pieces were attached to the SEM pins via a carbon tape layer. Just prior to imaging, samples were coated with Gold FTM layer of 10.0 nm thickness.

2.1.2.8   Thermogravimetric Analysis (TGA):

The rate of degradation of the polymer-polymer complexes as a function of time was measured using the thermogravimetric analysis instrument: Netzsch TG 209 F1 Libra. The samples were first dried overnight and then analyzed between 30 °C and 1100 °C at a heating rate of 10.0 °C/min.

2.1.3   Solution Preparations:

2.1.3.1 PVP-VA Stock Samples:

PVP-VA stock solution was prepared by dissolving the stock powder in 10 mM HEPES-150 mM NaCl (pH= 7.33) buffer yielding a final concentration of 100 mg/mL, denoted as 1X. A series of further dilutions were done yielding standard solutions of respective concentrations 0.5, 0.1, 0.05, and 0.01 X.

2.1.3.2 PVP-PS Stock Samples:

The concentration of the PVP-PS stock solution is 395.2 mg/mL, denoted as 1X. This stock solution was used to prepare a series of further dilutions in the same buffer yielding standard solutions of respective concentrations 0.5, 0.1, 0.05, and 0.01 X.

2.1.3.3 Titration of PPE-CO$_2$-7 with Different Polymer Ratios:

To optimize the PPE-CO$_2$-7/PVP-copolymer ratio, CPE solution with a final polymer concentration of 5 µg/mL was prepared in 10 mM HEPES 150 mM NaCl (pH=7.33) and maintained at 20.0 °C. Incremental amounts of the copolymers were subsequently added to the solution.

27

All the analyzed samples were prepared by dissolving 22 µL PPE-CO$_2$-7 (450 µg/mL) in 2 mL of 10 mM HEPES-150 mM NaCl (pH=7.33) before introducing different incremental amounts of the two polymers separately. Titration was done until reaching a saturation in the emission intensity. The final concentration of the polymer in the cuvette was calculated as follows:

$V_t = 2022$ µL + V_i (polymer) in µL.

$$[copolymer] = \frac{\frac{\sum(C1V1 + C2V2 + \cdots)}{Vi = \sum(V1 + V2 + \cdots)}}{2022 + Vi}$$

[PPE-CO$_2$-7] $_{final}$ in cuvette $= \frac{22 \text{ µL} \times 450 \text{ } \mu g/mL}{2022 \text{ µL}} = 4.90 \text{ } \mu g/mL$

2.1.3.4 Thermal Sensing:

To evaluate the thermal response of the polymer complex, the solution mixture was subjected to a gradual increase in temperature between 15.0 - 70.0 °C with a 5.0 °C increment.

Analyzed PVP-VA sample contains: 2 mL of 10 mM HEPES-150 mM NaCl mixture, 22 µL PPE-CO$_2$-7 (450 µg/mL), and different volumes of PVP-VA (5 mg/mL).

Analyzed PVP-PS sample contains: 2 mL of 10 mM HEPES-150 mM NaCl mixture, 22 µL PPE-CO$_2$-7 (450 µg/mL), and 10 µL PVP-PS (3.95 mg/mL) yielding a final concentration [PVP-PS] $_{final}$ in cuvette = 19.45 µg/mL.

2.1.3.5 Reversibility and Cycling:

To check for the reversibility of our proposed system, the PPE- CO_2-7/polymer mixture was cycled 10 times between 20.0 and 70.0 °C.

Analyzed PVP-VA sample contains: 2 mL of 10 mM HEPES-150 mM NaCl mixture, 22 µL PPE-CO_2-7 (450 µg/mL), and 2.5 µL of PVP-VA (5 mg/mL).

Analyzed PVP-PS sample contains: 2 mL of 10 mM HEPES-150 mM NaCl mixture, 22 µL PPE-CO_2-7 (450 µg/mL), and 10 µL PVP-PS (3.95 mg/mL).

2.2 Localized Catalysis Driven by the Induction Heating of Magnetic Nanoparticles

2.2.1 Materials:

The following materials have been used for our catalysis project: Resazurin sodium salt, $C_{12}H_6NNaO_4$, powder, Bio-Reagent, suitable for cell culture (Aldrich); Gold (III) chloride trihydrate, $HAuCl_4.3H_2O$ (Aldrich); Iron (II) chloride tetrahydrate, $FeCl_2.4H_2O$, puriss. p.a., ≥99.0 % (Aldrich); Iron (III) chloride hexahydrate, $FeCl_3.6H_2O$, reagent grade, ≥98 %, chunks (Aldrich); Poly (Diallyl dimethylammonium chloride) (PDDA), $(C_8H_{16}ClN)_n$, solution average Mw 100,000-200,000 (low molecular weight), 20 wt. % in H_2O (Aldrich); Trisodium citrate dihydrate, ≥99 %, FG (Aldrich); Sodium Hydroxide, NaOH, puriss., meets analytical specification, 98-100.5%, pellets (Aldrich); Hydroxylamine hydrochloride, ClH_4NO, 97% (Acros); Ammonium hydroxide, NH_4OH, ACS reagent, 28-30% solution in water (Acros); Difco LB agar lennox was obtained from BD Diagnostic; and Deionized water (18 $\mu\Omega$, Nanopure Diamond, CRSL, AUB) for solution preparations and dilutions.

2.2.2   *Methods:*

2.2.2.1   Absorption Spectra:

Absorption spectra were measured using Jasco, V-570 UV/VIS/NIR Spectrophotometer in a double beam mode. All solutions were placed in a 1 cm x 1 cm quartz cuvettes while keeping the total volume constant and equal to 2 mL. Before each measurement, the solution was allowed to homogenize and stabilize for 2-3 mins.

2.2.2.2   Dynamic Light Scattering (DLS):

The size of the synthesized particles was calculated using the NanoPlus HD software of the DLS machine.

 Samples were diluted then suspended in cuvettes containing 2 mL deionized water.

2.2.2.3   Steady State Fluorescent Spectroscopy:

Resazurin is a weak fluorescent blue dye that is widely used in applications.[71] Upon heating and in the presence of AuNP as a catalyst and the reducing agent hydroxylamine (NH$_2$OH), resazurin is reduced into resorufin, a strong fluorescence molecule. In this paper, the reduction of resazurin was done in a 2 mL-tube containing a mixture of 48.7 mg/mL MNPs/ 0.7 mg/mL AuNP, and 2mM resazurin. Fluorescence intensity of resorufin was obtained by first diluting the reaction mixture in a 0.5 mM NaOH. All solutions were placed in a 1 cm x 1 cm quartz cuvettes. Before each measurement, the solution was allowed to homogenize and stabilize for 2-3 mins. Steady-state fluorescent spectroscopy was acquired by exciting at 532 nm using a Thermo Scientific Lumina spectrophotometer while collecting the emissions between 545 nm and 700 nm.

2.2.2.4   Thermal Heating of Magnetic Nanoparticles- MagneTherm:

MagneTherm was used to generate an alternating magnetic field using a built-in-coil NAN201003 at a 109.6 KHz. The increase in temperature was tracked using the OAKTON WD-08516-83 FEP thermocouple, dipped in the solution and connected to a data-logger. Initially, the voltage was increased to its maximum value that is equal to 32 V. Once the solution temperature reached 45°C, the voltage was adjusted manually and monitored down to approximately 10 V to keep the solution thermally constant.

2.2.2.5   Temperature Tracking:

To ensure comparable experimental conditions and maintain a stable temperature, the thermal variations were measured and tracked via a thermocouple dipped inside the solution tube and connected to a data logger machine. Adjustments were manually introduced, when needed, to maintain a constant value.

2.2.2.6   Microscopy Imaging:

A 5% agar gel sample was prepared and molded onto a microscopic slide and then left to solidify. Using a 0.3 mm-thin insulin needle, few microliters of resazurin were injected into the gel. MNPs solution was poured on the gel's surface for a few minutes to allow the magnetic nanoparticles to fill the cracks created by the needle. The solution was wiped away, and the slide is imaged with an upright fluorescence microscope Leica DM6 B. We then poured a solution of MNPs/AuNPs mixed with NH_2OH on the top of the gel again and left it in an alternating magnetic field. After two hours of heating in the MagneTherm, the gel surface was wiped and imaged for the second time under the same experimental conditions (5x objective and 1.5s exposure). Fluorescence intensities were

quantified using the ImageJ software. For resazurin, a 541-551 nm excitation filter was used, and the emission was collected between 565 and 605 nm.

CHAPTER 3

FLUORESCENT THERMAL SENSING USING CONJUGATED

POLYELECTROLYTES IN THIN POLYMER FILMS

Thermal sensing in thin polymer films has been a significant drawback towards optimizing the heat dissipation in micro- and nano-electronic devices as well as many other thin film-based technologies. To account for the limitations of current nano-thermometry, presented in the previous chapter, we report in this project the development of a fluorescent-based conjugated polyelectrolyte, capable of detecting thermal fluctuations, in thin polymer films prepared from polyvinylpyrrolidone-co-vinyl acetate. The sensor was first optimized in solution by testing two polyvinylpyrrolidone (PVP) copolymers (co-vinyl acetate (VA) and co-polystyrene (PS)) before it was applied on thin films through spun casting the solution onto quartz slides and imaging at different temperatures. Our goal was to achieve a high thermal sensitivity inside the thin polymer films.

3.1 Introduction:

In recent years, many fluorescent based thermal sensors were developed to probe temperature fluctuations in solution and for sub-cellular applications.[10, 72, 73] However, very few reports have focused on measuring thermal variations in thin polymer films despite their use in many processed micro-electronics and -materials such as micro-electro mechanical systems (MEMS) where thermal fluctuations play a pivotal role in their operation. Thermal sensitive thin-films are not only useful to measure temperature variations produced within those films but certainly to map heat generated in other solid substrates and at the interface between solids and liquids. Examples for such applications include but not limited to, microfluidic devices, microheaters, and microwell arrays where many chemical, physical and biological processes are currently being explored without accurately controlling the heat generated at the microscale.[74] Also, calorimetric micro-biosensors, where thermal fluctuations are correlated to the concentration of the analyte, is another field where thin-polymer thermal sensitive materials are of great interest.[75] It would facilitate the micromachining of such devices making it rapid, and inexpensive.

Heat dissipation in solid material arises from either electron in metals or lattice vibrations or phonons in insulators and semiconductors are making it difficult to probe using traditional contact-based methods.[76] The most popular approach has been to correlate metal resistance to temperature measurements.[77, 78] For instance, Mclennan *et al.* have developed thin film thermistor consisting of tin-selenide sensing material.[79] Similarly, Urban *et al.* used a thin film of amorphous germanium which yielded a high-temperature sensitivity (2% per degree) and a fast response time of 3 ms.[80] Gold thin films have also

been used to measure the in-situ temperature of the polymer electrolyte in fuel cells.[81] Recently, the Seebeck coefficient of V_2O_5 films was used to obtain highly sensitive and transparent temperature sensors.[82]

While thin metal films have been successful, they have been, however, relatively limited, especially in measuring the spatial thermal fluctuations accurately. Fluorescent-based techniques have advanced in recent years allowing measurements with high resolution down to few nm.[83-85] Motivated by this advancement, few examples of fluorescent-based thin films have been reported recently.[86-88] Aizawa *et al.* reported an effective sensor in thin films by measuring the fluorescence lifetime of Cr doped Al_2O_3.[89] In another example, a silica sol-gel matrix was embedded with the temperature sensitive probe rhodamine B and used to measure the surface temperature of MEMS micro-hotplates.[88]

As such, there was a pressing need for new thermometers capable of measuring the thermal fluctuations in thin films. Conjugated polyelectrolyes, and PPE-CO2 in particular, appeared as a considerable candidate due to its relative properties discussed in chapter 1.

Despite their exceptional characteristics, PPE-CO2-7 (Figure 3.1), like other CPEs, still suffer from some limitations such as low photostability, photodegradation, blinking, and fast irreversible photobleaching. This, therefore, restricted their development and implementation into sensing applications and devices where the above drawbacks are essential requirements.[90]
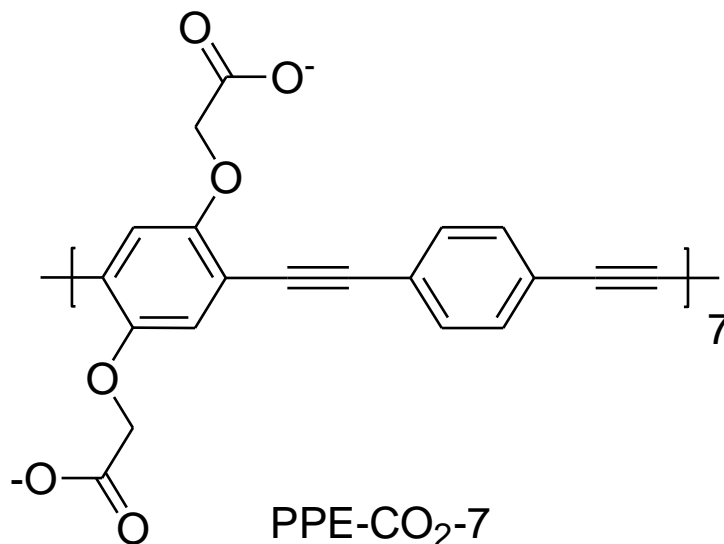
Figure 3.1: Schematic representation of the chemical structure referring to the short anionic conjugated polyelectrolyte poly (phenylene ethynylene) carboxylate with 7 repeating monomer-units (PPE-CO$_2$-7).

One suggested approach to prevail over this, while enhancing the PPE-CO$_2$-7 functionality and photostability, is to complex it with another polymer of desired properties. For instance, polyvinylpyrrolidone (PVP) is an amphiphilic polymer that, when used as a scaffold for the CPE, was found to extend the latter's backbone and prevent photodegradation. This polymer also led to a 23-fold increase in the quantum efficiency of the complexed CPE. Below is a detailed explanation on how PVP has enhanced our CPE-based thermal sensors, and how we'll implement them in our thin polymer film application.

Our laboratory has previously reported on the thermal sensitivity of short conjugated polyelectrolytes (CPEs), specifically poly-(phenylene ethynylene) (PPE-CO$_2$-7) when complexed to an amphiphilic polymer, polyvinylpyrrolidone (PVP).[41] The probe showed excellent sensitivity between 10 °C and 90 °C and a high relative sensitivity of 2.7% at 35 °C. A suggested speculation is that in the presence of PVP, the PPE-CO$_2$-7

aggregates are destabilized and the change in the solution temperature disaggregates the CPE chains in the excited state.[91] As a result, the emission spectra shifted between 520 nm and a brighter peak at 450 nm. The nanothermometer ratiometric signal was reversible with fast response time. The probe also showed an excellent thermal response in hydrogel materials specifically agarose and agar resulting in a respective maximum relative sensitivity of 2.0% and 1.9% at 45.0 °C.[92]

Building on this, we thought of expanding our probe through introducing two PVP derivatives of distinct and desired properties: poly(vinylpyrrolidone)-co-vinyl acetate (PVP-VA) and polyvinylpyrrolidone polystyrene (PVP-PS) (Figure 3.2). Some of the reasons behind choosing these two polymers are because (1) they both are copolymers of PVP which is apparently an important factor for the thermal response of PPE-CO_2 and (2) both could be prepared into thin films by a simple spin-coating technique.[85] Particularly, PVP-VA is known for its high binding affinity and film formation on both hydrophobic and hydrophilic surfaces. PVP-VA is also a good insulator which would be excellent for thermal sensing application in electronic devices.[86]
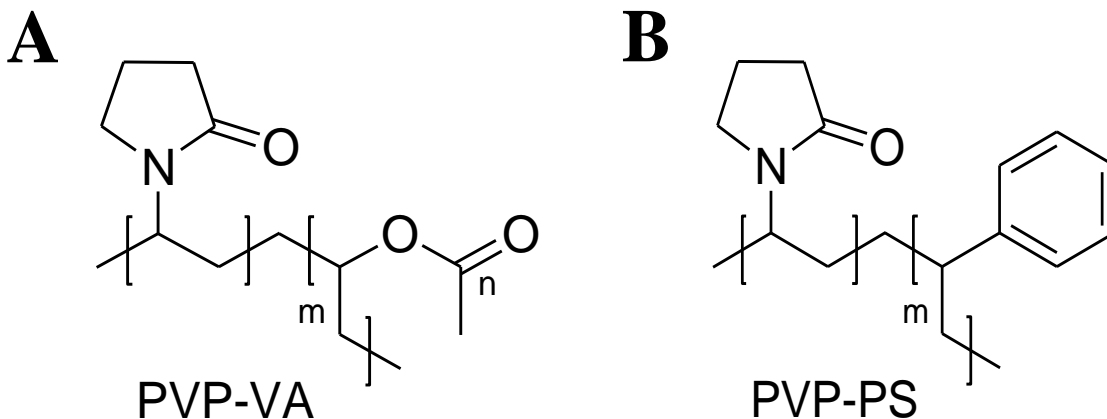
A PVP-VA

B PVP-PS

Figure 3.2: Schematic and chemical structure of the amphiphilic polymers (A) poly(vinylpyrrolidone)-co-vinyl acetate (PVP-VA) and (B) polyvinylpyrrolidone polystyrene (PVP-PS)

Herein, we report in this chapter on the optimization of poly (phenylene ethynylene) fluorescent-based conjugated polyelectrolyte in solution via its complexation with two polyvinylpyrrolidone (PVP) copolymers (co-vinyl acetate (VA) and co-polystyrene (PS)). Following our foremost goal, the thermal sensitive PPE-CO$_2$-7 is then implemented and tested in polymer films prepared from polyvinylpyrrolidone-co-vinyl acetate.

3.3 Results and Discussion:

In general, the photophysical behavior of conjugated polyelectrolytes is highly dependent on the polymer micro-environment. Specifically, we have shown that PPE-CO_2-7 thermal response depends on the pH, the buffer solution, and the polymer molecular weight and concentration to which it has been complexed; increasing the PVP concentration and its molecular weight, improved the thermal sensitivity of the CPE complex. [41, 91, 92]

In this study we picked two PVP co-polymers that could be easily prepared into thin films by a simple spin casting procedure. The first one, PVP-co-polystyrene, has a hydrophobic character which we assumed might favor a destabilized PPE-CO_2-7 structure. While the second polymer, PVP-co-vinyl acetate which has a slightly more hydrophilic character. In addition, both have other favorable properties that make them excellent materials for coating untreated metal and glass surfaces. [93, 94]

3.3.1 Absorbance Spectra:

We initiated our study by exploring the spectroscopic properties of PPE-CO$_2$-7 in solution in the presence of the two copolymers. When PPE-CO$_2$-7 was mixed with either PVP-VA or PVP-PS, a slight red shift in the absorbance was observed (Figure 3.3). This might indicate an extension in the CPE conjugation upon favorable complexation with the copolymers. The addition of PVP-PS particle lead to the appearance of a scattering tail which was also apparent when fluorescent measurements were later acquired.
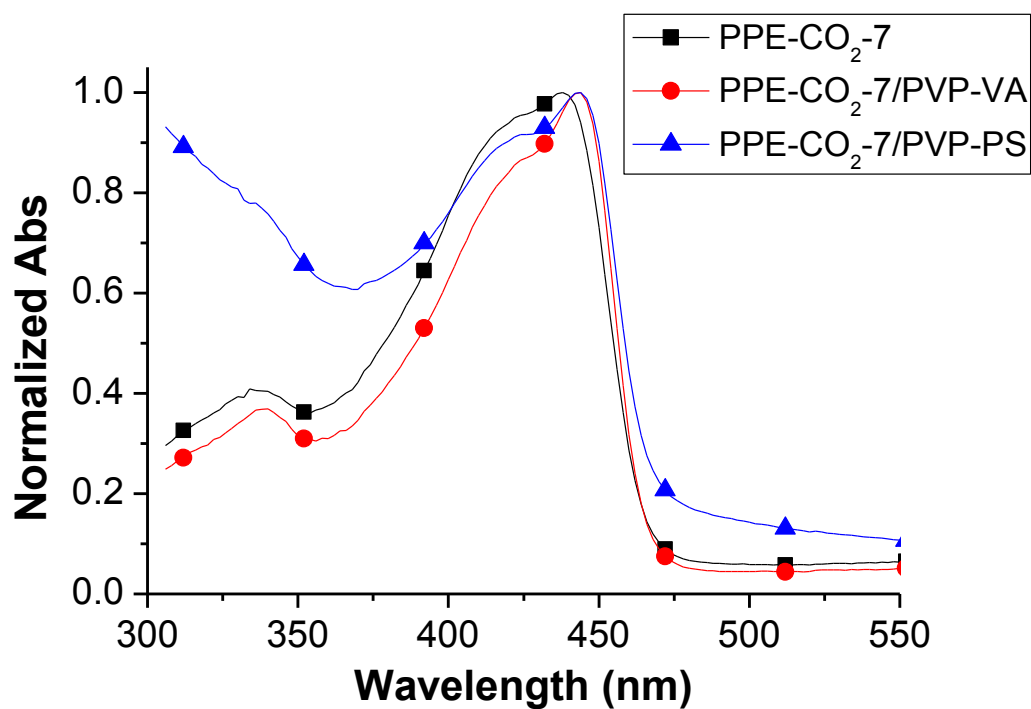
Figure 3.3: Absorbance spectra of PPE-CO$_2$-7 (■), PPE-CO$_2$-7/PVP-VA (●) and PPE-CO$_2$-7/PVP-PS (▲). Data are obtained in the form of continuous spectra,yet symbols are added for visual aid only.

3.3.2   *Excitation Spectra of PPE-CO$_2$-7 with PVP-VA:*

The excitation spectrum was acquired for the PPE-CO$_2$-7/PVP-VA over an excitation range 350 and 510 nm while collecting the emission at 530 nm (Figure 3.4). The obtained spectrum followed the same trend as the emission one, reported later in this chapter. Moreover, this spectrum was consistent with the absorbance obtained in figure 3.3 in terms of the peaks and general structure of the curves.
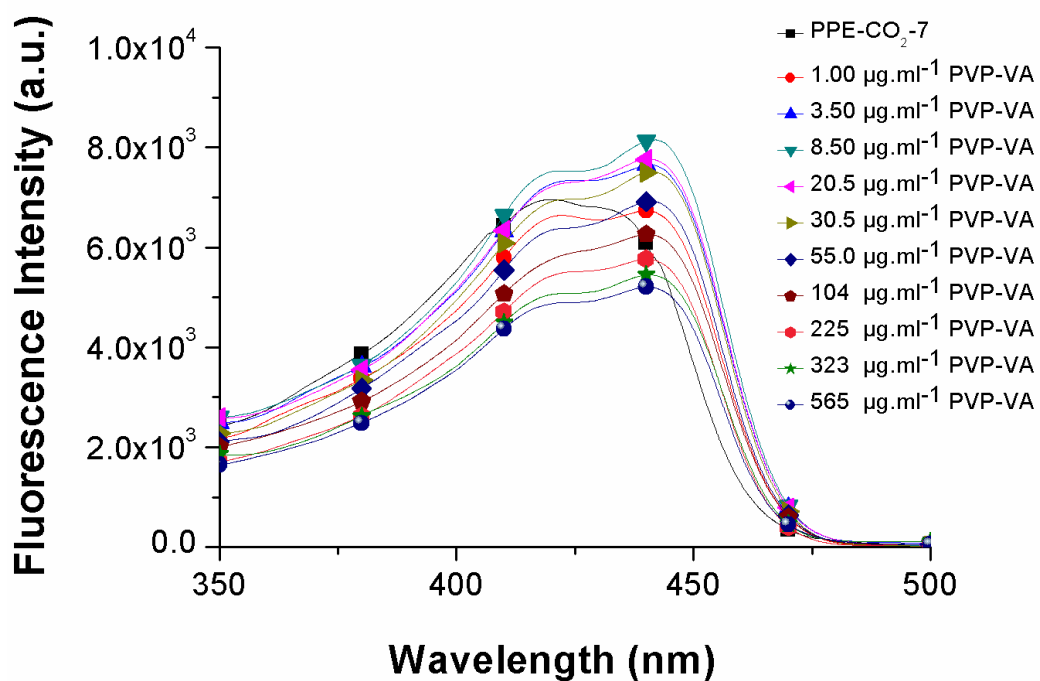
Figure 3.4: Excitation spectra of PPE-CO$_2$-7 (5 µg/mL) upon addition of incremental amounts of PVP-VA acquired at 20.0 ℃ in 10 mM HEPES and 150 mM NaCl. Spectra were collected at 520 nm. Data are obtained in the form of continuous spectra,yet symbols are added for visual aid only.

3.3.3 *Titrations:*

We then aimed to identify the concentration at which the copolymers would destabilize the PPE-CO$_2$-7 aggregates at room temperature by looking for a new emission peak at 450 nm. As such, when the complex is heated and the CPE chains are fully disaggregated, an increase in the emission at 450 nm is expected. To a solution of PPE-CO$_2$-7, an incremental amount of PVP-VA or PVP-PS was added at a constant temperature of 20 °C and continuously excited at 420 nm.

The addition of PVP-VA lead to a blue shift in the fluorescent emission with a small increase in intensity (Figure 3.5A). With the increase in the copolymer concentration, the non-aggregated emission peak at 450 nm became more apparent concomitant with the decrease in the aggregated intensity at 550 nm.

This behavior was similar to what we have previously observed and reported for PVP polymers when added to PPE-CO$_2$-7. PVP-PS addition did induce a blue shift in the fluorescent signal however a decrease in the signal was observed with the increase in the added polymer concentration (Figure 3.5B).

We speculate that this might be due to the scattering of the PVP-PS suspension. To assess the thermal sensitivity of the PPE-CO$_2$-7/copolymers, we picked the concentration at which the emission of the CPE is blue shifted, and the 450 nm peak is barely apparent; that corresponded to 6.17 µg/mL and 19.45 µg/mL for PVP-VA and PVP-PS respectively.

A

Legend:
- PPE-CO$_2$
- 1.0 µg.ml^{-1} PVP-VA
- 3.5 µg.ml^{-1} PVP-VA
- 8.5 µg.ml^{-1} PVP-VA
- 20.5 µg.ml^{-1} PVP-VA
- 30.5 µg.ml^{-1} PVP-VA

B

Legend:
- PPE-CO$_2$-7
- 0.005 mg.ml^{-1} PVP-PS
- 0.015 mg.ml^{-1} PVP-PS
- 0.035 mg.ml^{-1} PVP-PS
- 0.080 mg.ml^{-1} PVP-PS
- 0.120 mg.ml^{-1} PVP-PS
- 0.220 mg.ml^{-1} PVP-PS
- 0.410 mg.ml^{-1} PVP-PS
- 0.890 mg.ml^{-1} PVP-PS
- 1.280 mg.ml^{-1} PVP-PS
- 2.230 mg.ml^{-1} PVP-PS

44
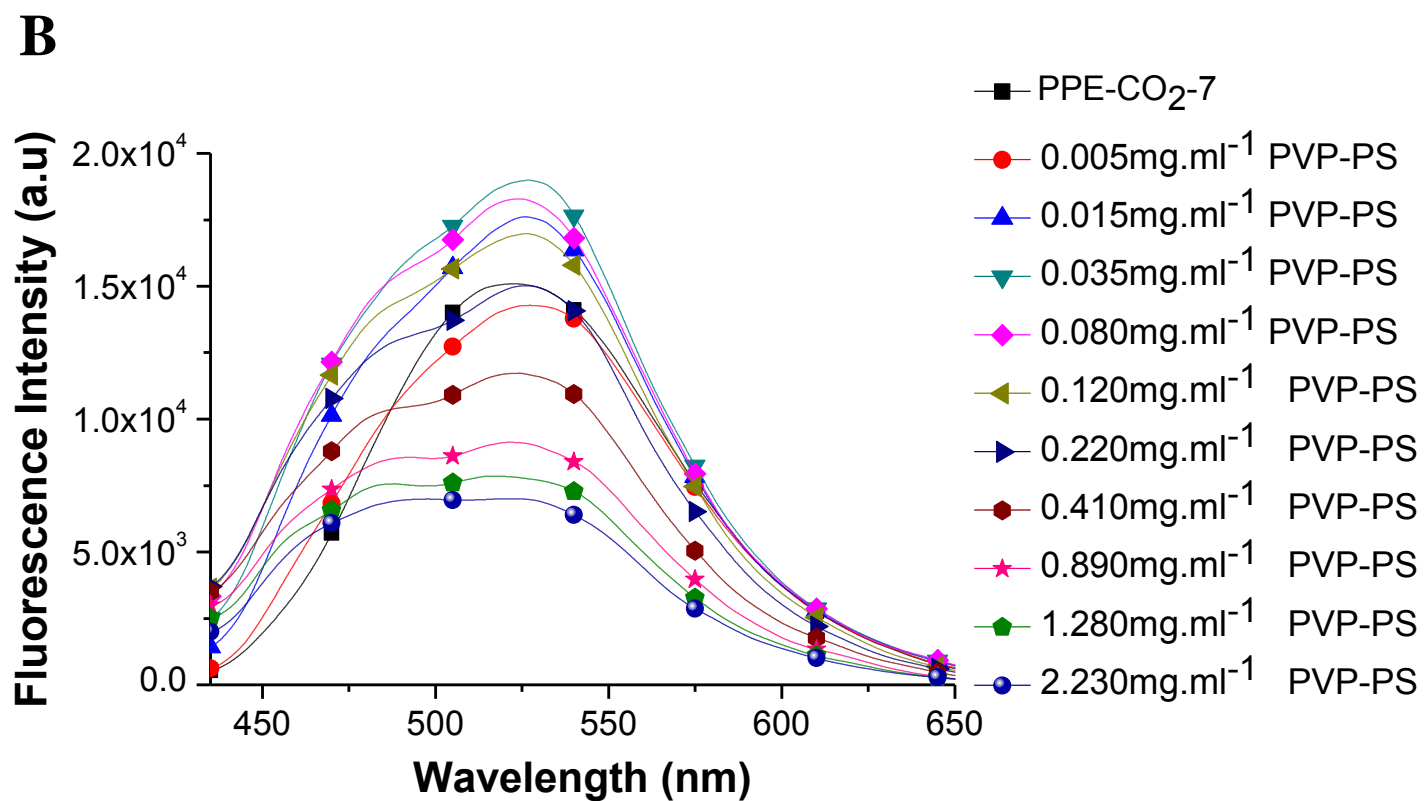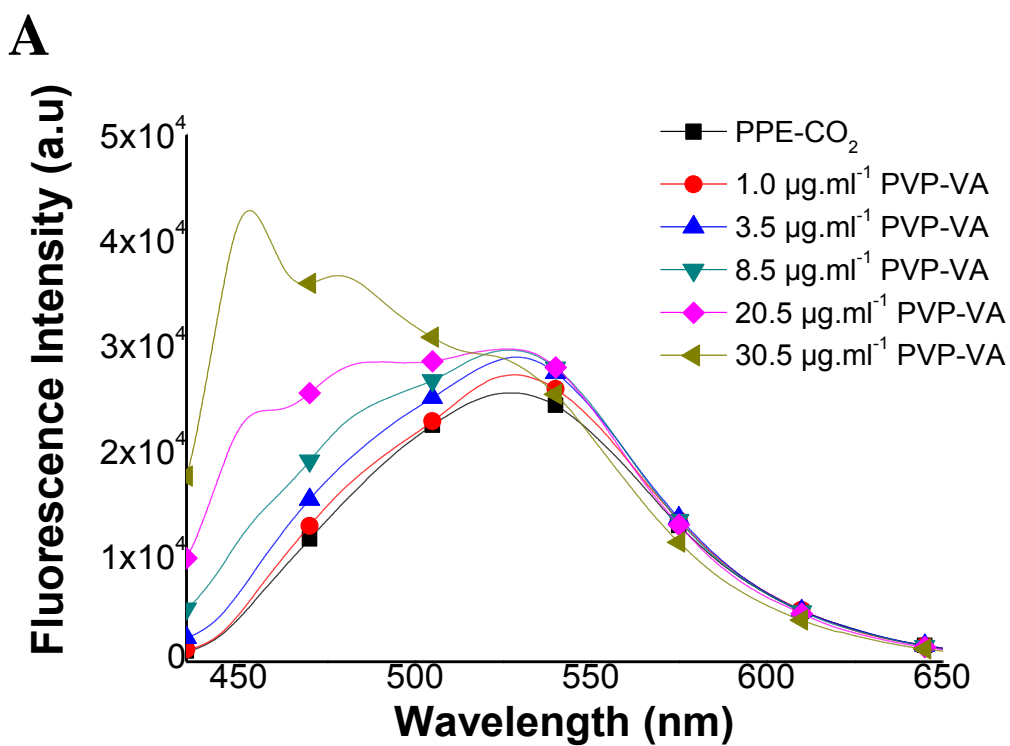
Figure 3.5: Fluorescent Emission Spectra of PPE-CO_2-7 (5 µg/mL) upon addition of incremental amounts of (A) PVP-VA and (B) PVP-PS acquired at 20.0 ℃ in 10 mM HEPES and 150 mM NaCl when excited at 420 nm. Data are obtained in the form of continuous spectra, yet symbols are added for visual aid only.

3.3.4   Thermal Sensing:

Using the polymer's critical concentration obtained above, the thermal sensitivity for the mixture PPE-CO_2/PVP copolymers was therefore assessed by subjecting the PPE-CO_2-7/PVP-VA or PPE-CO_2-7/PVP-PS to an incremental temperature increase between 15 °C and 70 °C at 5 °C steps and tracking the emission shift from the green to the blue emission region. The emission spectra were recorded after 5 minutes of stabilization.

For PVP-VA, a clear shift in the fluorescent emission was recorded from the destabilized state to the single chain peak at 450 nm with the increase in temperature (Figure 3.7A). PVP-PS, on the other hand, did not show a clear shift nor an increase at the 450 nm peak (Figure 3.9A). This trial was done in triplicates, the individual measurements of PVP-VA and PVP-PS were reported independently in figures 3.8 and 3.10, respectively.

To evaluate the probe's thermal sensitivity, the ratiometric signal was calculated by first integrating the intensity between 435 nm and 500 nm (I_{Blue}) and from 500 nm to 650 nm (I_{Green}) and then plotting the ratio $Q = \dfrac{I_{Blue}}{I_{Greem}}$ versus the temperature changes. The reported graphs correspond to the average of the integrated ratios of the three independent measurements. (Figure 3.7B and 3.9B).

For the thermal sensing of PPE-CO_2/PVP-VA, the spectra were first acquired at three different concentrations lying within the range of the critical concentration obtained above (Figure 3.6).
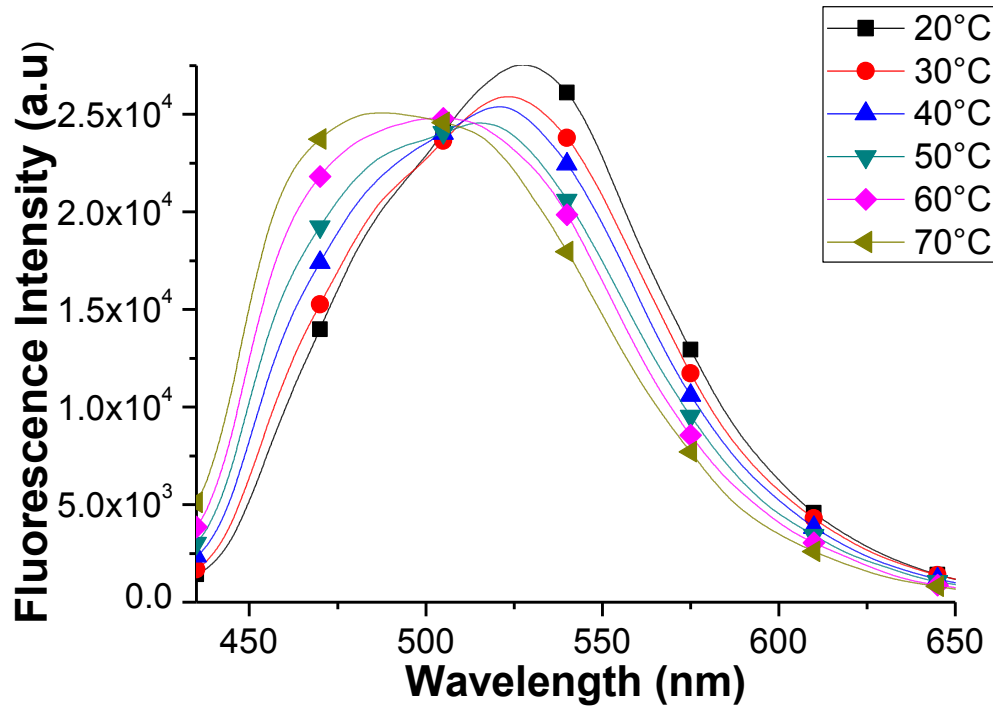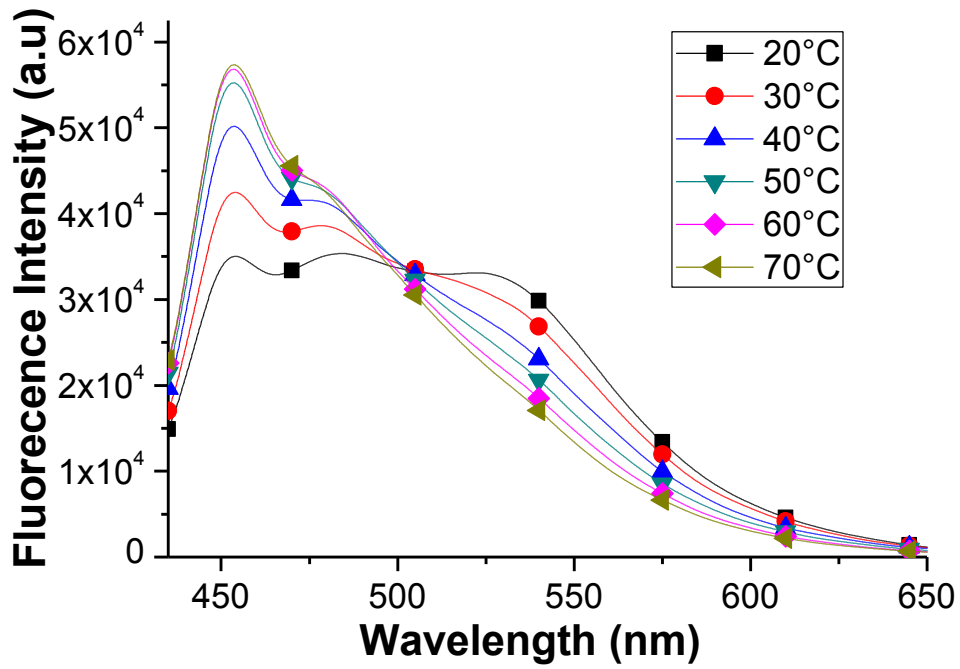
C
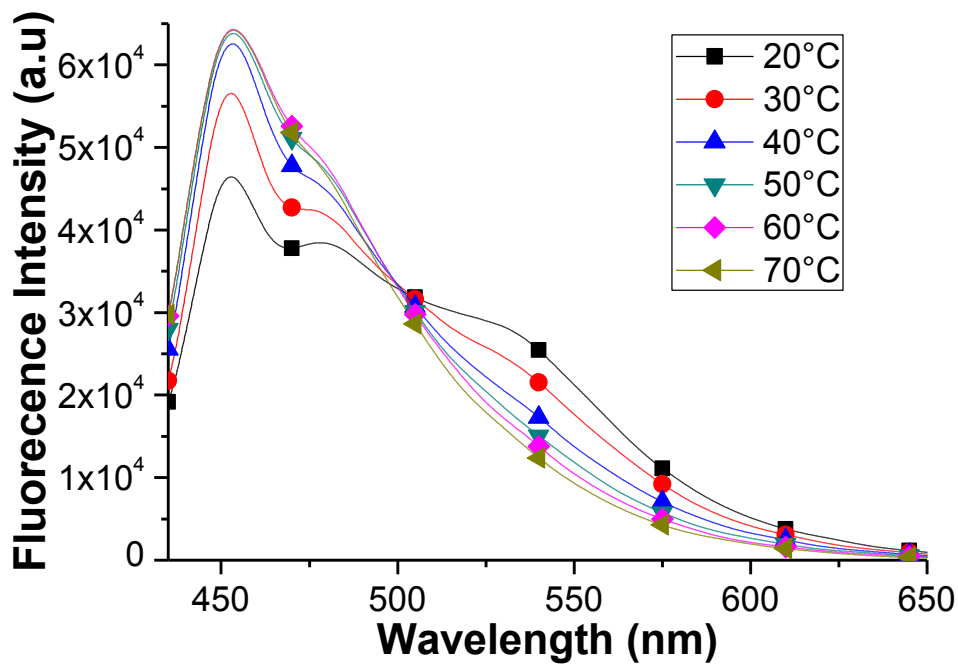
Figure 3.6: Thermal response of PPE-CO$_2$ (5 µg/mL) in complexation with (A) 2.47 5µg/mL, (B) 12.33 5µg/mL, and (C) 24.6 5µg/mL PVP-VA, prepared in 10 mM HEPES with 150 mM NaCl (pH=7.3) buffer solution, upon exciting at 420 nm acquired between 20.0 ℃ and 70.0 ℃, with 10 ℃ increment. Data are obtained in the form of continuous spectra, yet symbols are added for visual aid only.
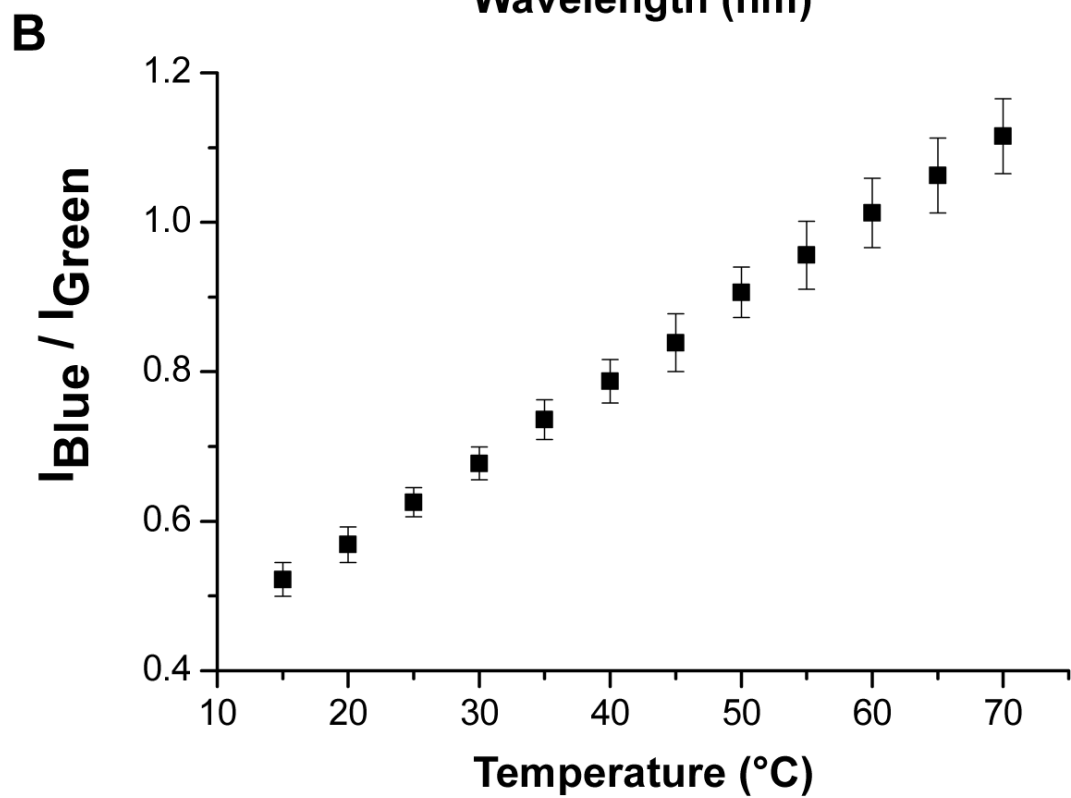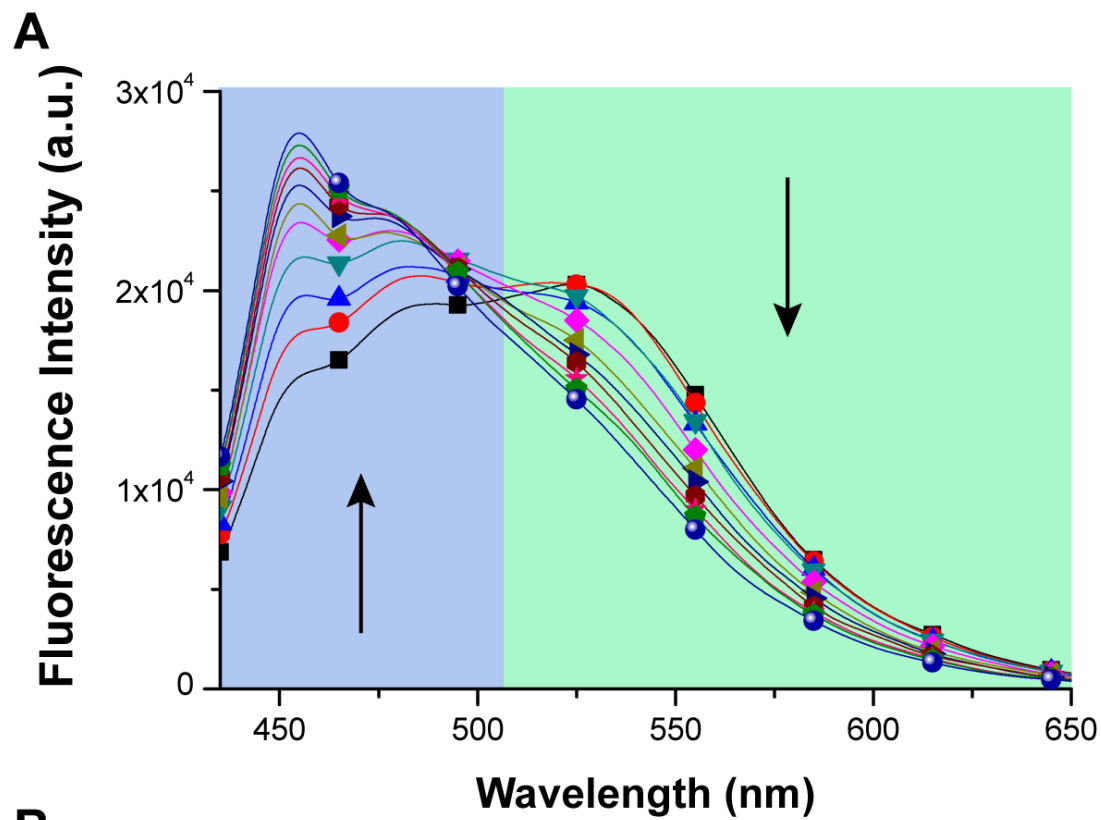
Figure 3.7: (A) Thermal response of PPE-CO_2-7 (5 µg/mL) in complexation with PVP-VA (6.17 µg/mL) prepared in 10mM HEPES with 150 mM NaCl (pH=7.3) buffer solution, upon exciting at 420nm acquired between 15.0°C and 70.0°C, with 5°C increment. (B) Average Integrated Fluorescent ratio, Q, of the blue region before (I_{blue}), to the green region (I_{green}) after the iso-emission point at 500 nm versus the temperature acquired between 20.0°C and 70.0°C - 5.0°C increment three independent thermal measurements. The individual measurements are shown in figure 3.8. Data are obtained in the form of continuous spectra, yet symbols are added for visual aid only.
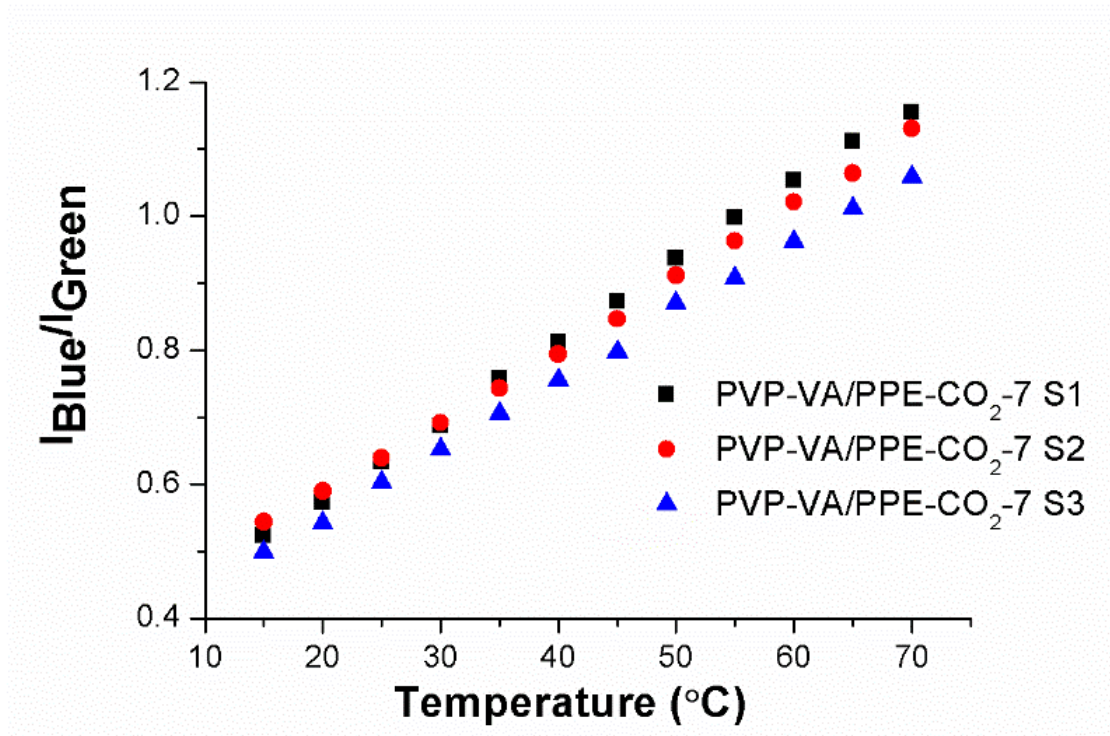
Figure 3.8: Thermal response of three individual PPE-CO_2/PVP-VA measurements. Reported is the fluorescent ratio, Q, of the blue region before (I_{blue}), to the green region (I_{green}) after the iso-emission point at 500 nm versus the temperature acquired between 15.0°C and 70.0°C - 5.0°C increment. Data are obtained in the form of continuous spectra, yet symbols are added for visual aid only.
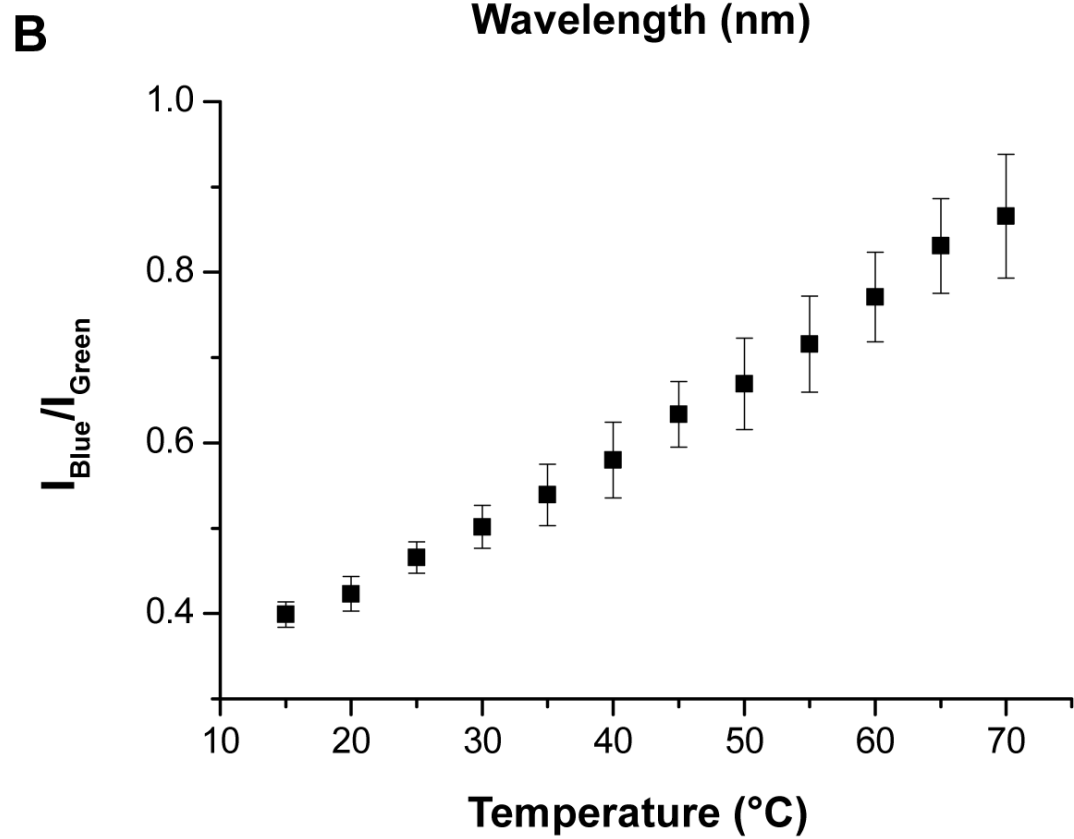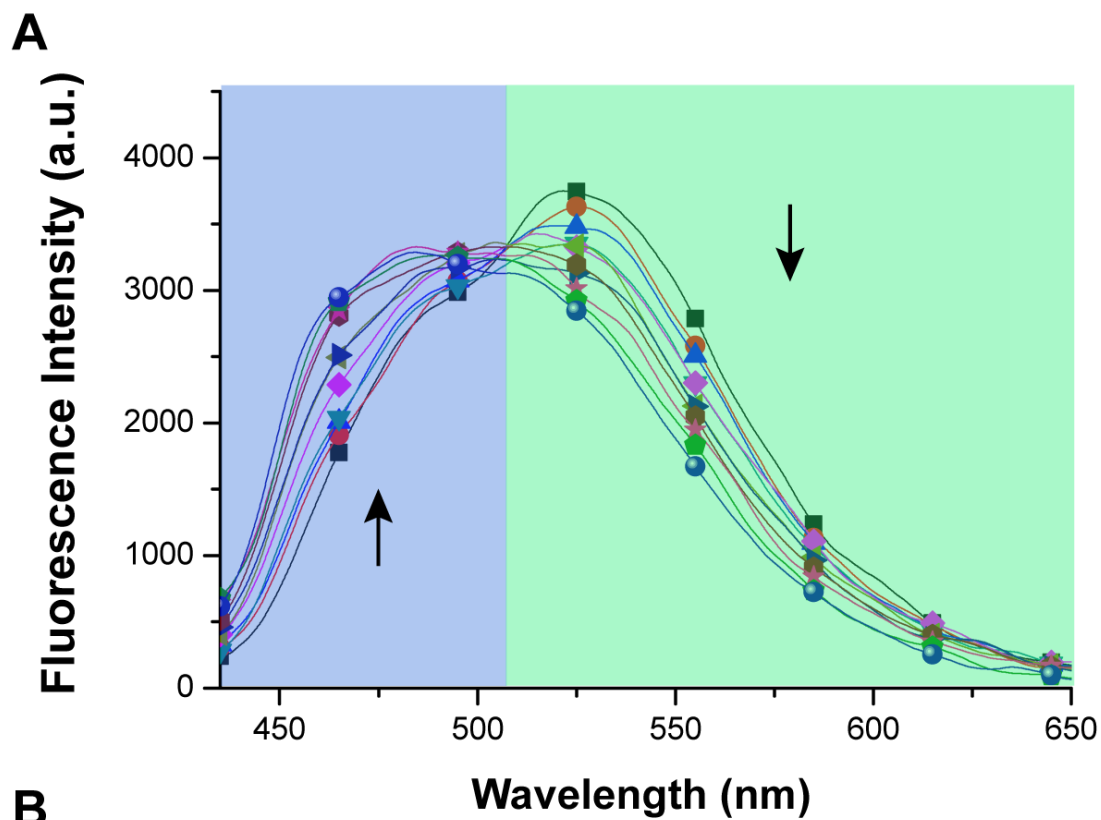
Figure 3.9 (A) Thermal response of PPE-CO_2 (5 µg/mL) in complexation with PVP-PS (19.45µg/mL) prepared in 10mM HEPES with 150 mM NaCl (pH=7.3) buffer solution, upon exciting at 420nm acquired between $15.0°C$ and $70.0°C, with$ 5°C increment. (B) Average Integrated Fluorescent ratio, Q, of the blue region before (I_{blue}), to the green region (I_{green}) after the iso-emission point at 500 nm versus the temperature acquired between $20.0°C$ and $70.0°C$ - $5.0°C$ increment three independent thermal measurements. The individual measurements are shown in figure 3.10. Data are obtained in the form of continuous spectra, yet symbols are added for visual aid only.
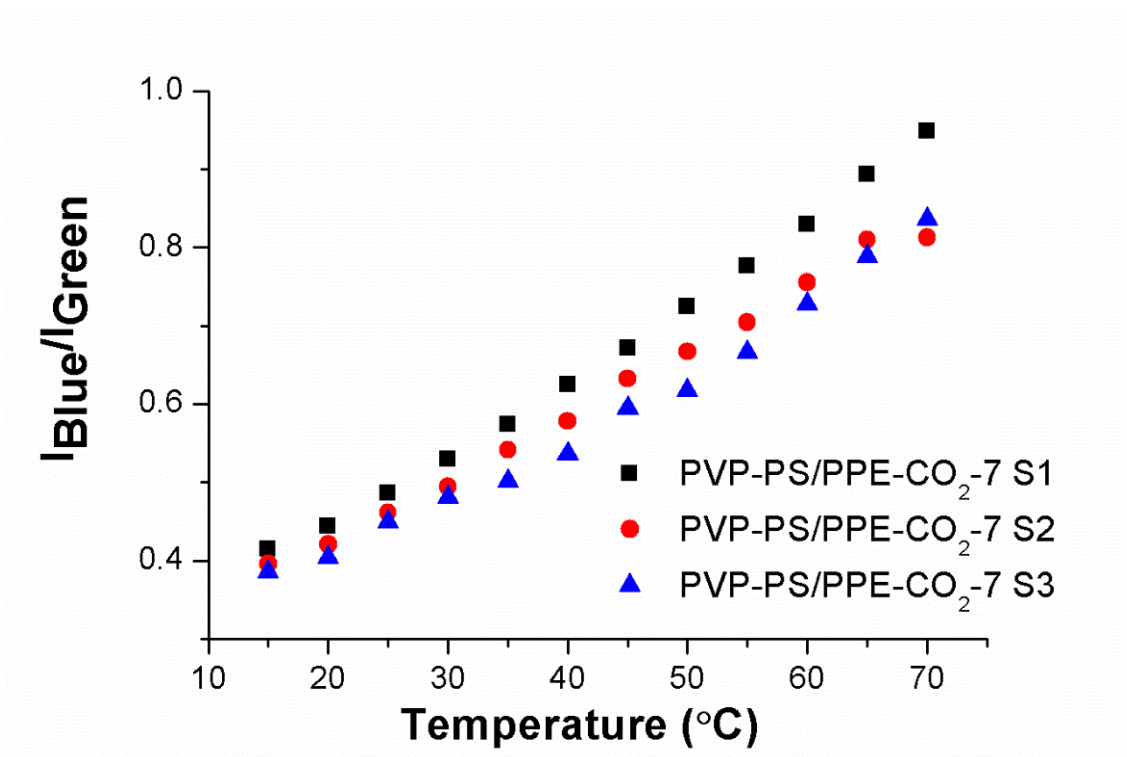
Figure 3.10: Thermal response of three individual PPE-CO_2/PVP-PS measurements. Reported is the fluorescent ratio, Q, of the blue region before (I_{blue}), to the green region (I_{green}) after the iso-emission point at 500 nm versus the temperature acquired between 15.0°C and 70.0°C - 5.0°C increment. Data are obtained in the form of continuous spectra, yet symbols are added for visual aid only.

3.3.5   *Relative Sensitivity*:

The relative thermal sensitivities were then calculated using the below function:

$$\left(\%S = \frac{\frac{dQ}{\partial T}}{Q} \times 100 \right)$$

The respectively calculated sensitivities for PVP-VA and PVP-PS were 2.35% and 1.455% (Figures 3.11 and 3.12). The PVP-VA sensitivity is comparable to our reported value for PVP alone in solution which was equal to 2.7% while that of PVP-PS is relatively low. The considerably lower sensitivity and the observed intensity reduction for PVP-PS led us to focus only on the PVP-VA.
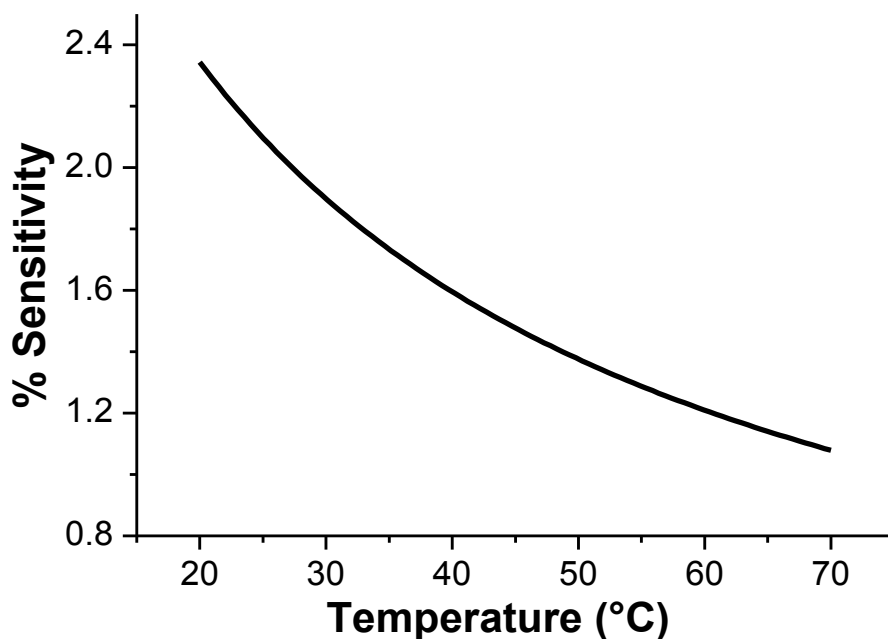
Figure 3.11: The relative sensitivity (% S) calculated from the thermal response ratio I_{blue}/I_{green} of PPE-CO$_2$-7/PVP-VA
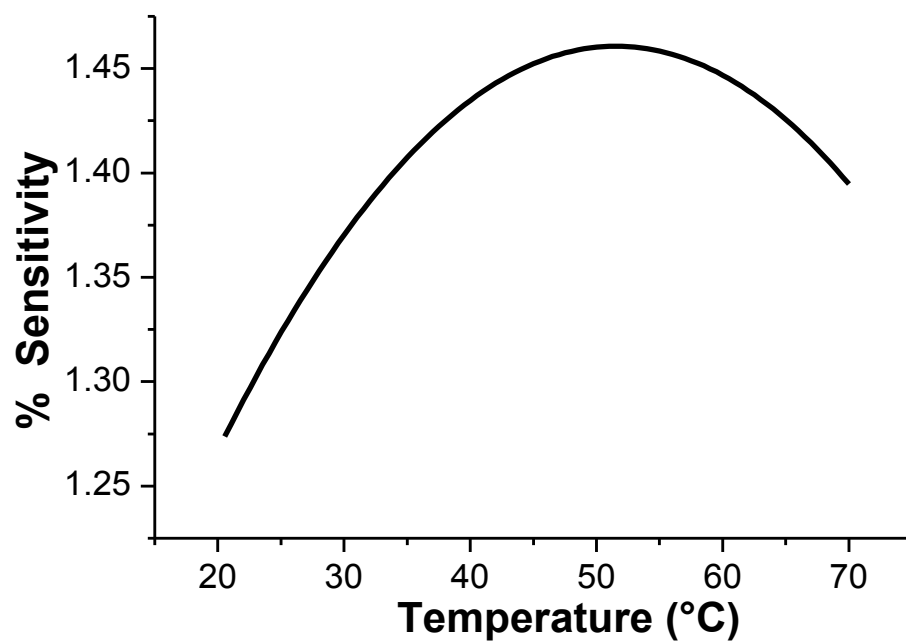
Figure 3.12: The relative sensitivity (% S) calculated from the thermal response ratio I_{blue}/I_{green} of PPE-CO$_2$-7/PVP-PS.

3.3.6   *Reversibility and Cycling*:

An important parameter to check for when using polymeric material in thermal sensing is reversibility. Polymers, in general, tend to form hysteresis as they cycle between relaxed configuration at high temperatures and a collapsed state at lower temperatures. This can lead to irreversibility in the reported fluorescent signal with the change in the CPE microenvironment. A solution of PPE-CO$_2$-7/PVP-VA was cycled multiple times between 20 °C and 70 °C and then the ratio I_{blue}/I_{green} was calculated and plotted (Figure 3.13). Over the 10 cycles, the thermal probe response was reversible with no observed hysteresis and a small signal deviation of 2.5 % reflecting its stability over the 3-4 hours experimental window. PVP-PS have shown similar results (Figure 3.14).
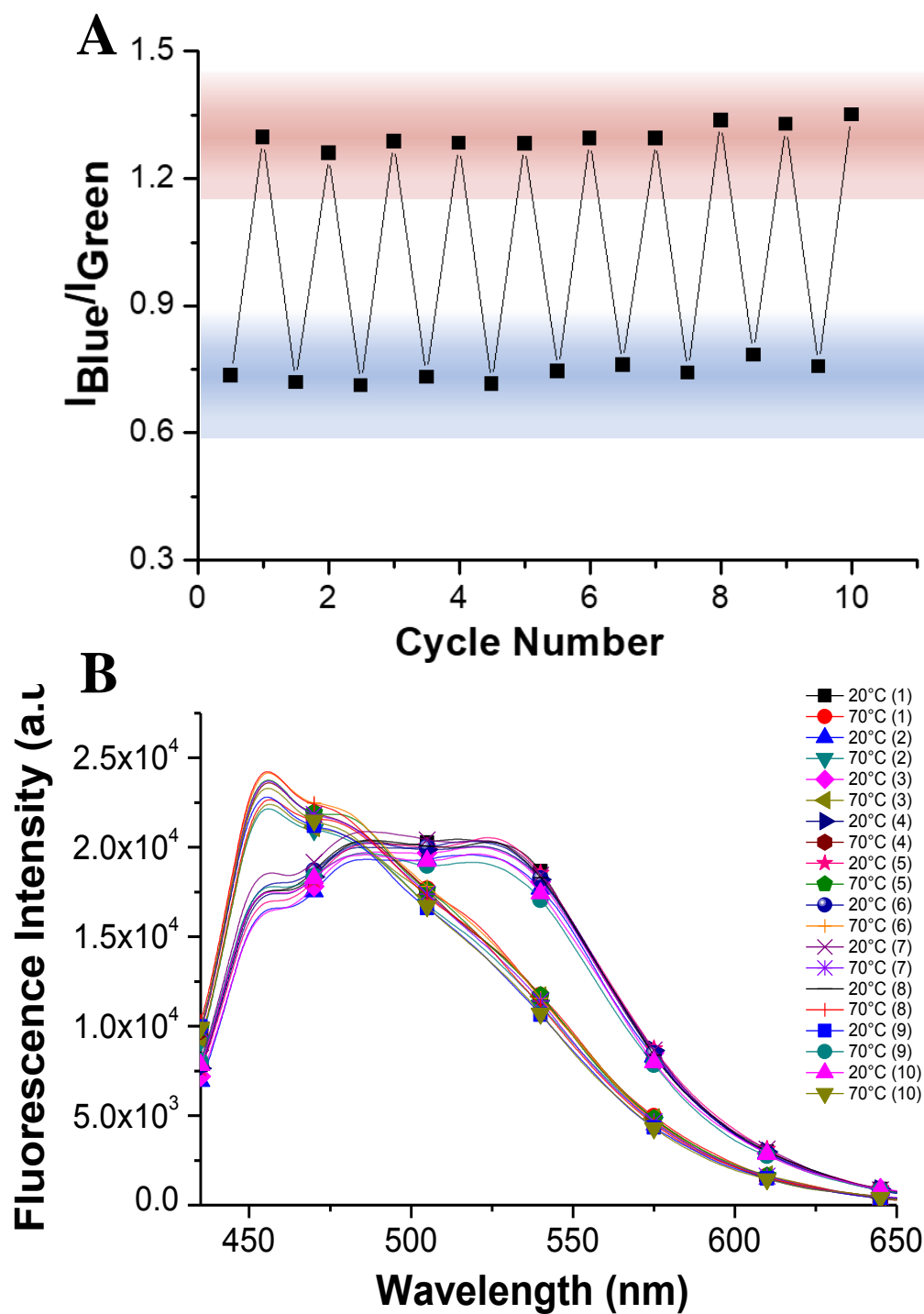
Figure 3.13: (A) Cycling PPE-CO$_2$-7 (5 µg/mL)/PVP-VA (6.17 µg/mL) between 20.0 °C (blue shade/Bottom) and 70.0 °C (red shade/Top). Lines connecting the experimental points are for visual aid only. (B) Respective emission spectra of PPE-CO$_2$ -7 /PVP-VA cycle between 20.0 ℃ and 70.0 ℃ when excited at 420 nm The experiment was performed in 10 mM HEPES in 150 mM NaCl (pH=7.3) buffer solution. The solution

was kept to stabilize for 5 min before each measurement. Data are obtained in the form of continuous spectra,yet symbols are added for visual aid only.
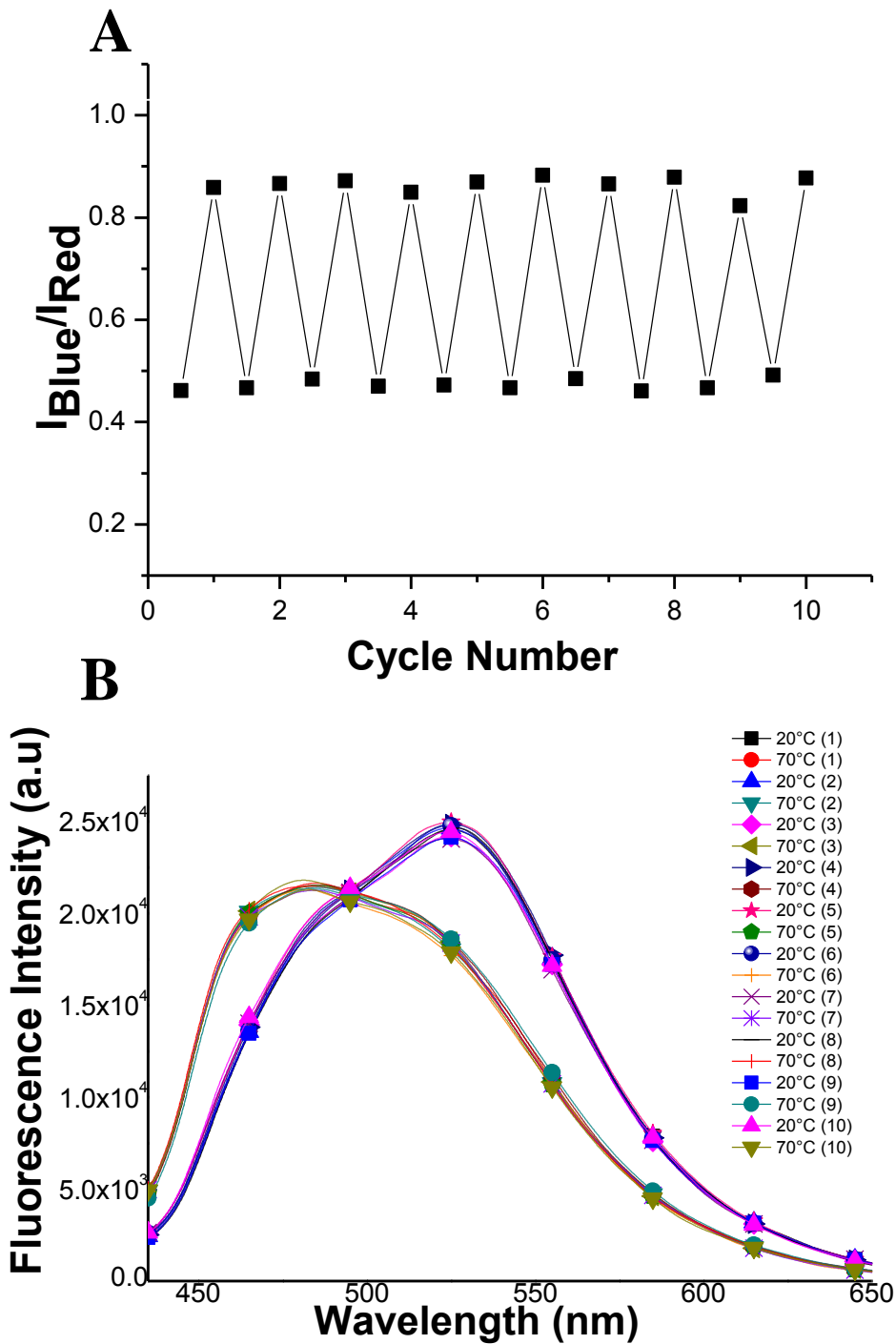
Figure 3.14: Cycling of PPE-CO_2 -7 (5 µg/mL)/PVP-PS (19.45 µg/mL) between 20.0°C and 70.0 °C , with its respective fluorescent emission spectra. Lines connecting the

experimental points are for visual aid only. (B) Respective emission spectra of PPE-CO$_2$ - 7/PVP-PS cycle between 20.0 ℃ and 70.0 ℃ when excited at 420 nm The experiment was performed in 10 mM HEPES with 150 mM NaCl (pH=7.3) buffer solution, and the solution was kept to stabilize for 5 min before each measurement. Data are obtained in the form of continuous spectra,yet symbols are added for visual aid only.

3.3.7 *Thin Polymer Film Assembly*:

3.3.7.1 Thermal Imaging of PPE-CO$_2$/PVP-VA Films:

To this point, we have demonstrated the possibility to observe a thermal response for PPE-CO$_2$-7 when complexed with PVP co-polymers in solution. Our interest, as stated earlier is to explore the thermal response in thin films. As such, the CPE was mixed with PVP-VA and spun cast onto a quartz slide. The ratio of the two polymers was kept equal to that optimized in solution.

Moving to a solid thin film sample implies dealing with many variables as the polymer micro-environment changes. In our previous work, PPE-CO$_2$-7 retained its ratiometric behavior in a hydrogel mixture. We adopted the same setup by placing the spun casted film of PVP-VA/PPE-CO$_2$-7 on a quartz slide which was placed on a Peltier cooler.[95] The excitation was done using a UV-lamp (365 nm), and the detection was recorded with a regular DSLR Canon 750D camera- 60mm macro lens- (exposure time 1/5 s, f/5.6, ISO 100). Figure 3.15 summarizes the collected images between 20 °C and 50 °C. To the naked eye, a slight change in the fluorescent emission is observed. The region of interest was selected and further analyzed using ImageJ to extract the average green and blue intensity channel since the ratiometric windows overlap those channels of the DSLR CMOS detector. Upon increasing the temperature, an increase in intensity was observed in both channels with a slightly more pronounced increase in the green window (Figure 3.16).

This behavior has been observed in solution at high PVP-VA concentration, where the PPE-CO$_2$-7 has been fully disaggregated by the polymer and an increase in temperature results in an overall increase in fluorescent intensity (Figure 3.8). Adjusting the CPE/PVP-VA ratio in films resulted in either a faint fluorescent signal or the same results. We believe in the film preparation process; the drying step is disaggregating the CPE chains and the increase in temperature is leading to an overall increase in the fluorescent intensity.
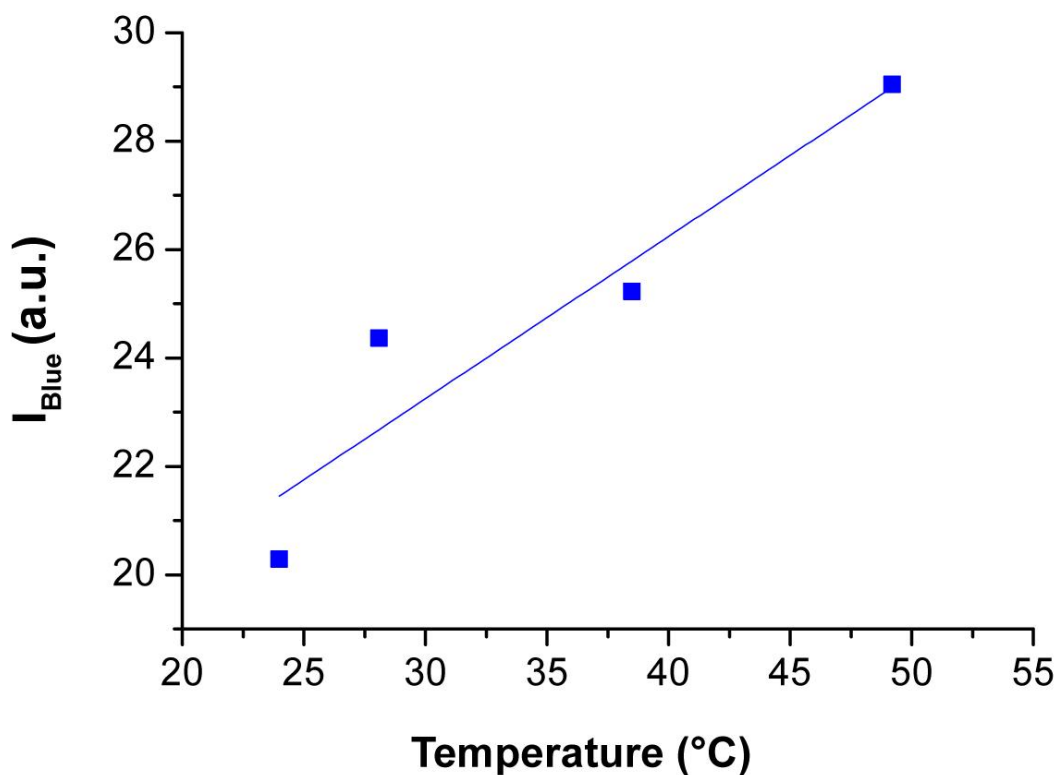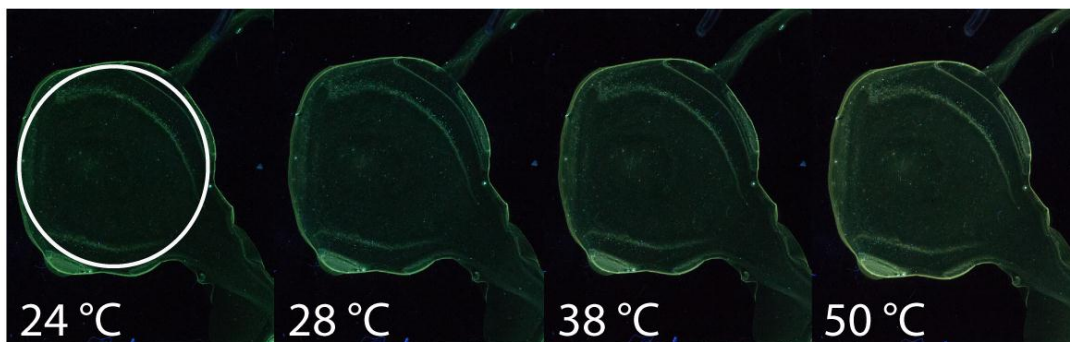
Figure 3.15: (A) Sequential images acquired using a DSLR camera upon exciting a film of PPE-CO_2-7/PVP-VA using a UV lamp when placed on a Peltier heater. The circle highlights the analyzed region of interest. (B) Average fluorescent intensity obtained by dissecting the images in (A) into their RGB components and plotting the blue channel intensity versus the measured temperature.
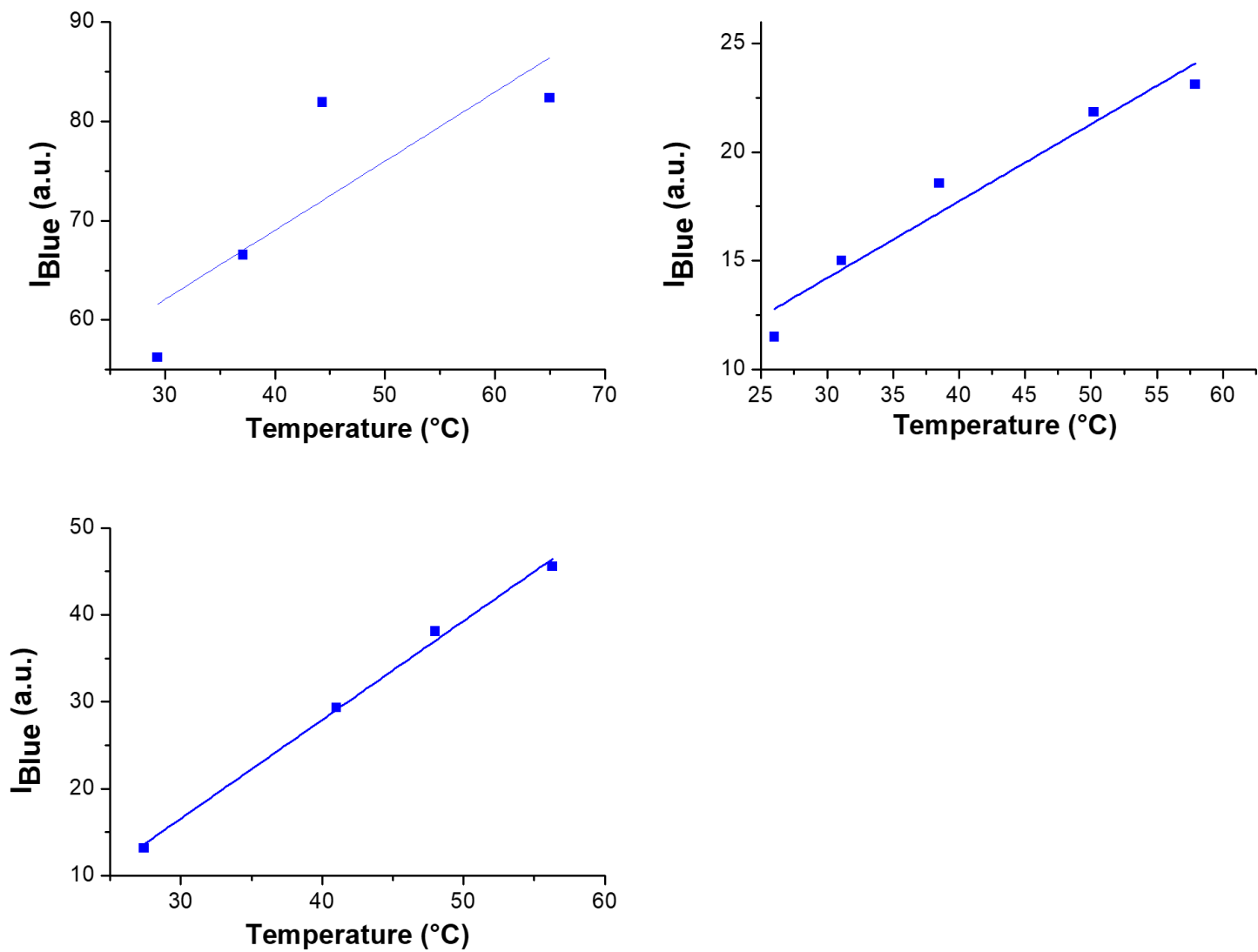
Figure 3.16: Average fluorescent intensity obtained by dissecting the images from three independent measurements into their RGB components and plotting the blue channel intensity versus the measured temperature.

3.3.7.2 Thermal Imaging of Rh/PPE-CO₂/PVP-VA:

While the ratiometric signal was not attainable in the prepared films, the increase in signal is still advantageous compared to the traditional fluorescent dye thermal response which decreases with the temperature increase making it difficult to decouple it from photobleaching. The fluorescent-based method can be expanded to three-dimensional imaging and spatial resolutions down to a few nms. As such, in recent years, only a few thermochromic fluorescent-based sensors were reported. Poly (vinylidene fluoride) with 4,40-bis(2-benzoxazolyl), as an example, exhibited a reversible thermochromic transition between blue and green fluorescence.[96] The composite films showed thermo-responsive control of RGB coloration with high reversibility through structural changes of nanoscale aggregates of the leuco.[97]

To add a second layer of certainty to our thermal measurements in thin films, we introduced a temperature sensitive dye Rhodamine B. The same procedure was followed, and a mixture of PPE-CO₂-7/PVP-VA and Rhodamine B was spun cast onto a quartz glass. Images were acquired upon excitation with a UV lamp (365 nm) and later analyzed with ImageJ (Figure 3.17 and Figure 3.18). When the intensity in the three channels (green, blue and red) was deconvoluted, we observed an increase in the blue channel consistent with the previous result of PPE-CO₂-7 alone. The red channel which captures photon between ca. 600 nm and 850 nm and overlaps Rhodamine B emission, revealed a decrease in fluorescent intensity over the same tested temperature window. The ratio of the average intensity of the two channels gave a linear thermal response with a slope of 0.010. The

addition of Rhodamine B has allowed us to obtain a ratiometric thermal response in thin

polymer films when imaged with a regular DSLR camera.
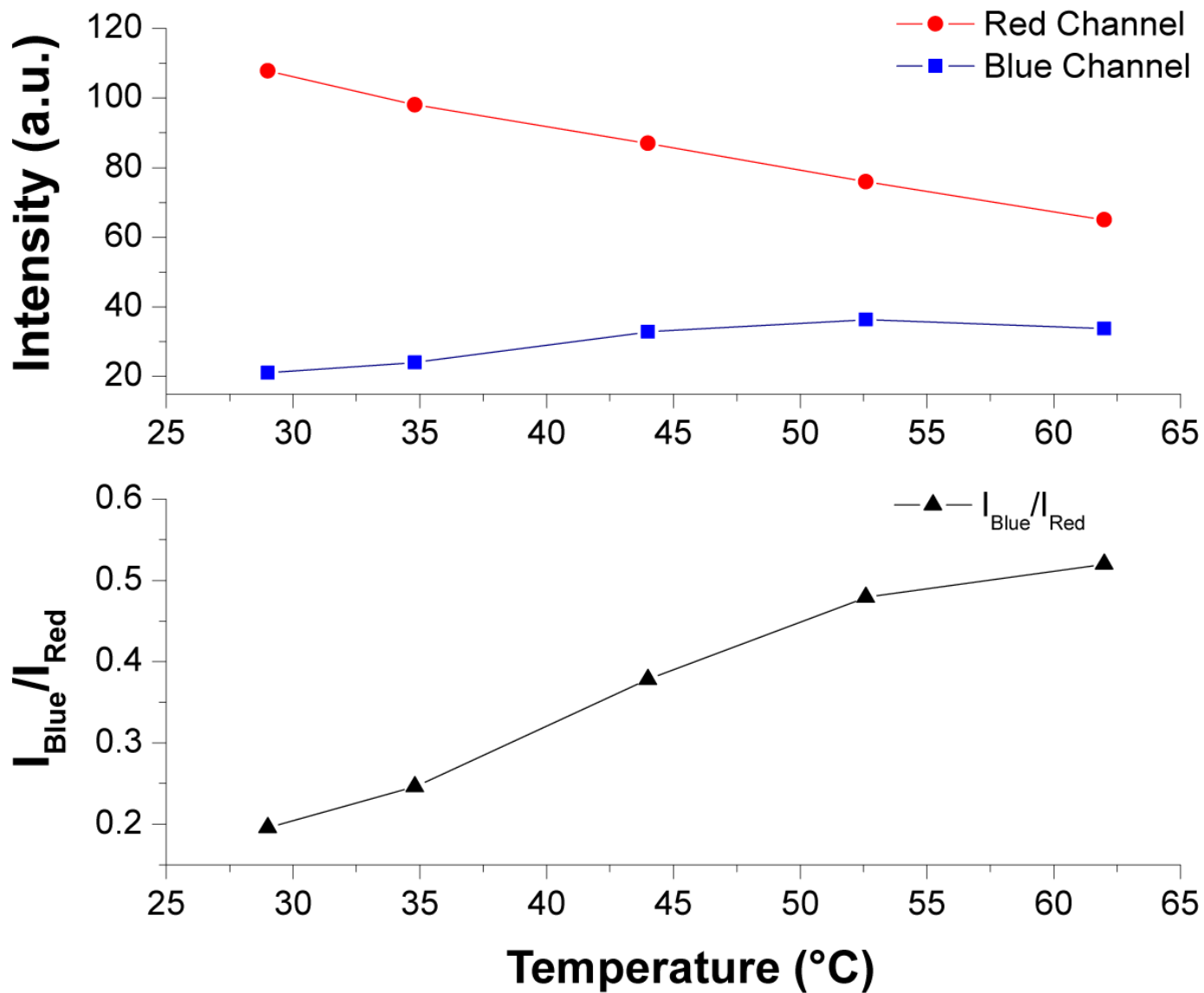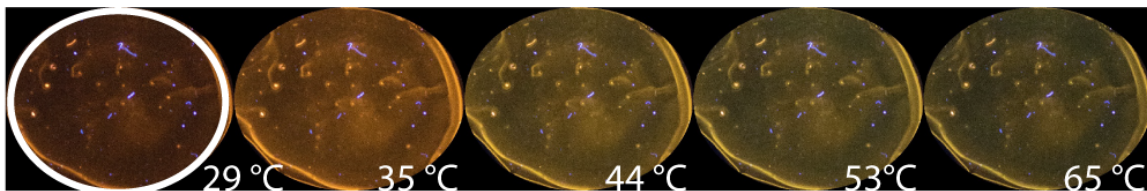
Figure 3.17: Sequential images acquired using a DSLR camera upon exciting a film of PPE-CO$_2$-7/PVP-VA + Rhodamine B using a UV lamp when placed on a Peltier heater. The circle highlights the analyzed region of interest. (B) Average fluorescent intensity

obtained by dissecting the images in (A) into their RGB components and plotting the red and blue channel intensities versus the measured temperature. (C) The ratio of the average intensities of the two channels plotted in (B) versus the measured temperature.
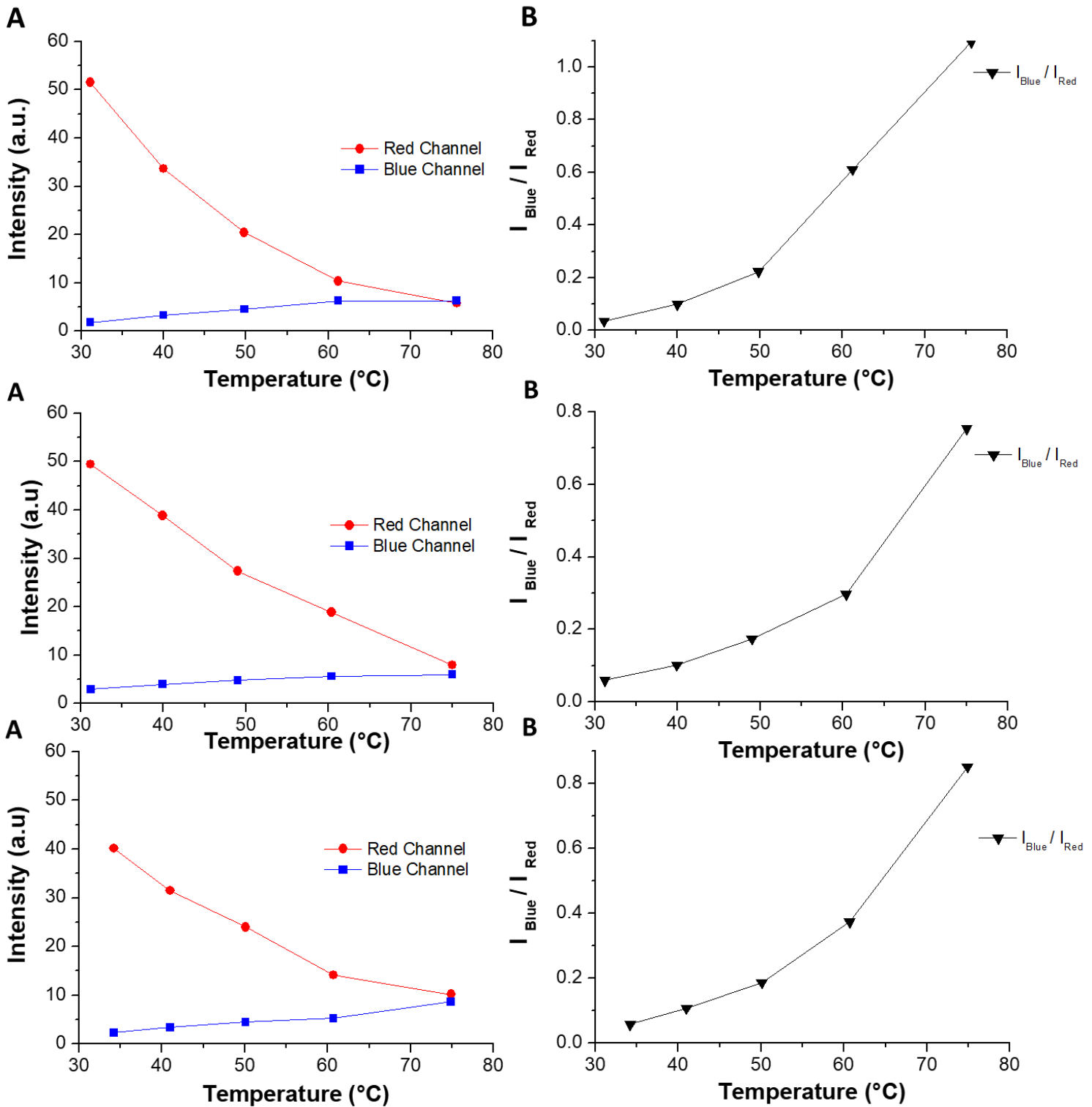
Figure 3.18: Three independent thermal response base on the imaging trials of Rh/PPE-CO_2/PVP-VA obtained by dissecting the images into their RGB components and plotting

the red and blue channel intensities versus the measured temperature. (B) The ratio of the average intensities of the two channels plotted versus the measured temperature.

3.3.8 *Thin Polymer Films Characterization*:

3.3.8.1 Scanning Electron Microscopy (SEM):

Thin polymer films were spun-casted on a small glass substrate, and their morphology was determined by scanning electron microscopy (SEM) using a MIRA3 Tescan. Before imaging, the sample was sputtered with a 10 nm layer of gold.
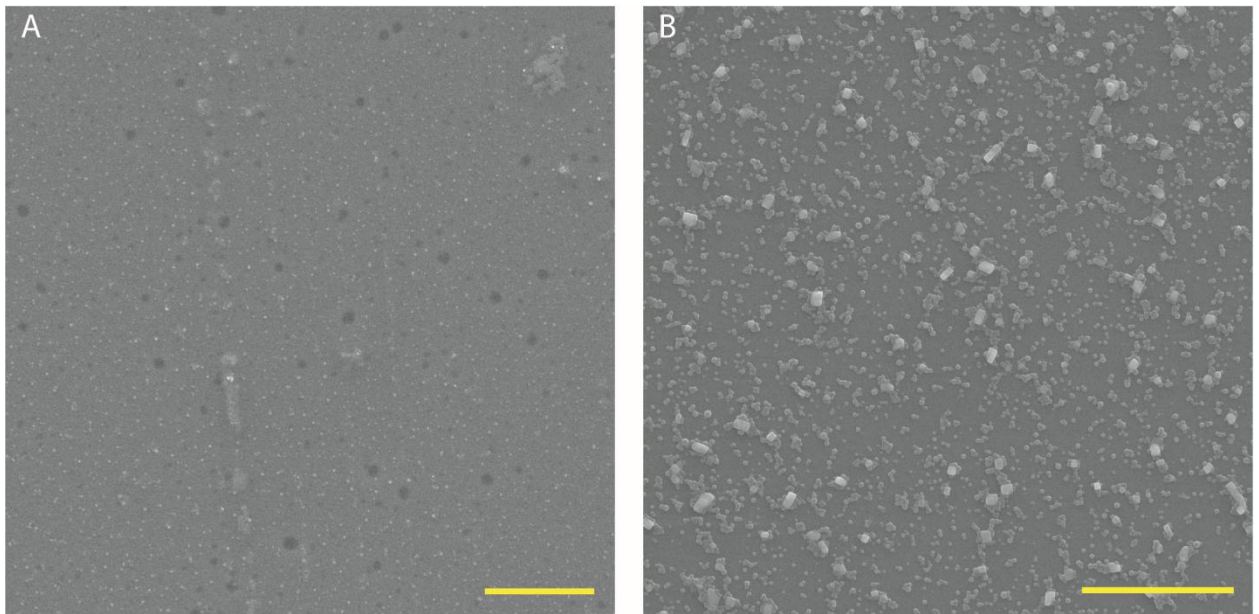
Figure 3.19: SEM images for spin-coated PVP-VA and PVP-PS films. Scale is equal to 5 μm.

The film thickness was measured using tilted SEM and was found to be equal to *ca.* 550 nm PVP-VA and *ca.* 1500 nm for the PVP-PS.
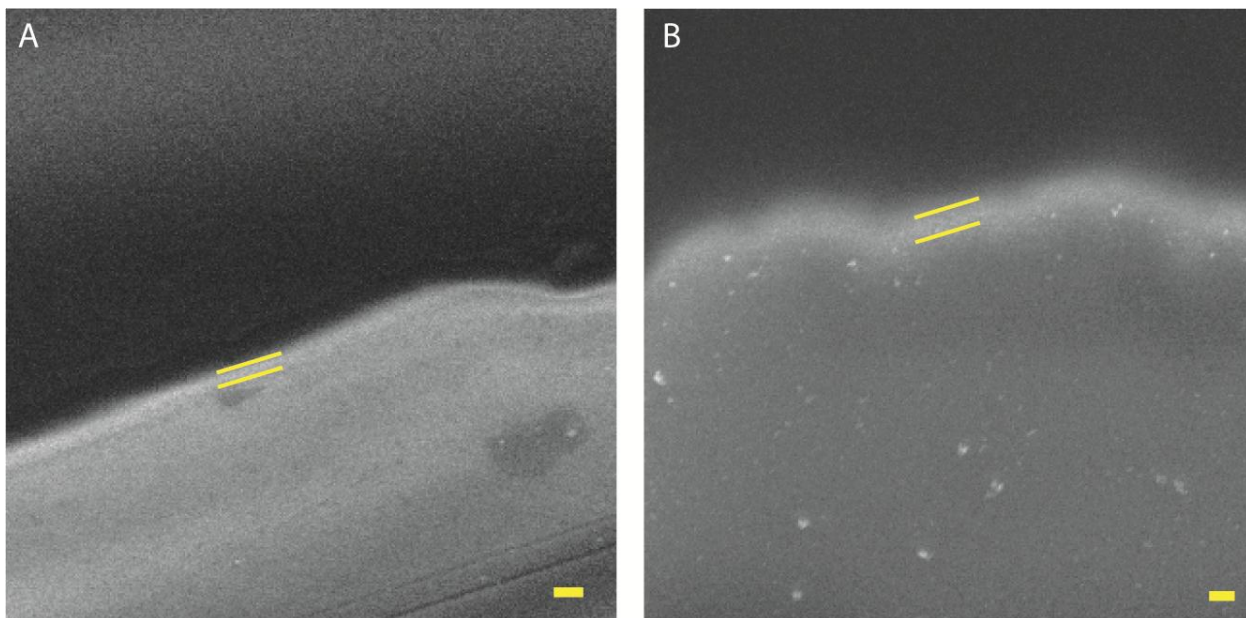
Figure 3.20: Tilted SEM images showing the film thickness of (A) PVP-VA and (B) PVP-PS.

3.3.8.2 Thermogravimetric Analysis (TGA):

For the thermogravimetric analysis, a Netzsch TG 209 F1 Libra instrument was used. The samples were first dried overnight and then analyzed between 30 °C and 1100 °C (but only reported until 600 °C) at a heating rate of 10.0 °C/min. PVP-VA/ PPE-CO_2-7, and PVP-VA/ PPE-CO_2-7/Rhodamine B. The results show that both co-polymers are stable up to temperatures around 300 °C. PPE-CO_2-7 polymers are stable up to 800 °C. Rhodamine B seems to degrade at temperatures above 100 °C.
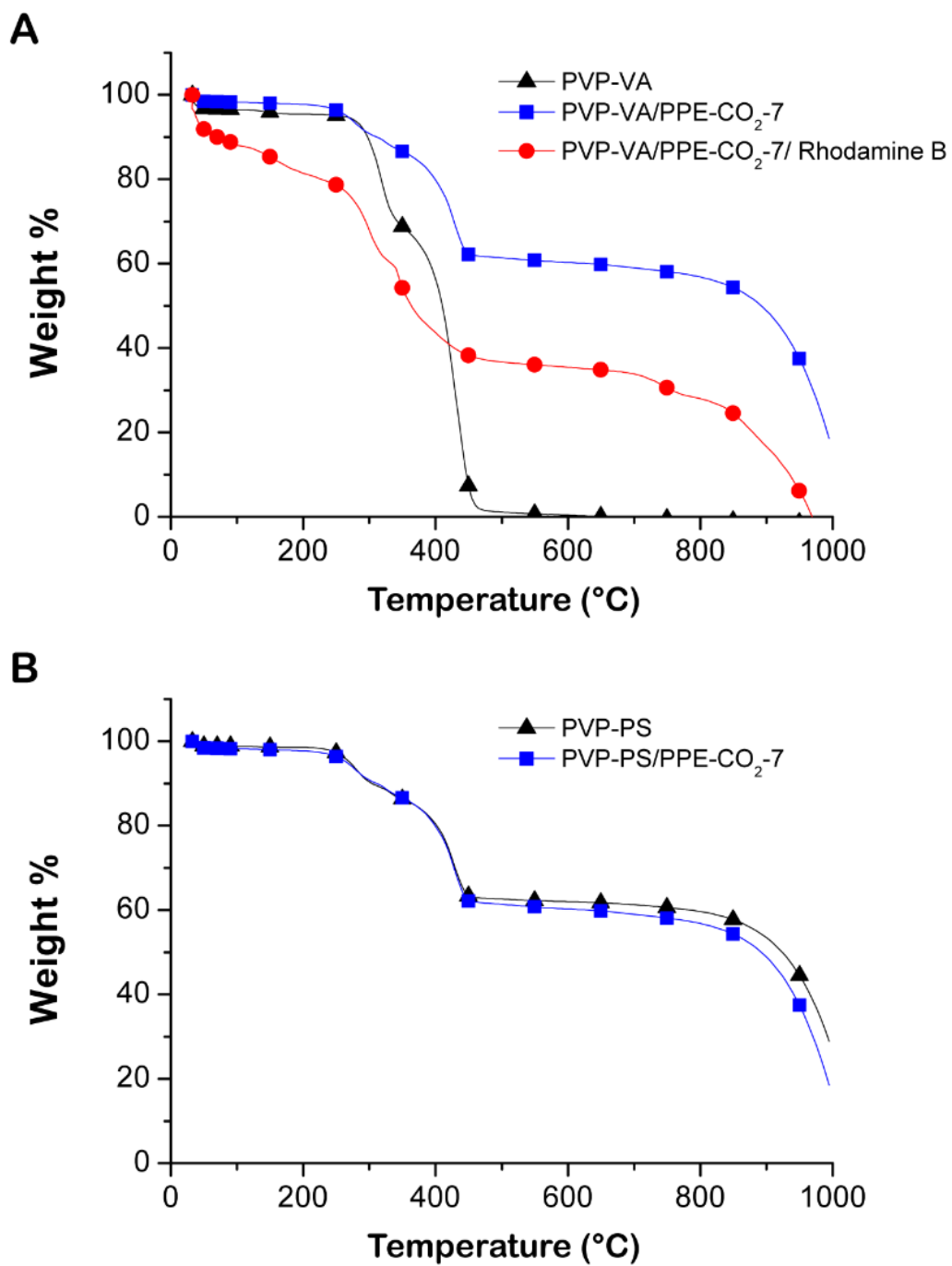
Figure 3.21: Thermogravimetric analysis for (A) PVP-VA, PVP-VA/ PPE-CO$_2$-7, and PVP-VA/ PPE-CO$_2$-7/Rhodamine B and (B) PVP-PS, PS/PPE-CO$_2$-7. Data are obtained in the form of continuous spectra,yet symbols are added for visual aid only.

3.3.9 *Stability of Thin Films at Different UV Irradiation Times:*

Film stability was assessed under continuous UV irradiations at 1 min intervals. The intensity was integrated and plotted versus time. The decay would affect the thermal response mostly for the non-ratiometric system (PVP-VA/PPE-CO_2-7). However, little effect would be observed on raitometric systems as it was shown by our group previously (Figures 3.13 and 3.14).
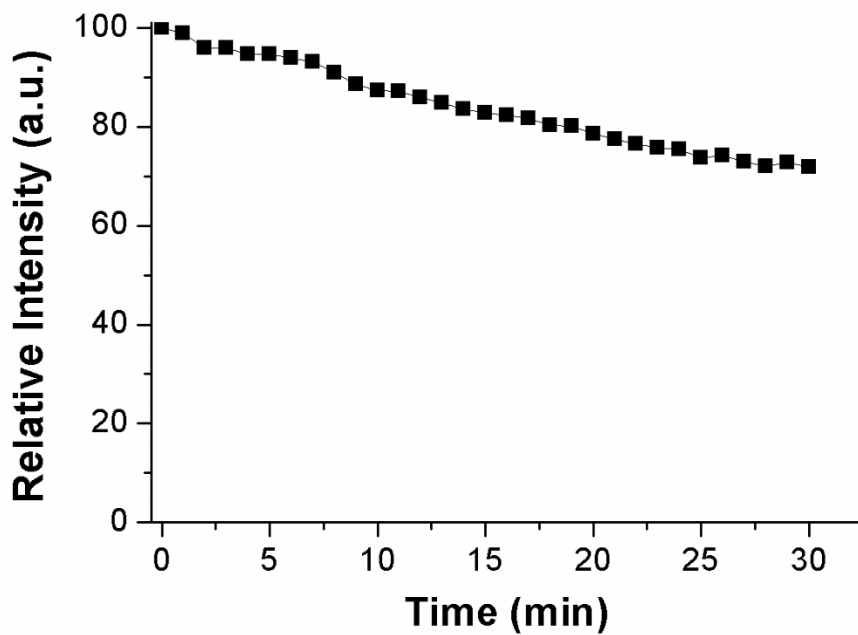
Figure 3.22: Relative fluorescent intensity upon continuous exposure under UV light at 0.02W/cm^2.

3.4 Conclusion:

The thermal sensing challenge in thin films was approached mostly by developing optical films that change colors in response to external temperature stimulation. While these methods provide a great way to estimate the temperature of the film, they are limited to the depth of information they can provide. In this work, we show that thermochromic response of PPE-CO$_2$-7 conjugated polyelectrolytes in solution is not restricted to PVP but is also observed with PVP co-polymers with a measured relative sensitivity of 2.35% and 1.455% for PVP-VA and PVP-PS, respectively. The thermal response was preserved in films but with no detectable ratiometric change in their signal, yet when mixed with Rhodamine B, the desired ratiometric signal was detected and was measured using a DSLR camera. This work has the potential to allow the measurements of thermal fluctuations in microelectronic devices such as MEMS, hence leading to the optimization of their performance.

CHAPTER 4

LOCALIZED CATALYSIS DRIVEN BY THE INDUCTION

HEATING OF MAGNETIC NANOPARTICLES

Controlling temperature with high spatial resolution has been a challenge and the bottleneck for advancing scientific discoveries at the micro-scale level. Particularly, localized catalysis is one of the major fields in chemistry affected by the thermal drawbacks highlighted in chapter 1. For this, we believe that the ability to deliberately generate heat with exquisite spatial resolution will affect how we perform local catalysis significantly.

In chapter three, we reported the development of a fluorescent-based sensor where a thermally-sensitive conjugated polyelectrolyte (PPE-CO$_2$-7) is implemented in thin-polymer films prepared from polyvinylpyrrolidone-co-vinyl acetate (PVP-VA). Our ability to build this thermal sensor motivated us to develop new strategies to locally control thermally-driven reactions at the nanoscale.

Herein, we aimed in this chapter to exploit the heat generated from magnetic nanoparticles when placed in an alternating magnetic field to drive catalytic chemical reactions. Specifically, and as a proof of concept, we focused on monitoring the catalysis reduction of resazurin into resorufin. Our major aim was to locally activate the catalytic reaction when placed in the magnetic field while comparing its efficiency to that of a solution heated by an external source under the same conditions.

4.1 Introduction:

Driving and manipulating thermally-dependent chemical reactions at the nano-scale is critical for a more efficient catalysis at the surface level. Understanding the principles of the surface chemical reactions is quite challenging because of the low resolution along with the limitations in the available techniques.[98]

While the science of the 21st century focuses on unraveling phenomena at the sub-micron level, the temperature is still being applied using large heat sources relative to the size of the studied system. The lack of available methods to accurately manipulate the temperature at the micro-scale has limited the advancement of both fundamental studies and small technologies.

For instance, cellular and even sub-cellular thermal processes are studied using temperature-controlled chambers or heated glass coverslips, leading to a non-homogenous thermal distribution.[99-101] Thermally activated pro-drugs are yet another example where micro-particles degradation are studied and optimized in large reaction volumes.[102-104] While these selected two examples are widely reported in the literature, many more examples could be cited from the different fields of science and engineering.[105, 106] There is, therefore, a pressing need to deliberately generate heat with exquisite spatial resolution. This ability will have a tremendous effect on how we perform and understand chemical and biological processes at the sub-micron scale.

Our ability to develop a thermal sensor in thin polymer films, discussed in chapter 3, motivated us to develop new strategies to control thermally-driven reactions at the nanoscale. Particularly, sensing with a low thermal resolution and a spatially-uncontrolled heating is a major drawback that researchers still suffer from.

Gold nanoparticles (AuNPs) can be plasmonically heated upon light excitation to enhance catalytic reactions on either the gold particle itself or when coupled to other metallic surfaces.[107, 108] Scaiano *et al.* reported the photocatalytic reduction of resazurin using the local heat generated from the plasmonic excitation of gold nanoparticles.[109] When compared to a reaction performed in a water bath at 80 °C, the conversion was much more efficient. This approach, however promising, might be limited for two reasons: (1) the high laser power needed to excite the gold nanoparticles can be disruptive to many organic matrices, in general, and living organs in particular, and (2) the penetration depth of visible and near-IR light sources is limited in opaque or semi-transparent materials. Magnetic nanoparticles (MNPs), on the other hand, generate heat when placed in an alternating magnetic field while presenting no harm to organic matrices and have large penetration depth in a wide range of materials (plastic, human tissues, etc.).[110-112]

Given this, recent thermochemical techniques highly rely on magnetic nanoparticles, that when placed in an alternating magnetic field, generate heat to the surface. This phenomenon, referred to as hyperthermia, has been proven to be an effective therapeutic strategy for cancer by potentially increasing the tumor oxygenation and radio/chemo sensitivity of solid tumors with the ability to restrict heating to the tumor area without it dissipating and destroying the surrounding cellular environment. In other words,

once they accumulate in a tumor, the localized heat induces apoptosis.[113, 114] Despite the stated advantages, the scope of work where MNPs are currently used is still rather limited.

In this chapter, we demonstrate the use of magnetic nanoparticles as local heat sources to catalyze chemical reactions of interest on the surface of metal nanoparticles. To this end, we assembled iron oxide and gold nanoparticles into a micro-catalytic structure. The heat generated by the magnetic particles is transferred to the metal surface to catalyze the reduction conversion of resazurin to the highly fluorescent product resorufin in the presence of NH_2OH (Figure 4.1). This strategy allowed us to improve the reaction efficiency by more than 100% when compared to a reaction placed in a water bath under the same experimental conditions.
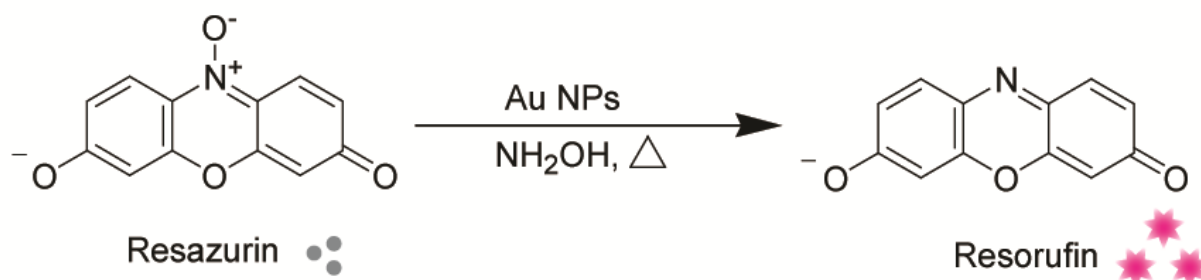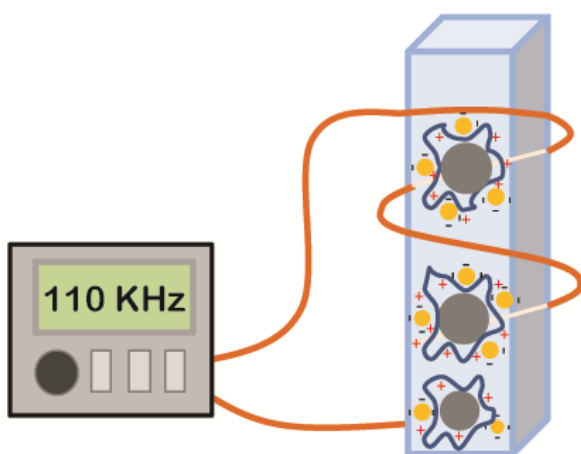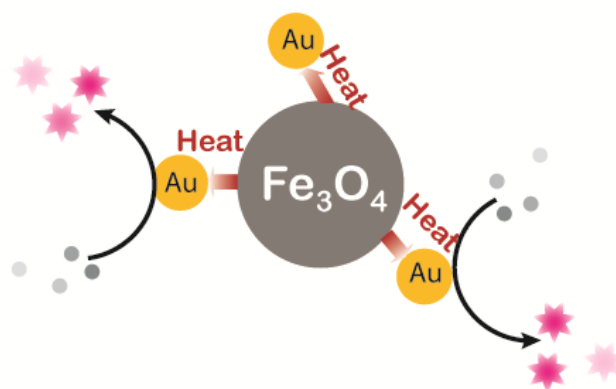
Figure 4.1: (A) the catalytic reduction reaction of resazurin to the fluorescent resorufin in the presence of gold nanoparticles and NH_2OH. (B) Schematic representation of the heat induction setup; a frequency generator is connected to a coil where the micro-catalytic MNPs/AuNPs solution is placed and subjected to an alternating magnetic field (frequency=110 KHz). (C) The assembly of the prepared micro-catalytic MNPs/AuNPs structure is driven by the electrostatic interaction between negatively charged MNPs and AuNPs using positively charged polyelectrolytes (PDDA).

4.2 Synthesis:

4.2.1   Synthesis of Iron Oxide Magnetic Nanoparticles (MNPs):

Iron oxide magnetic nanoparticles (MNPs) were synthesized using a previously published procedure.[115] Briefly, equimolar masses of Iron (II) chloride $FeCl_2.4H_2O$ (1.2g) and Iron (III) chloride $FeCl_3.6H_2O$ (3.25g) were dissolved in 80 mL deionized water. Next, 10 mL of ammonium hydroxide solution (28% w/v) was added while mechanical stirring. Twenty minutes later, 4.4g of trisodium citrate dihydrate powder was dissolved and the whole mixture was stirred while the temperature was raised and maintained at 90 °C for 30 min. After cooling down to room temperature, the magnetic nanoparticles produced were collected by an external magnet, decanted, and then re-suspended in 10 mL deionized water (Figure 4.2) yielding an estimated 139 mg/mL solution of particle size equal to *ca.* 257 nm (Table 4.1).
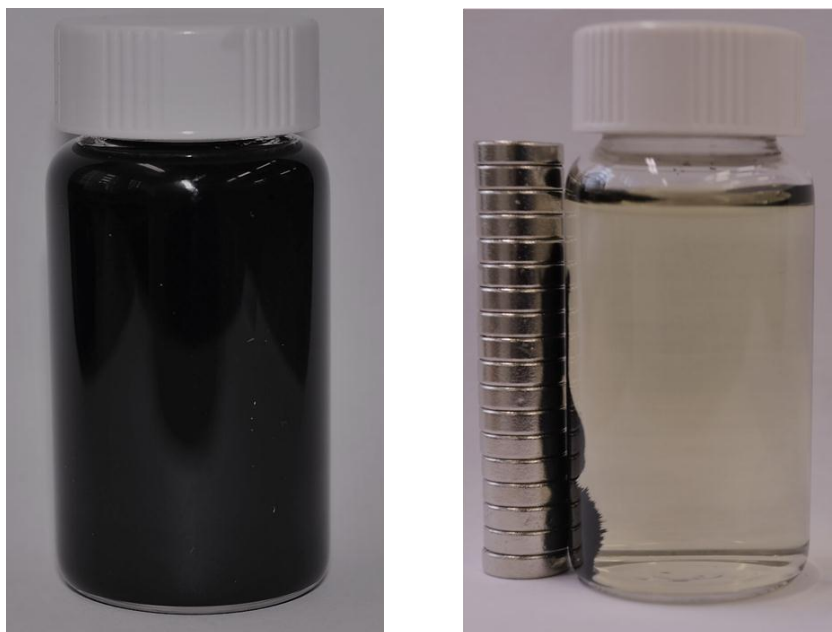
Figure 4.2: Iron oxide magnetic nanoparticles (MNPs) before and after applying an external magnetic field.

4.2.2   Synthesis of Gold Nanoparticles (AuNPs):

The gold nanoparticles (AuNPs) were prepared following the sodium citrate reduction method.[116] In short, 80 µL of a 0.2 g/mL gold (III) chloride trihydrate ($HAuCl_4.3H_2O$) solution was diluted in 10 mL deionized water and stirred till boiling. Then, 1.5 mL of 3% trisodium citrate dihydrate was added to form a momentarily colorless solution that rapidly turns into wine-red. The gold's concentration in the resulting suspension was estimated to be 1.4 mg/mL while its hydrodynamic radius was calculated to be *ca.* 92 nm (Table 4.1).

Here, we assumed that the degree of conversion of gold salt into gold nanoparticles is 100%. As such, all the reported concentrations of AuNPs are reported to be equal to that of the gold salt initially used.

4.2.3   Assembling the Gold-Magnetic Nanoparticle Catalytic Micro-Catalytic Structure:

The assembly of the catalytic micro-structure was achieved by the addition of a positively charged polyelectrolyte: Poly (Diallyl Dimethyl ammonium chloride) -PDDA- to a mixture of 1:1 Fe_3O_4: AuNPs by volume, followed by vortexing for 15 mins. This resulted in the assembly of MNPs/AuNPs macro structures with the heat generating element and the catalytic surface closely positioned (Figure 4.3).
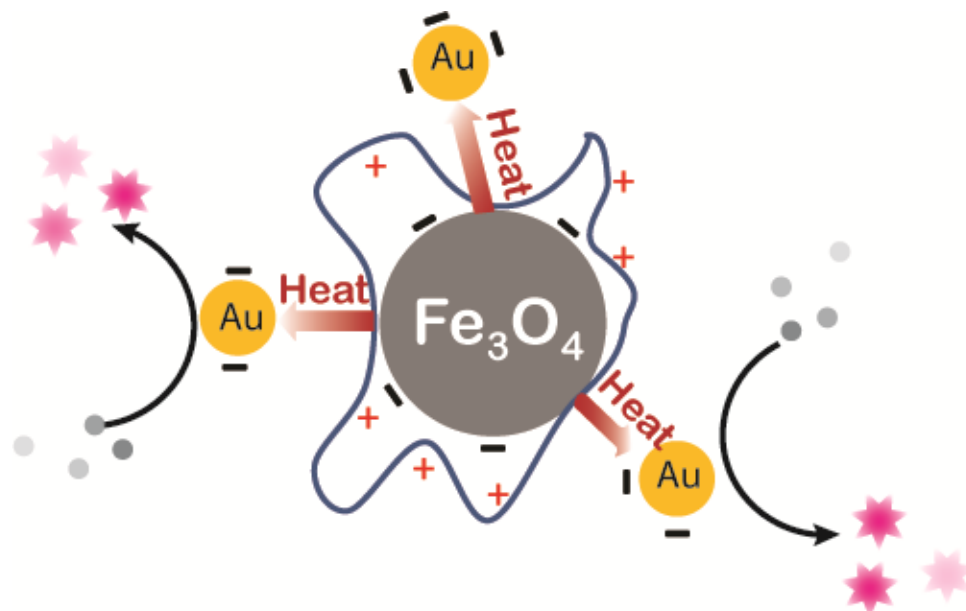
Figure 4.3: Scheme showing the assembly of the MNPs/AuNPs into micro-catalytic structures. Positively charged polyelectrolyte, PDDA, was used to bring together negatively charged magnetic and gold particles.

4.3 Results and Discussions:

4.3.1   Characterizations of the Assembled MNPs/AuNPs:

4.3.1.1   <u>Absorption Spectra</u>**:**

We characterized the MNPs/AuNPs structures in terms of morphology, size, and degree of assembly through first monitoring the absorption of gold nanoparticles before and after the collection by magnet and comparing them to that of a solution of pristine gold nanoparticles. The absence of any detectable absorption that can be attributed to gold nanoparticles in the supernatant implies the efficient assembly of the desired MNPs/AuNPs catalytic complex (Figure 4.4). The result was evident by even the naked eye when the characteristic red color of the gold nanoparticle solution was not observed after applying an external magnetic field (Figure 4.5)
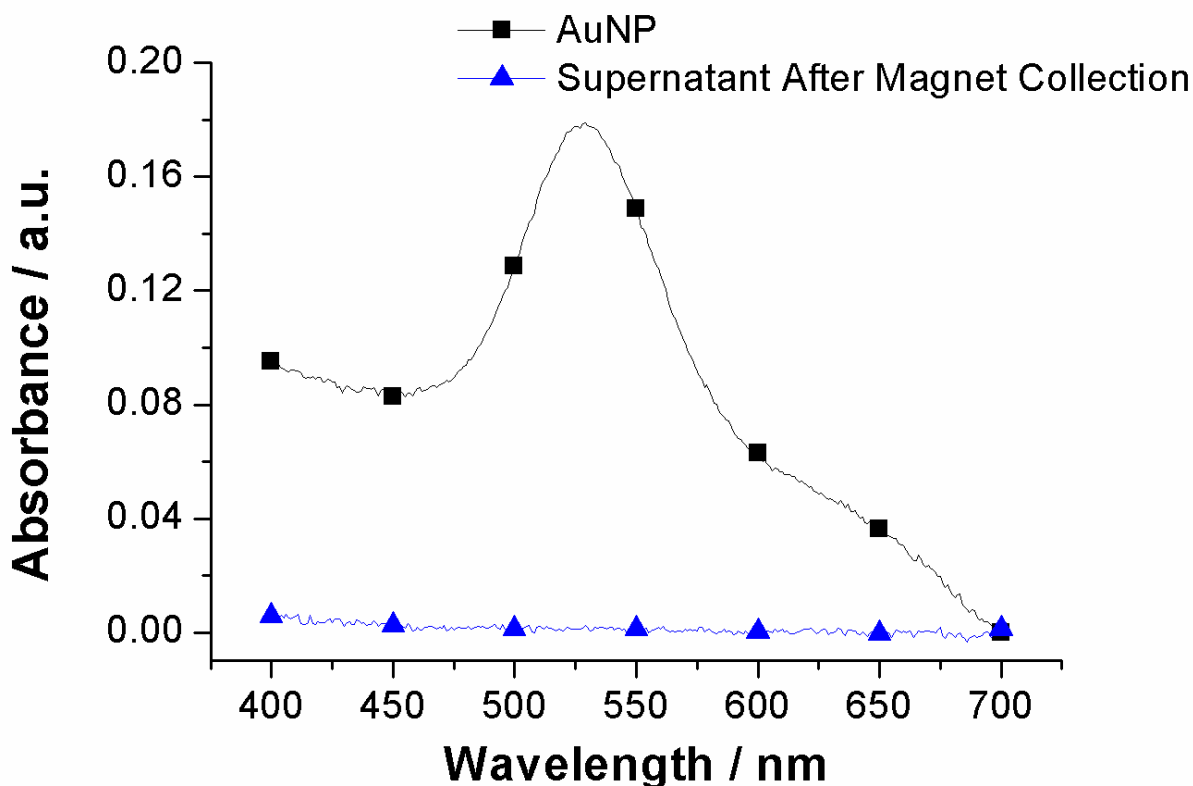
Figure 4.4: Absorption spectra of pristine gold NPs solution and of the supernatant of a MNPs/AuNPs sample upon separation. Data are obtained in the form of continuous spectra,yet symbols are added for visual aid only.

Figure 4.5: The assembly of the micro-catalytic structure was evident by the clear supernatant upon applying an external magnetic field.

4.3.1.2   Dynamic Light Scattering (DLS):

To further confirm the assembly, we resorted to compare the hydrodynamic radius of the MNPs/AuNPs mixture to that of MNPs and AuNPs solutions. The increase in the cumulant diameter from 257 nm and 92 nm for MNP and AuNP respectively, to 3800 nm in the assembled solution supports the suggested attachment (Table 4.1).

Sample	Cumulant Diameter (nm)	Polydispersity Index
MNP	257	0.19
AuNP	92	0.159
Mixture	3800	0.637

Table 4.1: Hydrodynamic radius for the prepared particles and assembled micro-catalytic structure measured using NanoPlus HD.

4.3.2   Optimization of the Catalytic Reaction:

The catalytic reaction condition was optimized in a water bath maintained at 65 °C. by varying the concentrations of each of gold nanoparticles, NH_2OH, and the positively charged polyelectrolyte (PDDA) (Figures 4.6-4.8). Our aim was to reach the optimal conditions at which the reaction is almost blocked at room temperature, yet it proceeds faster at higher temperatures without being completely saturated so we can observe the ehnacement as a function of time.

The reaction efficiency was judged by monitoring the fluorescence intensity of resorufin produced under different experimental conditions at different time points. The choice of concentrations took into consideration not only the conversion efficiency but also the technical aspect of the experiment such as avoiding large aggregates, signal scattering, or quenching of the fluorescent signal by the gold nanoparticles.

The reaction temperature was controlled by placing the solution in a water bath. The optimized solution was then tested at different temperatures between 25.0 °C and 85.0 °C with a step increment of 10.0 °C (Figure 4.9). The temperature was monitored and tracked using a thermocouple connected to a data logger.

To maintain normalized results, the reaction is blocked once introducing the sample into the cuvette, and the fluorescence measurements are obtained at room temperature.

4.3.2.1   Optimization of the Gold Nanoparticles Concentration:

The gold nanoparticles concentration was optimized by increasing their final concentration in the reaction mixture (Figure 4.6). Results showed that a gold NPs concentration greater than 0.35 mg/mL leads to a saturation in the fluorescent signal.
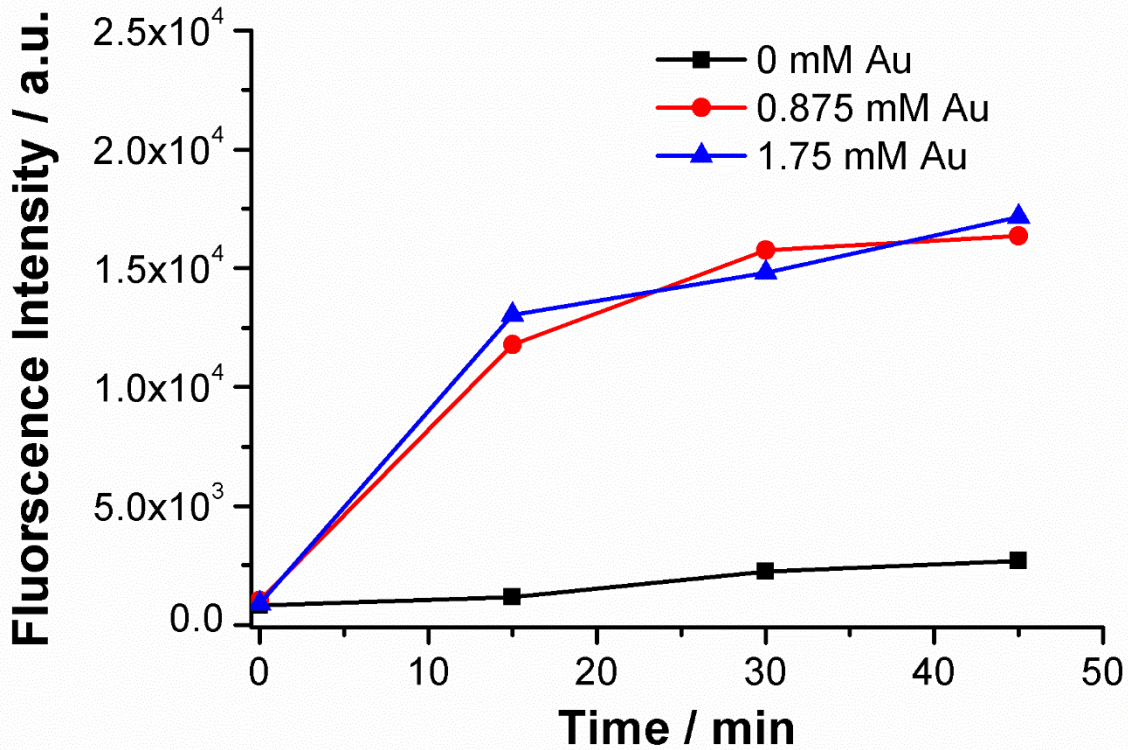
Figure 4.6: The maximum fluorescence intensities of resorufin acquired at different gold nanoparticles final concentrations. The results were obtained at 4 different time points: 0, 15, 30, and 45 min.

4.3.2.2   Optimization of Hydroxylamine- NH_2OH Concentration:

The concentration of the reducing agent NH_2OH was varied to check for its optimum amount needed for the reduction (Figure 4.7). The increase in the concentration of NH_2OH was found to increase the fluorescence intensity. We, thus, agreed on taking 7.5 mM as the final concentration of the reducing agent in the catalytic reaction.
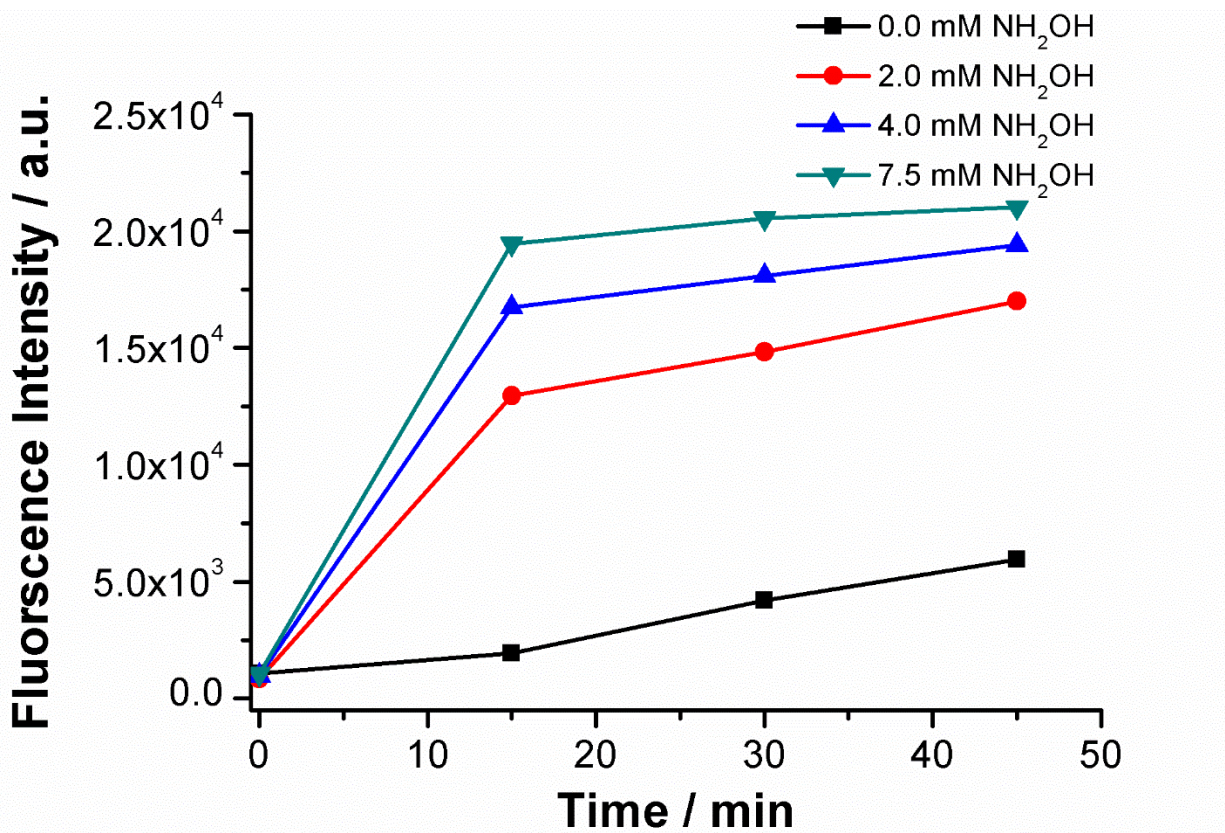
Figure 4.7: The maximum fluorescence intensities of resorufin acquired at different hydroxylamine concentrations. The results were obtained at 4 different time points: 0, 15, 30, and 45 min.

PDDA is used to assemble the catalytic micro-structure by electrostatically gluing the negatively charged magnetic and gold nanoparticles. Samples with different concentrations of PDDA were tested and the fluorescent signal of resorufin was measured (Figure 4.8). Due to the considerable enhancement in the fluorescence intensity in the solution containing 64.3 mM of PDDA, the latter was taken as the standard final concentration for the upcoming trials.
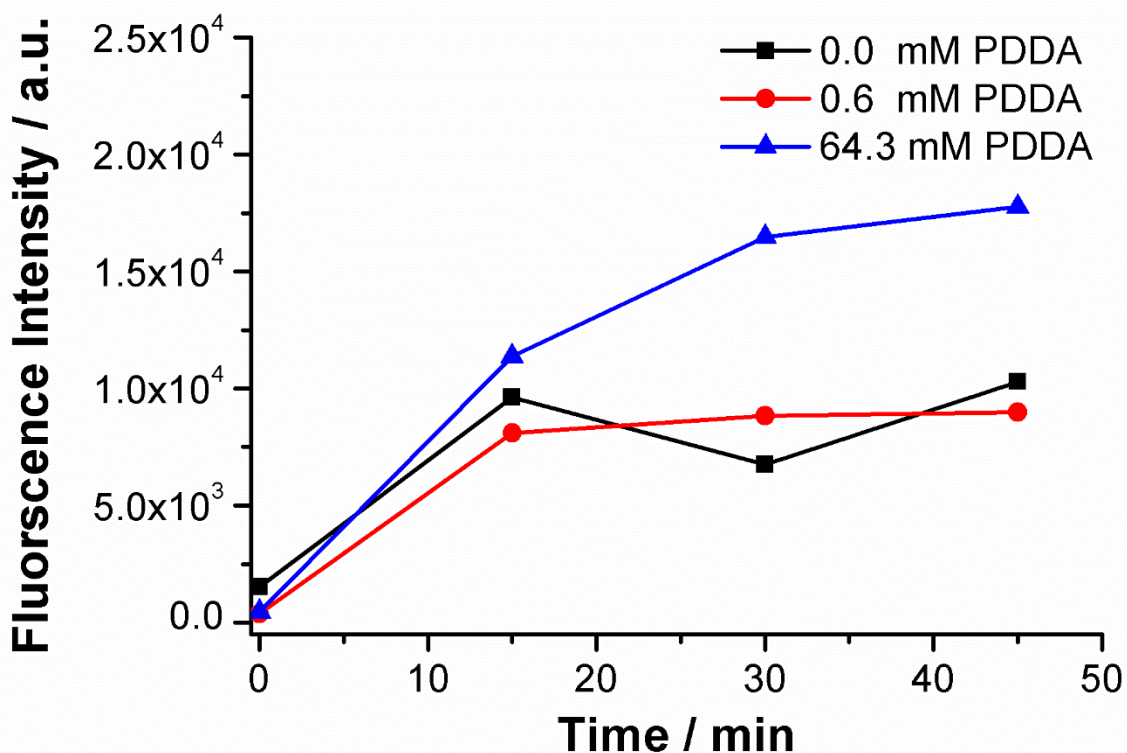
Figure 4.8: The maximum fluorescence intensities of resorufin acquired at different poly diallyl dimethyl ammonium chloride (PDDA) concentrations. The results were obtained at 4 different time points: 0, 15, 30, and 45 min.

4.3.2.4   Optimization of Temperature:

To check for the optimum temperature at which the reaction is neither saturated, nor sluggish, a series of experiments were done at different water bath temperatures ranging from 25 to 85 °C. All trials were performed using identical mixtures based on the aforementioned optimized standard conditions. To insure consistency with the MagneTherm trials and to account for the expected decrease in the reaction's rate in the MagneTherm due to the presence of magnetic nanoparticles, the temperature optimization in the water bath was done while mixing MNP with the reduction solution mixture (Figure 4.9). Above 55 °C, the reaction starts to saturate, thus 45 °C was chosen as a standard temperature for further trials
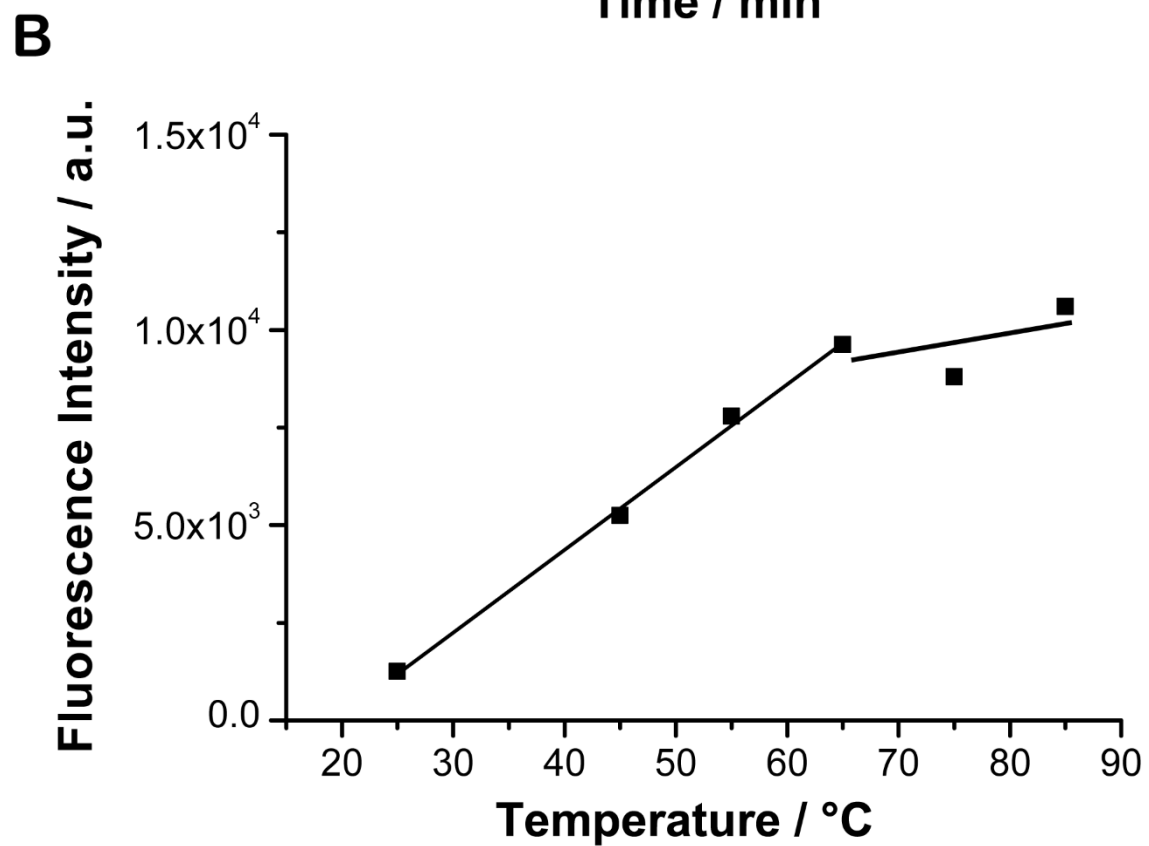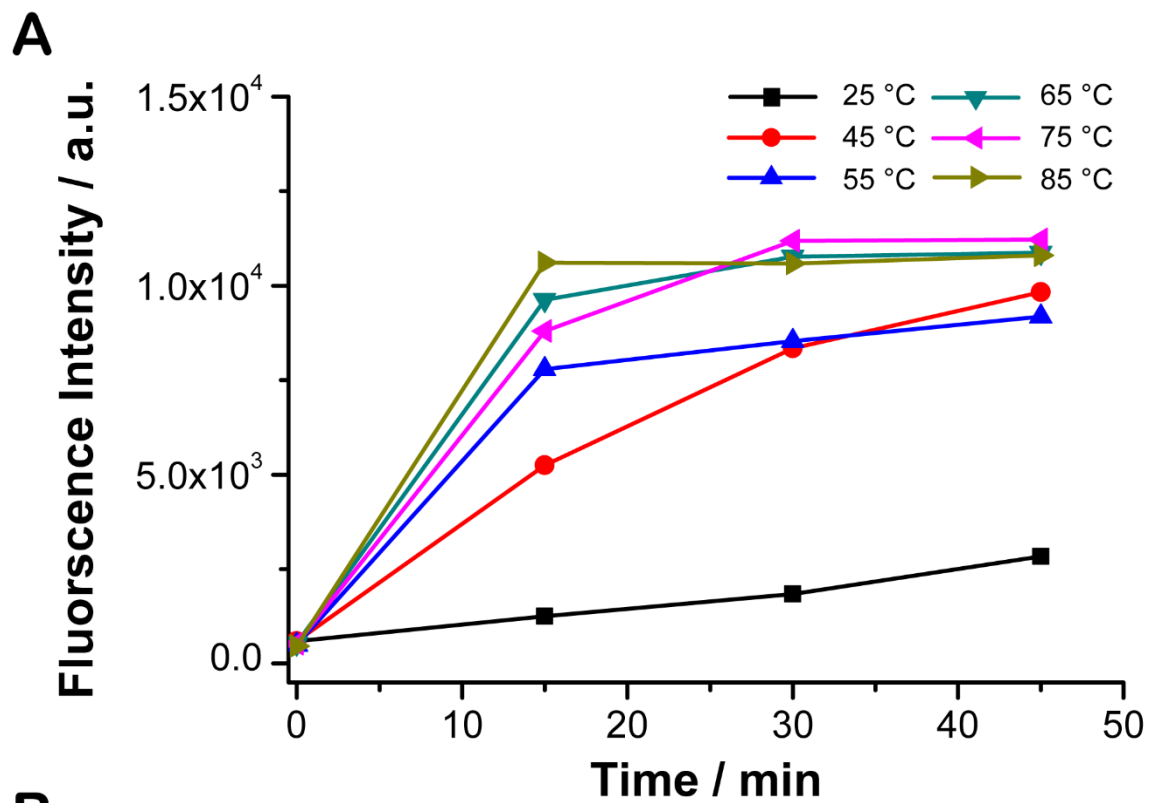
Figure 4.9: (A) The maximum fluorescence intensities of resorufin acquired at different temperatures between 25.0 °C and 85.0 °C with a step increment of 10.0 °C in a water bath. Measurements were obtained at 4 different time points: 0, 15, 30, and 45 min. (B) The maximum fluorescence intensities of resorufin at 15 min time point versus temperature.

4.3.3 Heating by Induction Versus Water Bath Trials:

The efficiency of the locally induced heat was compared, under the same experimental conditions, to that of a water bath and measured by comparing the fluorescence intensity of resorufin (Figure 4.10). This experiment was repeated two more times for consistency (Figure 4.11).

Both solutions corresponding to the water bath and the heat induction trials included similar AuNPs, NH_2OH, PDDA, and iron oxide MNPs concentrations. Magnetic nanoparticles were added to the solution heated by inside a water bath to maintain consistency with that of the heat induction.

As such, we carried the catalytic reaction at 45.0 °C. At this temperature, the reaction kinetics would allow us to observe the enhancement, if any, in the conversion of resazurin when carried out in a water bath and compare it to that in a solution heated by the MNPs when placed in an alternating magnetic field. At different time intervals, the fluorescent signal of the resorufin was sampled and compared. Within the first 15 minutes, the catalytic micro-structure showed an enhanced catalytic conversation as compared to a water bath solution, and reached, in some cases, a 120 % enhanced efficiency (Figures 4.10 & 4.11). Results obtained after 30min showed a decrease in the degree of enhancement due to the saturation in the conversion of resazurin into resorufin as a function of time.

87

While the solution temperature in both experiments was maintained at 45.0 °C, we believe the local surface temperature of the gold nanoparticles is higher than the solution temperature, allowing a more efficient conversion of resazurin to resorufin. This hypothesis is supported by previously reported studies; Pellegrino *et al.* probed the distance-dependent temperature as generated by magnetic nanoparticles using a thermos-sensitive molecule.[117] The local temperature surrounding the MNPs was found to be approximately 45 °C greater than the solution temperature. Zink *et al.* also reported a temperature gradient with a measured MNPs surface temperature of 42 °C and a solution temperature was equal to 19 °C.[71]

Although all trials consistently showed an increase in efficiency, it varied from one sample to another. The micro-catalytic structure has a tendency to aggregate in solution. Despite taking many measures to homogenize the solution before making any transfer to the reaction mixture, we believe our effort did not lead to completely eliminate this error.
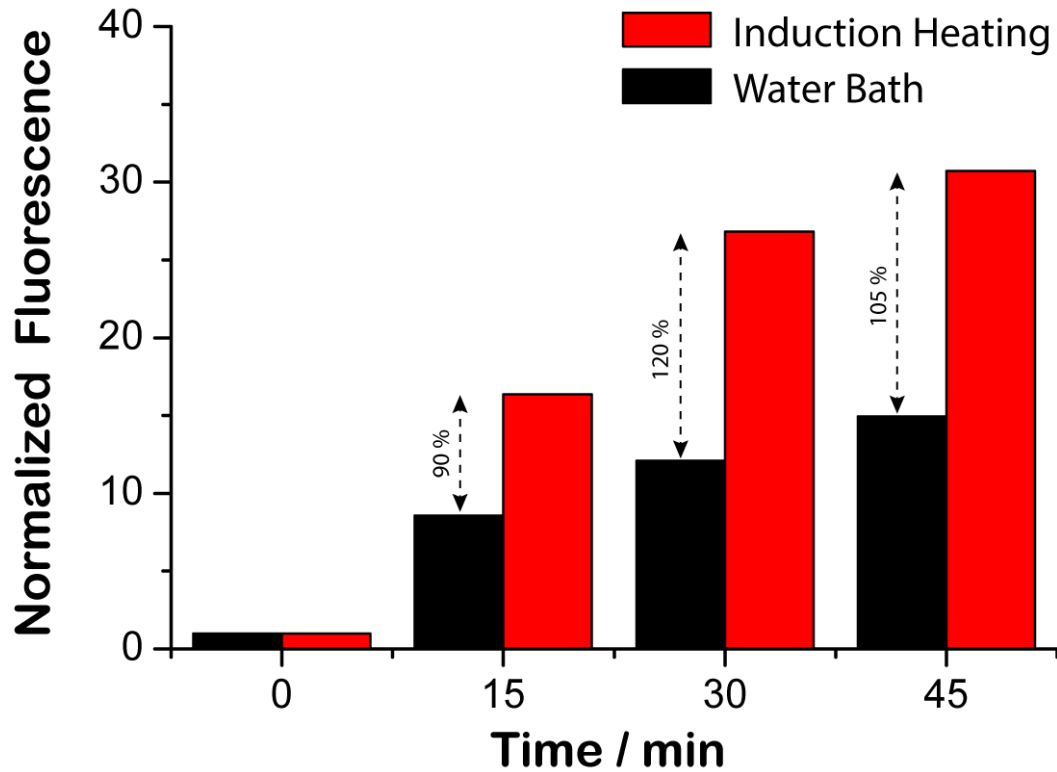
Figure 4.10: Comparing the fluorescence intensities of resorufin produced by the catalytic reduction of resazurin when heated by either an external heat source or by the micro-catalytic MNPs/AuNPs structure. Both solution temperatures were maintained at 45.0 °C.
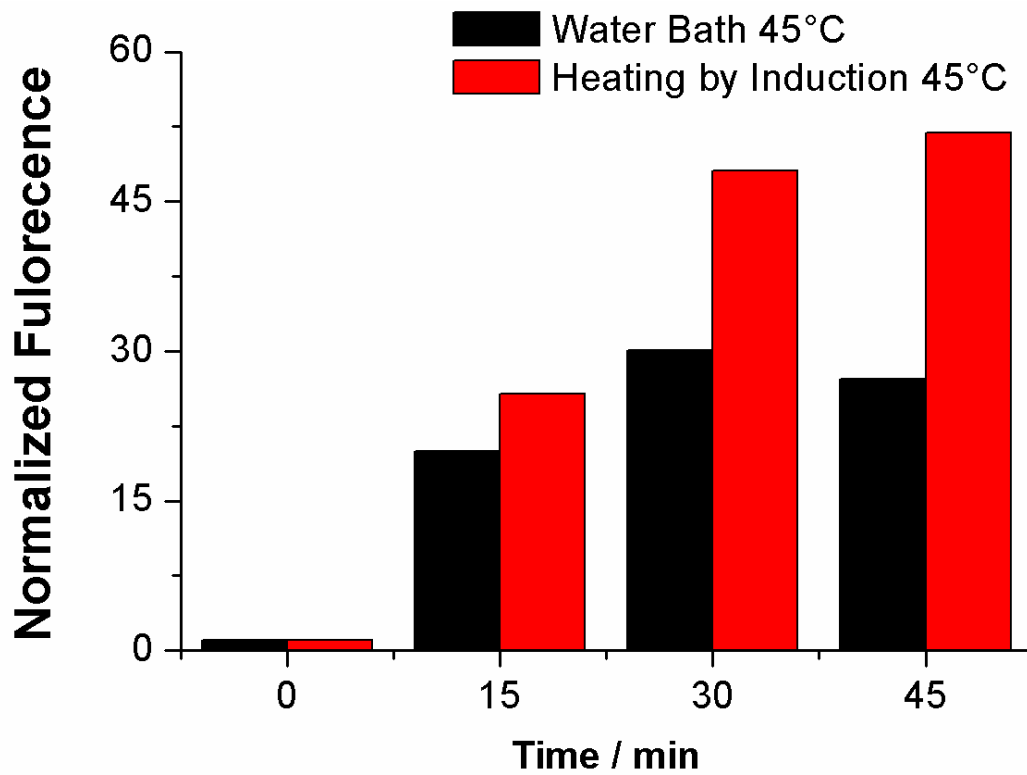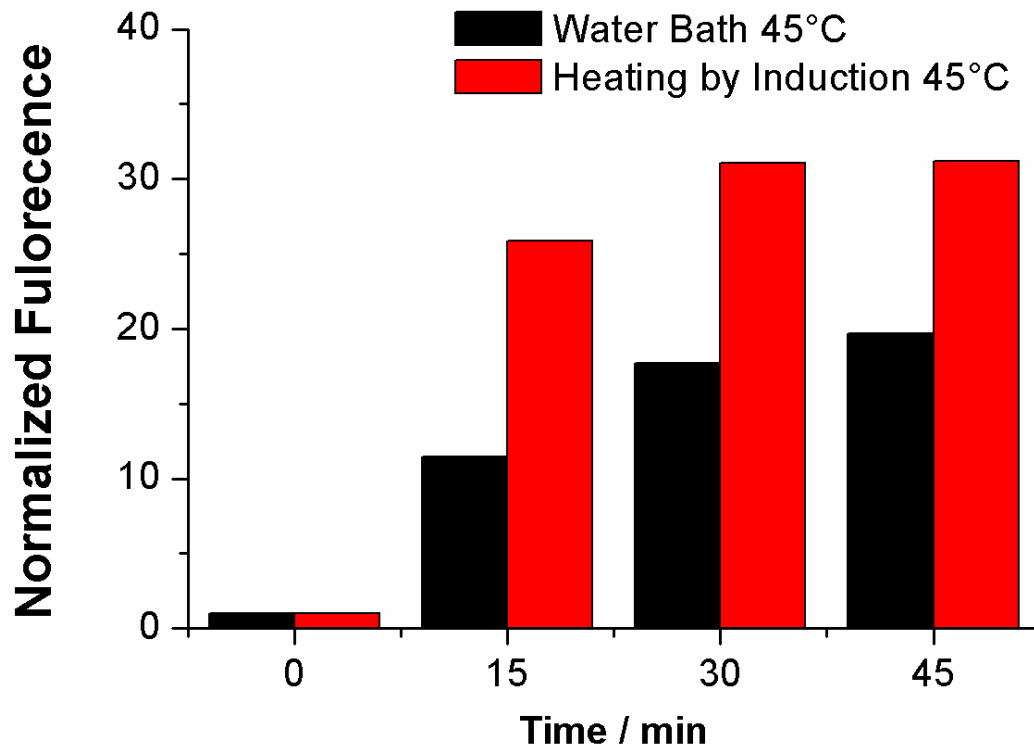
Figure 4.11: Comparing the fluorescence intensities of resorufin produced by the catalytic reduction of resazurin and heated either in a water bath or by induction using magnetic nanoparticles. Solution temperatures were maintained at 45.0 °C.

4.3.4   Temperature Tracking:

To ensure comparable experimental conditions and maintain a stable temperature, the thermal variations were measured and tracked via a thermocouple dipped inside the solution tube and connected to a data logger machine. Adjustments were manually introduced, when needed, to maintain a constant value. Figure 4.12 shows an example of the thermal tracking. Both solutions reached steady values within the first few minutes and remained relatively constant throughout the experiment.
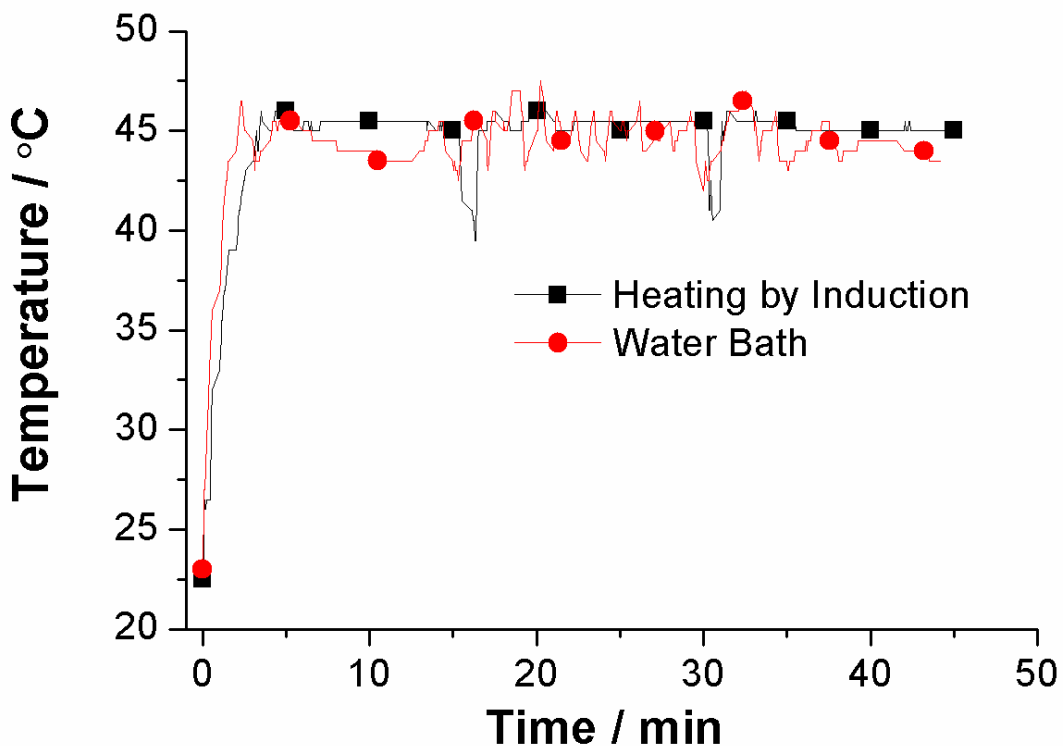
Figure 4.12: Plot tracking the increase in temperature of the solution as a function of time, recorded via a data logger. Solution 1 was inserted in the MagneTherm while the other in a water bath at 45°C. Data are obtained in the form of continuous spectra,yet symbols are added for visual aid only.

4.3.5   Microscopy Imaging:

Based on these promising findings, we argued that these localized catalytic reactions would allow the deliberate production of molecules of interests in a spatially confined volume even when a small amount of the micro-catalytic structure is introduced Hydrogels have been used in chemistry and biology to mimic soft matrices including but not limited to extracellular medium.[118, 119] We wanted to check if it is possible to catalyze chemical reactions in small localized volumes in soft materials. The success in achieving this could translate, in the future, toward in-situ drug generation, for instance.[120]

For this purpose, a thin agar gel layer (5%) was prepared and molded onto a microscopic slide and then left to solidify. Using a 0.3mm-thin insulin needle, few microliters of resazurin were injected into the gel. MNPs solution was poured on the gel's surface for few minutes to allow the magnetic nanoparticles to fill the cracks created by the needle. The solution was wiped away, and the slide is imaged with an upright fluorescence microscope Leica DM6 B. We then poured a solution of MNPs/AuNPs mixed with NH_2OH on the top of the gel again and left it in an alternating magnetic field. After two hours of heating in the MagneTherm, the gel surface was wiped and imaged for the second time under the same experimental conditions (5x objective and 1.5s exposure). Fluorescence intensities were quantified using the ImageJ software (Figure 4.13). For resazurin, a 541-551 nm excitation filter was used, and the emission was collected between 565 and 605 nm.

Integrated intensity showed an increase between 100 and 150 %, which is consistent with the results obtained from the steady-state fluorescent spectroscopic measurements. The observed range of increased fluorescence intensity might be the result of the variable amount of the micro-catalytic structures introduced to the gel.
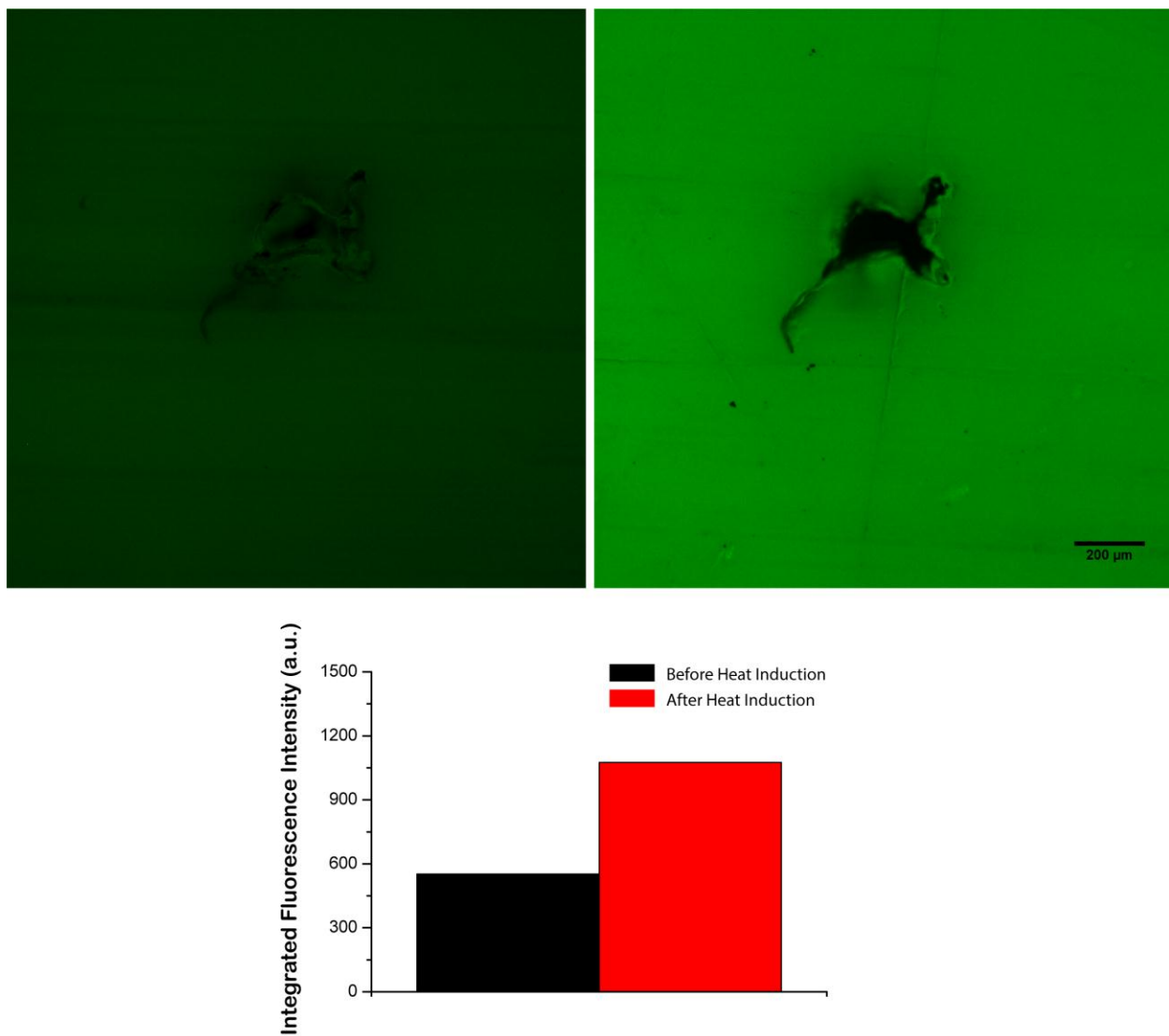
Figure 4.13: Fluorescent microscopy images of agar gel before and after exposure to an alternating magnetic field in the presence of resazurin, NH_2OH, and MNPs/AuNPs complex along with their integrated fluorescence intensities. Images were acquired using a 5× objective with NA= 0.8 coupled with an excitation filter of 541-551 nm, and the emission was collected between 565-605 nm
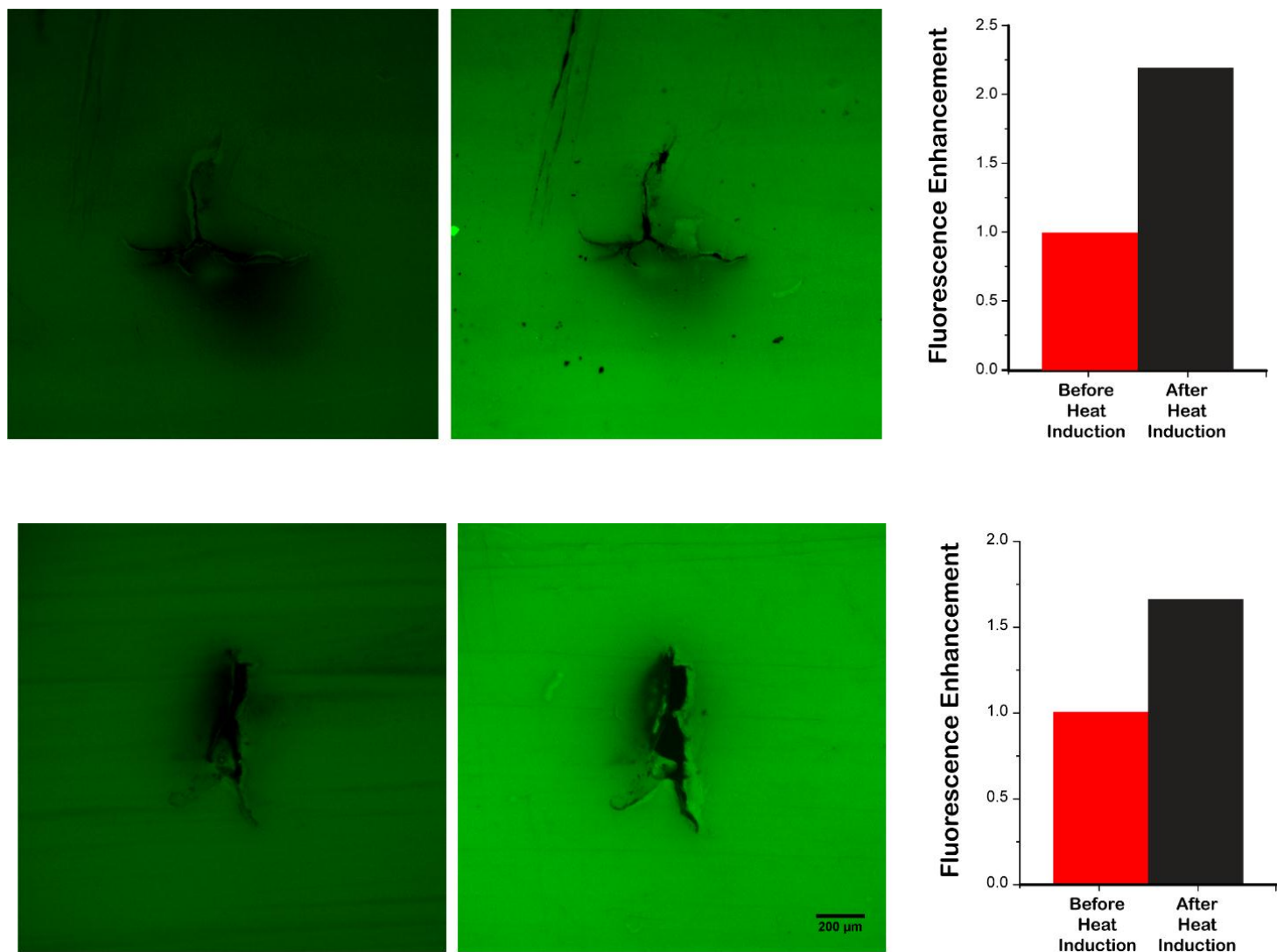
Figure 4.14: Fluorescent microscopy images of agar gel before and after exposure to an alternating magnetic field in the presence of resazurin, NH_2OH, and MNPs/AuNPs complex along with their fluorescence-enhancement levels. Images were acquired using a $5\times$ objective with NA= 0.8 coupled with an excitation filter of 541-551 nm and the emission was collected between 565-605 nm.

4.3.6   Visual Analysis:

The increase in the fluorescence intensity detected under the microscope, was consistent with what was obtained through visual analysis of the color changes in the cuvette prior its fluorescence measurements (Figure 4.15). The resazurin (blue) is reduced into the resorufin (pink) as a function of time. These results further confirm the efficiency of our initially proposed local catalysis setup.
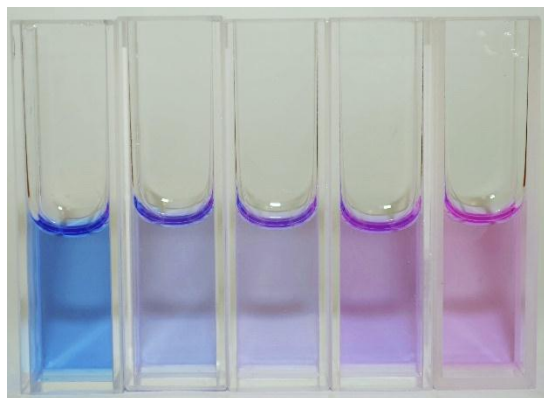
Figure 4.15: Photograph of the changes in color of the different solution samples a function of time.

4.4 Conclusion:

In conclusion, we successfully report the use of heat generated at the microscale to drive chemical reactions with significantly higher catalytic efficiency when compared to a water bath maintained at the same temperature. This proof-of-concept experiment will eventually pave the way to thermally control reactions with a high spatial resolution which would allow, for instance, the production of drugs with surgical precision. Prodrugs, such as endoperoxides, could be delivered to the organs of interest, and their uncaging could then be catalyzed upon local heating to release reactive oxygen species intracellularly with surgical spatial control. Molecular printing, nanofabrication, or even local molecular enrichment are just some of the many applications that one might contemplate.

CHAPTER V

CONCLUSION

In chapter 3, we reported our design of a thermal sensor efficient for measurements in thin films. Our system includes an optical film capable of changing colors upon external thermal stimulations. We first studied the effect of complexing PVP derivatives (PVP-VA and PVP-PS) with the short conjugated polyelectrolyte PPE-CO$_2$-7 in a solution and measured their relative sensitivies; 2.35% for PVP-VA and 1.455% for PVP-PS. Showing promising results in solutions, the PVP-VA/ PPE-CO$_2$-7 complex was preserved in thin films through spun casting the solution of the mixture on the top of a quartz slide. Films were then imaged using a DSLR camera under UV-light exposure and analyzed based on the enhancements in the 3 main color-components.

In order to improve the ratiometric change in the obtained signal, we resorted to mix the CPE/polymer complex with the fluorescent Rhodamine B. The desired ratiometric signal was then detected after imaging and analyzing the respective films.

This work has the potential to allow the measurements of thermal fluctuations in microelectronic devices such as MEMS, hence leading to the optimization of their performance.

Building on the successful results achieved in chapter 3, we believed that the ability to drive chemical reactions using locally generated heat while maintaining a high spatial resolution, would add significantly to this achievement.

As such, we aimed in chapter 4, to exploit the heat generated from magnetic nanoparticles when placed in an alternating magnetic field to drive catalytic chemical reactions. Specifically, and as a proof of concept, we focused on monitoring the catalysis reduction of resazurin into resorufin. Our major aim was to locally activate the catalytic reaction when placed in the alternating magnetic field while comparing its efficiency to that of a solution heated by an external source under the same conditions.

We initially focused on synthesizing the iron oxide magnetic nanoparticles and optimizing the respective thermal responses. The catalytic conditions for the rezasurin to be reduced into resorufin, were then optimized in a water bath maintained at 65 °C. Next, the optimized reaction's solution was placed in an alternating magnetic field, maintained at 45 °C where the rate of the reduction was monitored and the fluorescence intensity of resorufin produced was constantly measured. The efficiency of the locally induced heat was compared, under the same experimental conditions, to that of a water bath at 45 °C. Within the first 15 minutes, the catalytic micro-structure showed an enhanced catalytic conversation as compared to a water bath solution, and reached, in some cases, a 120 % enhanced efficiency

Conclusively, we report the successful use of heat generated at the microscale to drive chemical reactions with significantly higher catalytic efficiency when compared to a water bath maintained at the same temperature. This proof-of-concept experiment will eventually pave the way to thermally control reactions with a high spatial resolution which would allow, for instance, the production of drugs with surgical precision.

CHAPTER VI

REFERENCES

1.   Fischer LH, Harms GS, Wolfbeis OS. Upconverting nanoparticles for nanoscale thermometry. Angewandte Chemie International Edition. 2011;50(20):4546-51.

2.   Seymour RS. Biophysics and physiology of temperature regulation in thermogenic flowers. Bioscience reports. 2001;21(2):223-36.

3.   Okabe K, Inada N, Gota C, Harada Y, Funatsu T, Uchiyama S. Intracellular temperature mapping with a fluorescent polymeric thermometer and fluorescence lifetime imaging microscopy. Nature communications. 2012;3:705.

4.   Lowell BB, Spiegelman BM. Towards a molecular understanding of adaptive thermogenesis. Nature. 2000;404(6778):652.

5.   Monti M, Brandt L, Ikomi‑Kumm J, Olsson H. Microcalorimetric investigation of cell metabolism in tumour cells from patients with non‑Hodgkin lymphoma (NHL). Scandinavian journal of haematology. 1986;36(4):353-7.

6.   McCabe KM, Hernandez M. Molecular thermometry. Pediatric research. 2010;67(5):469.

7.   Wu Y, Liu J, Ma J, Liu Y, Wang Y, Wu D. Ratiometric nanothermometer based on rhodamine dye-incorporated F127-melamine-formaldehyde polymer nanoparticle: preparation, characterization, wide-range temperature sensing, and precise intracellular thermometry. ACS applied materials & interfaces. 2016;8(23):14396-405.

8.   Liu J, Guo X, Hu R, Xu J, Wang S, Li S, et al. Intracellular fluorescent temperature probe based on triarylboron substituted poly N-isopropylacrylamide and energy transfer. Analytical chemistry. 2015;87(7):3694-8.

9.   Stockbridge RB, Lewis CA, Yuan Y, Wolfenden R. Impact of temperature on the time required for the establishment of primordial biochemistry, and for the evolution of enzymes. Proceedings of the National Academy of Sciences. 2010;107(51):22102-5.

10.   Tanimoto R, Hiraiwa T, Nakai Y, Shindo Y, Oka K, Hiroi N, et al. Detection of Temperature Difference in Neuronal Cells. Scientific Reports. 2016;6:22071.

11.   Hartmann J, Voigt P, Reichling M. Measuring local thermal conductivity in polycrystalline diamond with a high resolution photothermal microscope. Journal of applied physics. 1997;81(7):2966-72.

12.   Bal NC, Maurya SK, Sopariwala DH, Sahoo SK, Gupta SC, Shaikh SA, et al. Sarcolipin is a newly identified regulator of muscle-based thermogenesis in mammals. Nature medicine. 2012;18(10):1575.

13.   Iyer PV, Ananthanarayan L. Enzyme stability and stabilization—aqueous and non-aqueous environment. Process biochemistry. 2008;43(10):1019-32.

14.   Lagendijk J. Hyperthermia treatment planning. Physics in Medicine & Biology. 2000;45(5):R61.

15.   Stauffer P, Goldberg S. Introduction: thermal ablation therapy. International Journal of Hyperthermia. 2004;20(7):671-7.

16. Mazur P. Freezing of living cells: mechanisms and implications. American journal of physiology-cell physiology. 1984;247(3):C125-C42.

17. Scully K, editor Laser line heating. Ship Production Symposium; 1987.

18. Liu J, Detrembleur C, De Pauw-Gillet M-C, Mornet S, Vander Elst L, Laurent S, et al. Heat-triggered drug release systems based on mesoporous silica nanoparticles filled with a maghemite core and phase-change molecules as gatekeepers. Journal of Materials Chemistry B. 2014;2(1):59-70.

19. McDaniel JR, Callahan DJ, Chilkoti A. Drug delivery to solid tumors by elastin-like polypeptides. Advanced drug delivery reviews. 2010;62(15):1456-67.

20. Rassaei L, Compton RG, Marken F. Microwave-Enhanced Electrochemistry in Locally Superheated Aqueous− Glycerol Electrolyte Media. The Journal of Physical Chemistry C. 2009;113(8):3046-9.

21. Geitenbeek RG, Nieuwelink A-E, Jacobs TS, Salzmann BB, Goetze J, Meijerink A, et al. In Situ Luminescence Thermometry To Locally Measure Temperature Gradients during Catalytic Reactions. ACS catalysis. 2018;8(3):2397-401.

22. Zhou X, Xu W, Liu G, Panda D, Chen P. Size-dependent catalytic activity and dynamics of gold nanoparticles at the single-molecule level. Journal of the American Chemical Society. 2009;132(1):138-46.

23. Chen P, Zhou X, Shen H, Andoy NM, Choudhary E, Han K-S, et al. Single-molecule fluorescence imaging of nanocatalytic processes. Chemical Society Reviews. 2010;39(12):4560-70.

24. Huo M, Wang L, Chen Y, Shi J. Tumor-selective catalytic nanomedicine by nanocatalyst delivery. Nature communications. 2017;8(1):357.

25. Khalid A, Kontis K. 2D surface thermal imaging using rise-time analysis from laser-induced luminescence phosphor thermometry. Measurement Science and Technology. 2009;20(2):025305.

26. Graham EM, Iwai K, Uchiyama S, de Silva AP, Magennis SW, Jones AC. Quantitative mapping of aqueous microfluidic temperature with sub-degree resolution using fluorescence lifetime imaging microscopy. Lab on a Chip. 2010;10(10):1267-73.

27. Burchfield JD. Lord Kelvin and the Age of the Earth: University of Chicago Press; 1990.

28. Lee J, Kotov NA. Thermometer design at the nanoscale. Nano Today. 2007;2(1):48-51.

29. Kolodner P, Tyson JA. Remote thermal imaging with 0.7‐μm spatial resolution using temperature‐dependent fluorescent thin flims. Applied Physics Letters. 1983;42(1):117-9.

30. Campbell CW, El Latif A, Foster JW. Application of thermography to karst hydrology. Journal of Cave and Karst Studies. 1996;58(3):163-7.

31. Vetrone F, Naccache R, Zamarrón A, Juarranz de la Fuente A, Sanz-Rodríguez F, Martinez Maestro L, et al. Temperature sensing using fluorescent nanothermometers. ACS nano. 2010;4(6):3254-8.

32. Kiyonaka S, Kajimoto T, Sakaguchi R, Shinmi D, Omatsu-Kanbe M, Matsuura H, et al. Genetically encoded fluorescent thermosensors visualize subcellular thermoregulation in living cells. Nature methods. 2013;10(12):1232.

33.   Oyama K, Takabayashi M, Takei Y, Arai S, Takeoka S, Ishiwata Si, et al. Walking nanothermometers: spatiotemporal temperature measurement of transported acidic organelles in single living cells. Lab on a Chip. 2012;12(9):1591-3.

34.   Albers AE, Chan EM, McBride PM, Ajo-Franklin CM, Cohen BE, Helms BA. Dual-emitting quantum dot/quantum rod-based nanothermometers with enhanced response and sensitivity in live cells. Journal of the American Chemical Society. 2012;134(23):9565-8.

35.   Wei L, Ma Y, Shi X, Wang Y, Su X, Yu C, et al. Living cell intracellular temperature imaging with biocompatible dye-conjugated carbon dots. Journal of Materials Chemistry B. 2017;5(18):3383-90.

36.   Wang C, Xu Z, Cheng H, Lin H, Humphrey MG, Zhang C. A hydrothermal route to water-stable luminescent carbon dots as nanosensors for pH and temperature. Carbon. 2015;82:87-95.

37.   Balabhadra S, Debasu ML, Brites CD, Nunes LA, Malta OL, Rocha J, et al. Boosting the sensitivity of Nd 3+-based luminescent nanothermometers. Nanoscale. 2015;7(41):17261-7.

38.   Takei Y, Arai S, Murata A, Takabayashi M, Oyama K, Ishiwata Si, et al. A nanoparticle-based ratiometric and self-calibrated fluorescent thermometer for single living cells. ACS nano. 2013;8(1):198-206.

39.   Zhou Y, Zhang D, Zeng J, Gan N, Cuan J. A luminescent Lanthanide-free MOF nanohybrid for highly sensitive ratiometric temperature sensing in physiological range. Talanta. 2018;181:410-5.

40.   Shen X, Yan B. Polymer hybrid thin films based on rare earth ion-functionalized MOF: photoluminescence tuning and sensing as a thermometer. Dalton Transactions. 2015;44(4):1875-81.

41.   Darwish GH, Koubeissi A, Shoker T, Shaheen SA, Karam P. Turning the heat on conjugated polyelectrolytes: an off–on ratiometric nanothermometer. Chemical Communications. 2016;52(4):823-6.

42.   Ye F, Wu C, Jin Y, Chan Y-H, Zhang X, Chiu DT. Ratiometric temperature sensing with semiconducting polymer dots. Journal of the American Chemical Society. 2011;133(21):8146-9.

43.   Chen C-Y, Chen C-T. A PNIPAM-based fluorescent nanothermometer with ratiometric readout. Chemical communications. 2011;47(3):994-6.

44.   Chandrasekharan N, Kelly LA. A dual fluorescence temperature sensor based on perylene/exciplex interconversion. Journal of the American Chemical Society. 2001;123(40):9898-9.

45.   Chang K, Liu Y, Hu D, Qi Q, Gao D, Wang Y, et al. Highly stable conjugated polymer dots as multifunctional agents for photoacoustic imaging-guided photothermal therapy. ACS applied materials & interfaces. 2018;10(8):7012-21.

46.   Lee W, Seo JH, Woo HY. Conjugated polyelectrolytes: A new class of semiconducting material for organic electronic devices. Polymer. 2013;54(19):5104-21.

47.   Liu B, Bazan GC. Conjugated polyelectrolytes: fundamentals and applications: John Wiley & Sons; 2013.

48.   Skotheim TA, Reynolds J. Handbook of Conducting Polymers, 2 Volume Set: CRC press; 2007.

49.   Hennebicq E, Pourtois G, Scholes GD, Herz LM, Russell DM, Silva C, et al. Exciton migration in rigid-rod conjugated polymers: an improved Förster model. Journal of the American Chemical Society. 2005;127(13):4744-62.

50.   Ngo AT, Karam P, Cosa G. Conjugated polyelectrolyte–lipid interactions: opportunities in biosensing. Pure and Applied Chemistry. 2010;83(1):43-55.

51.   Rochat Sb, Swager TM. Conjugated amplifying polymers for optical sensing applications. ACS applied materials & interfaces. 2013;5(11):4488-502.

52.   Schwartz BJ. Conjugated polymers as molecular materials: How chain conformation and film morphology influence energy transfer and interchain interactions. Annual review of physical chemistry. 2003;54(1):141-72.

53.   Tan C, Atas E, Müller JG, Pinto MR, Kleiman VD, Schanze KS. Amplified quenching of a conjugated polyelectrolyte by cyanine dyes. Journal of the American Chemical Society. 2004;126(42):13685-94.

54.   Scholes GD. Long-range resonance energy transfer in molecular systems. Annual review of physical chemistry. 2003;54(1):57-87.

55.   Jiang H, Taranekar P, Reynolds JR, Schanze KS. Conjugated polyelectrolytes: synthesis, photophysics, and applications. Angewandte Chemie International Edition. 2009;48(24):4300-16.

56.   Tan C, Pinto MR, Schanze KS. Photophysics, aggregation and amplified quenching of a water-soluble poly (phenylene ethynylene). Chemical Communications. 2002(5):446-7.

57.   Walters KA, Ley KD, Schanze KS. Photophysical consequences of conformation and aggregation in dilute solutions of π-conjugated oligomers. Langmuir. 1999;15(17):5676-80.

58.   Levitus M, Schmieder K, Ricks H, Shimizu KD, Bunz UH, Garcia-Garibay MA. Steps to demarcate the effects of chromophore aggregation and planarization in poly (phenyleneethynylene) s. 1. Rotationally interrupted conjugation in the excited states of 1, 4-bis (phenylethynyl) benzene. Journal of the American Chemical Society. 2001;123(18):4259-65.

59.   Kim J, Swager T. Control of conformational and interpolymer effects in conjugated polymers. Nature. 2001;411(6841):1030.

60.   Thomas SW, Joly GD, Swager TM. Chemical sensors based on amplifying fluorescent conjugated polymers. Chemical reviews. 2007;107(4):1339-86.

61.   Liang W. Excitons. Physics Education. 1970;5(4):226.

62.   Swager TM, Gil CJ, Wrighton MS. Fluorescence studies of poly (p-phenyleneethynylene) s: the effect of anthracene substitution. The Journal of Physical Chemistry. 1995;99(14):4886-93.

63.   Zhou Q, Swager TM. Fluorescent chemosensors based on energy migration in conjugated polymers: the molecular wire approach to increased sensitivity. Journal of the American Chemical Society. 1995;117(50):12593-602.

64.   Chen L, McBranch DW, Wang H-L, Helgeson R, Wudl F, Whitten DG. Highly sensitive biological and chemical sensors based on reversible fluorescence quenching in a conjugated polymer. Proceedings of the National Academy of Sciences. 1999;96(22):12287-92.

65.   Karam P, Ngo AT, Rouiller I, Cosa G. Unraveling electronic energy transfer in single conjugated polyelectrolytes encapsulated in lipid vesicles. Proceedings of the National Academy of Sciences. 2010;107(41):17480-5.

66.	Zhao X, Jiang H, Schanze KS. Polymer chain length dependence of amplified fluorescence quenching in conjugated polyelectrolytes. Macromolecules. 2008;41(10):3422-8.

67.	Ricks HL, Choudry UH, Marshall AR, Bunz UH. Rod vs coil: molecular weight comparison of a poly (dialkyl-p-phenyleneethynylene) with its reduced poly (2, 5-dialkyl-p-xylylene). Macromolecules. 2003;36(5):1424-5.

68.	Arnt L, Tew GN. New poly (phenyleneethynylene) s with cationic, facially amphiphilic structures. Journal of the American Chemical Society. 2002;124(26):7664-5.

69.	Tan C, Pinto MR, Kose ME, Ghiviriga I, Schanze KS. Solvent‐Induced Self‐Assembly of a Meta‐Linked Conjugated Polyelectrolyte. Helix Formation, Guest Intercalation, and Amplified Quenching. Advanced Materials. 2004;16(14):1208-12.

70.	Zhao X. Conjugated polyelectrolytes based on poly (arylene ethynylene): Synthesis, solution photophysics and applications to sensors and solar cells2007.

71.	Dong J, Zink JI. Taking the temperature of the interiors of magnetically heated nanoparticles. ACS nano. 2014;8(5):5199-207.

72.	Okabe K, Inada N, Gota C, Harada Y, Funatsu T, Uchiyama S. Intracellular temperature mapping with a fluorescent polymeric thermometer and fluorescence lifetime imaging microscopy. Nat Commun. 2012;3:705.

73.	Donner JS, Thompson SA, Kreuzer MP, Baffou G, Quidant R. Mapping Intracellular Temperature Using Green Fluorescent Protein. Nano Letters. 2012;12(4):2107-11.

74.	Verhoeven H, Boettger E, Flöter A, Reiss H, Zachai R. Thermal resistance and electrical insulation of thin low-temperature-deposited diamond films. Diamond and Related Materials. 1997;6(2-4):298-302.

75.	Xie B, Danielsson B, Norberg P, Winquist F, Lundström I. Development of a thermal micro-biosensor fabricated on a silicon chip. Sensors and Actuators B: Chemical. 1992;6(1-3):127-30.

76.	Cahill DG, Goodson K, Majumdar A. Thermometry and thermal transport in micro/nanoscale solid-state devices and structures. Journal of Heat Transfer. 2002;124(2):223-41.

77.	Cain CP, Welch AJ. Thin-film temperature sensors for biological measurements. IEEE transactions on Biomedical Engineering. 1974(5):421-3.

78.	Agarwal RP, Kajanto I, Friberg AT. Silicon thin films for optoelectronic temperature sensors. Thin solid films. 1988;158(1):1-5.

79.	McLennan W, Ooten R, Bynum D, Palmer J, Pendley K, Baxter C. A thin film temperature sensor. Journal of Vacuum Science and Technology. 1975;12(1):71-3.

80.	Urban G, Jachimowicz A, Kohl F, Kuttner H, Olcaytug F, Kamper H, et al. High-resolution thin-film temperature sensor arrays for medical applications. Sensors and Actuators A: Physical. 1990;22(1-3):650-4.

81.	He S, Mench MM, Tadigadapa S. Thin film temperature sensor for real-time measurement of electrolyte temperature in a polymer electrolyte fuel cell. Sensors and Actuators A: Physical. 2006;125(2):170-7.

82.	Bianchi C, Loureiro J, Duarte P, Marques J, Figueira J, Ropio I, et al. V2O5 Thin Films for Flexible and High Sensitivity Transparent Temperature Sensor. Advanced Materials Technologies. 2016;1(6):1600077.

83.	Rust MJ, Bates M, Zhuang X. Sub-diffraction-limit imaging by stochastic optical reconstruction microscopy (STORM). Nature methods. 2006;3(10):793-6.
84.	Hariri AA, Hamblin GD, Gidi Y, Sleiman HF, Cosa G. Stepwise growth of surface-grafted DNA nanotubes visualized at the single-molecule level. Nature chemistry. 2015;7(4):295-300.
85.	Hell SW, Wichmann J. Breaking the diffraction resolution limit by stimulated emission: stimulated-emission-depletion fluorescence microscopy. Optics letters. 1994;19(11):780-2.
86.	Yarimaga O, Lee S, Ham DY, Choi JM, Kwon SG, Im M, et al. Thermofluorescent Conjugated Polymer Sensors for Nano‐and Microscale Temperature Monitoring. Macromolecular Chemistry and Physics. 2011;212(12):1211-20.
87.	Chauhan VM, Hopper RH, Ali SZ, King EM, Udrea F, Oxley CH, et al. Thermo-optical characterization of fluorescent rhodamine B based temperature-sensitive nanosensors using a CMOS MEMS micro-hotplate. Sensors and Actuators B: Chemical. 2014;192:126-33.
88.	Gui L, Ren CL. Temperature measurement in microfluidic chips using photobleaching of a fluorescent thin film. Applied Physics Letters. 2008;92(2):024102.
89.	Aizawa H, Kano Y, Katsumata T, Komuro S, editors. Temperature sensor application of fluorescence film. SICE, 2007 Annual Conference; 2007: IEEE.
90.	Darwish GH, Karam P. Nanohybrid conjugated polyelectrolytes: highly photostable and ultrabright nanoparticles. Nanoscale. 2015;7(37):15149-58.
91.	Darwish GH, Abouzeid J, Karam P. Tunable nanothermometer based on short poly (phenylene ethynylene). RSC Advances. 2016;6(71):67002-10.
92.	Darwish GH, Fakih HH, Karam P. Temperature Mapping in Hydrogel Matrices Using Unmodified Digital Camera. The Journal of Physical Chemistry B. 2017;121(5):1033-40.
93.	Ng HM. Optimization of dye-sensitized solar cells with poly (1-vinylpyrrolidone-co-vinyl acetate) gel polymer electrolytes containing binary salts and ionic liquid/Ng Hon Ming: University of Malaya; 2016.
94.	Whitbourne RJ. Bonding layers for medical device surface coatings. Google Patents; 2001.
95.	Darwish GH, Fakih HH, Karam P. Temperature Mapping in Hydrogel Matrices Using Unmodified Digital Camera. The Journal of Physical Chemistry B. 2017.
96.	Bao S, Fei B, Li J, Yao X, Lu X, Xin JH. Reversible thermochromic switching of fluorescent poly (vinylidene fluoride) composite containing bis (benzoxazolyl) stilbene dye. Dyes and Pigments. 2013;99(1):99-104.
97.	Ogasawara K, Nakamura K, Kobayashi N. Thermally controlled dual-mode display media with red-green-blue coloration and fluorescence via energy transfer between emission materials and leuco dyes. Journal of Materials Chemistry C. 2016;4(21):4805-13.
98.	Raghuraman S, Elinski MB, Batteas JD, Felts JR. Driving surface chemistry at the nanometer scale using localized heat and stress. Nano letters. 2017;17(4):2111-7.
99.	Steinberg I, Tamir G, Gannot I. A reconstruction method for the estimation of temperatures of multiple sources applied for nanoparticle-mediated hyperthermia. Molecules. 2018;23(3):670.
100.	Çakır M, Çalışkan D, Bütün B, Özbay E. Planar indium tin oxide heater for improved thermal distribution for metal oxide micromachined gas sensors. Sensors. 2016;16(10):1612.

101.   He X, Duan F, Liu J, Lan Q, Wu J, Yang C, et al. Transparent electrode based on silver nanowires and polyimide for film heater and flexible solar cell. Materials. 2017;10(12):1362.

102.   Ha W, Yu J, Song X-y, Chen J, Shi Y-p. Tunable temperature-responsive supramolecular hydrogels formed by prodrugs as a codelivery system. ACS applied materials & interfaces. 2014;6(13):10623-30.

103.   Lee HJ, Liu Y, Zhao J, Zhou M, Bouchard RR, Mitcham T, et al. In vitro and in vivo mapping of drug release after laser ablation thermal therapy with doxorubicin-loaded hollow gold nanoshells using fluorescence and photoacoustic imaging. Journal of Controlled Release. 2013;172(1):152-8.

104.   Xiao C, Ding J, Ma L, Yang C, Zhuang X, Chen X. Synthesis of thermal and oxidation dual responsive polymers for reactive oxygen species (ROS)-triggered drug release. Polymer Chemistry. 2015;6(5):738-47.

105.   Chen S, Wan C, Wang Y. Thermal analysis of lithium-ion batteries. Journal of power sources. 2005;140(1):111-24.

106.   Fuller TF, Newman J. Water and thermal management in solid‐polymer‐electrolyte fuel cells. Journal of the Electrochemical Society. 1993;140(5):1218-25.

107.   Adleman JR, Boyd DA, Goodwin DG, Psaltis D. Heterogenous catalysis mediated by plasmon heating. Nano letters. 2009;9(12):4417-23.

108.   Wang F, Li C, Chen H, Jiang R, Sun L-D, Li Q, et al. Plasmonic harvesting of light energy for Suzuki coupling reactions. Journal of the American Chemical Society. 2013;135(15):5588-601.

109.   Alejo CJB, Fasciani C, Grenier M, Netto-Ferreira JC, Scaiano JC. Reduction of resazurin to resorufin catalyzed by gold nanoparticles: dramatic reaction acceleration by laser or LED plasmon excitation. Catalysis Science & Technology. 2011;1(8):1506-11.

110.   Vallejo-Fernandez G, Whear O, Roca A, Hussain S, Timmis J, Patel V, et al. Mechanisms of hyperthermia in magnetic nanoparticles. Journal of Physics D: Applied Physics. 2013;46(31):312001.

111.   Obaidat I, Issa B, Haik Y. Magnetic properties of magnetic nanoparticles for efficient hyperthermia. Nanomaterials. 2015;5(1):63-89.

112.   Ghosh R, Pradhan L, Devi YP, Meena S, Tewari R, Kumar A, et al. Induction heating studies of Fe3O4 magnetic nanoparticles capped with oleic acid and polyethylene glycol for hyperthermia. Journal of Materials Chemistry. 2011;21(35):13388-98.

113.   Pankhurst QA, Connolly J, Jones S, Dobson J. Applications of magnetic nanoparticles in biomedicine. Journal of physics D: Applied physics. 2003;36(13):R167.

114.   Ito A, Shinkai M, Honda H, Kobayashi T. Medical application of functionalized magnetic nanoparticles. Journal of bioscience and bioengineering. 2005;100(1):1-11.

115.   Zhou H, Lee J, Park TJ, Lee SJ, Park JY, Lee J. Ultrasensitive DNA monitoring by Au–Fe3O4 nanocomplex. Sensors and Actuators B: Chemical. 2012;163(1):224-32.

116.   Salgueiriño-Maceira V, Correa-Duarte MA, Farle M, López-Quintela A, Sieradzki K, Diaz R. Bifunctional gold-coated magnetic silica spheres. Chemistry of Materials. 2006;18(11):2701-6.

117.   Riedinger A, Guardia P, Curcio A, Garcia MA, Cingolani R, Manna L, et al. Subnanometer local temperature probing and remotely controlled drug release based on azo-functionalized iron oxide nanoparticles. Nano letters. 2013;13(6):2399-406.

118.   Lee KY, Mooney DJ. Hydrogels for tissue engineering. Chemical reviews. 2001;101(7):1869-80.

119.   Drury JL, Mooney DJ. Hydrogels for tissue engineering: scaffold design variables and applications. Biomaterials. 2003;24(24):4337-51.

120.   Sershen S, Westcott S, Halas N, West J. Temperature‐sensitive polymer–nanoshell composites for photothermally modulated drug delivery. Journal of Biomedical Materials Research: An Official Journal of The Society for Biomaterials, The Japanese Society for Biomaterials, and The Australian Society for Biomaterials and the Korean Society for Biomaterials. 2000;51(3):293-8.